2016

INTEGRATION AND TESTING OF AN ADVANCED CONFORMABLE CNG TANK IN A FULL-SIZED LIGHT-DUTY PICKUP

Abayomi Famuyiwa
Michigan Technological University, aafamuyi@mtu.edu

INTEGRATION AND TESTING OF AN ADVANCED CONFORMABLE CNG TANK IN A FULL-SIZED LIGHT-DUTY PICKUP

By
Abayomi Famuyiwa

A THESIS
Submitted in partial fulfillment of the requirements for the degree of
MASTER OF SCIENCE
In Mechanical Engineering

MICHIGAN TECHNOLOGICAL UNIVERSITY
2016

This thesis has been approved in partial fulfillment of the requirements for the Degree of MASTER OF SCIENCE in Mechanical Engineering.

Department of Mechanical Engineering – Engineering Mechanics

Thesis Advisor: *Jeremy Worm*

Committee Member: *Greg Odegard*

Committee Member: *Scott Miers*

Department Chair: *William W. Predebon*

Table of Contents

List of Figures

List of Tables

Acknowledgements

I would like to express my sincere gratitude to my advisor Jeremy Worm for the continuous support throughout my graduate career with my research and my teaching assistant courses with motivation, leadership, and vast knowledge. His guidance and encouragement helped me learn how to be a dynamic and efficient research engineer as well as a confident teaching assistant with relatively new subjects.

Besides my advisor, I would like to thank the rest of the committee: Dr. Greg Odegard and Dr. Scott Miers, for their guidance and encouragement with my research as well as other school and professional related matters.

I would also like to thank my fellow labmates working on the project and at the APSRC: Tucker Aslup, Josh Dillon, Dr. Odegard's FEA team, Rafael Figueroa, REL Inc., Chris Davis, and Chris Morgan, for the inspiring conversations during meetings and assistance with various parts of the project.

Last of all but not least, I would like to thank my family: my parents, Abiodun and Maria, and my brothers, Deji and Tunde, for encouraging me since day one and helping my get through my graduate degree.

Acronyms

ARPA-e- Department of Energy's Advanced Research Project Agency-Energy

APSRC- Advanced Power Systems Research Center

BMEP- Brake Mean Effective Pressure

BSFC- Brake Specific Fuel Consumption

BSPP- British Standard Pipe Parallel

cDAQ – Compact Data Acquisition

CG – Center of Gravity

CNG- Compressed Natural Gas

CO- Carbon Monoxide

CO_2- Carbon Dioxide

FEA- Finite Element Analysis

FKM- Fluoroelastomer standard

GGE- Gasoline Gallon Equivalent

MAP- Manifold Absolute Pressure

NACTO-National Association of City Transportation Officials

NPT- National Pipe Thread

OBD- On-board Diagnostics

OEM- Original Equipment Manufacturer

PXM- Industrial Metric Pressure Transducer

SAE- Society of Automotive Engineers

SI- Spark Ignited Engine

VI – Virtual Instrument

Abstract

Michigan Technological University is collaborating with Southwestern Energy and REL Inc. to develop and integrate a compressed natural gas (CNG) matrix tank that enables efficient packaging, increases range, and reduced cost for CNG vehicle applications. The vehicle being used in this project is a light-duty pickup truck to take advantage of the open space underneath the body and bed of the vehicle. With today's cylindrical CNG tanks consuming cargo space, a solution is to develop a tank capable of being shaping to the underbody of the truck to free cargo space. University faculty and graduate students utilizes Finite Element Analysis (FEA), material property testing, and dynamic vehicle testing to integrate the REL produced tank to a 2015 Chevy Silverado.

This thesis specifically covers the tank integration and vehicle testing portion of the project. The four different tank configuration phases of the project are described in detail to provide a frame of reference. In addition, the procedure to integrate the first phase of REL matrix tanks to the vehicle is included. Certain instrumentation and testing procedures were required to obtain the data, so the process and development of selecting the required instrumentation and the test procedures are included. To conclude, data from the first three phases of the project are compared and contrasted to view the effects of the conformable matrix tanks. The data shows that the placement and weight of the CNG tanks does directly affect static and dynamic parameters such as lowering the vehicle center of gravity and increasing the vehicle acceleration time.

Chapter 1 Project Background

1.1 United States Energy Distribution

There is a need for cleaner and renewable fuels in the transportation sector of United States and around the world. Currently, the United States is heavily dependent on foreign fossil fuels such as diesel and gasoline that are dominating the transportation sector, but these are limited resources. The dominance of petroleum in the Unites States transportation sector in 2015 can be seen in Figure 1.1. A solution needs to be found before this source runs out, so researchers are testing and developing new fuels and technologies that can be used in the transportation sector to help reduce this dependence as well as the amount of greenhouse gases emitted into the atmosphere. Some of these developing renewable fuels and technologies are biodiesel, bioethanol, hydrogen cell, solar energy, and natural gas [1]. A key reason that gasoline and diesel are constantly used is because of the higher energy density. The higher energy density allows them to achieve farther distances as described by a figure in "6 Application of biomass derived fuels for internal combustion engines with a focus on transportation" [2]. Natural gas, on the other hand, has a lower density and is even lower when the gas is not compressed, so natural gas needs to be compressed to be viable as a transportation option. In the figure, natural gas is simplified to methane. Methane (4) is pressurized to 25 MPa absolute at 20 °C and achieves 183 km more than Methane (7) which is not pressurized at 101.3 kPa and 20 °C [2]. Of the listed alternatives above, compressed natural gas (CNG) has become increasingly popular for many transportation systems around the world. With more than 16.7 million natural gas powered vehicles operating around the world at the end of 2012, it is difficult to ignore the impact that natural gas can have in the transportation as the next leading dominant fuel used in the transportation sector [3].

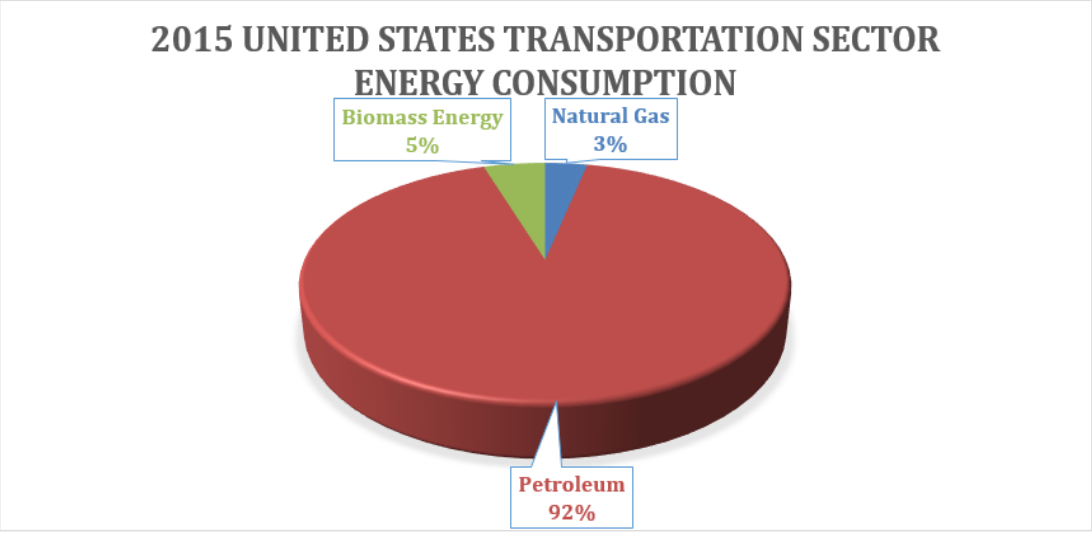

Figure 1.1: A proportional graph of the fuels used in the United States transportation sector.

1.2 Natural Gas Benefits

There are several benefits of natural gas in transportation. The most prominent benefits are that the fuel has lower cost, and cleaner emissions. With qualities including having a higher octane number than gasoline, natural gas fuels are able to gain a couple perks with engine operation. It is more tolerant to knock, enabling higher compression ratio, and optimal combustion phasing. Both of which improve engine efficiency [4]. When compared to gasoline with testing a spark ignited (SI) engine, it was found that CNG has 22% less brake specific fuel consumption (BSFC) and 13% higher fuel conversion efficiency [5]. What most people do not realize is that natural gas is around them more than they think. More than 60 million homes and businesses in the United States use natural gas, primarily for their heating [6]. If people were inclined to fuel their natural gas vehicles, they could just tap into their existing natural gas system at home and just pay for their monthly vehicle transportation costs with their natural gas bill. With the current low price of natural gas, consumers in the transportation sector would be able to save money and pay back the investment of their natural gas vehicle. In addition, natural gas burns cleaner than gasoline in more areas than one. When compared to gasoline in the emissions realm, there is a 40-87% reduction of unburned hydrocarbons emissions, 20-98% reduction of carbon monoxide (CO) emissions. Because of the increased efficiency,

and reduced carbon mass, there is a 8-20% reduction in carbon dioxide (CO_2) emissions [5].

1.3 Drawbacks of Natural gas Vehicles

As with all things in this world, there are always drawbacks to developing technologies such as natural gas powered vehicles. Since the fuel is a vapor instead of the standard liquid gasoline, the natural gas needs to be compressed at high pressures to minimize the space of the fuel container and still be able to store enough useable natural gas to fuel the engine for a comparable distance to gasoline. With these high pressures, specialized containers have to be designed and constructed to tolerate the same abuse and other extreme exposures that a gasoline container would experience [7]. There are numerous safety standards that need to be followed when handling CNG fuels such as FMVSS 304, NGV2, ISO 11439, NFPA 52 [8]. All of these standards are referenced and followed during this project to ensure the safety of the researchers, research facility, by-standers at test locations, and other researchers and by-standers in the future.

Other factors that contribute to the drawbacks are the size and weight of the tanks, and the reduction in engine power and torque. For those more interested in the power and torque that their truck can provide for hauling, the reduced volumetric efficiency and lower flame speed of CNG leads to an 8-16% reduction in brake torque, brake power, and brake mean effective pressure (BMEP) [5]. In general, the cylindrical CNG tanks in the pickup truck sector can take up to 50% of the cargo space in the bed of the truck [9]. Additionally, there is added weight from the tank relative to a liquid tank as well as the additional fueling components to inject the fuel into the engine if it is a bi-fuel system, not a CNG only system. These components tend to increase the vehicle cost which then leads to a longer payback time for the higher initial investment [10].

1.4 Alternative Solutions

Researchers around the world have been developing and testing solutions to make the CNG tanks as lightweight as possible and also find a way to move the large tank out of the bed of pick-up trucks. In general, pickup truck consumers buy their trucks to be able

to haul cargo in the bed of their truck. If a large tank is occupying more than a third of the cargo space, then they are less inclined to sacrifice that important space for a currently expensive natural gas pickup truck that is limiting their hauling capabilities. As the CNG tanks have developed, the researchers have been able to make them more lightweight moving away from metal as the main component. There are currently four types of approved natural gas containers that can be purchased for use. The earliest type 1 containers are produced using all metal, usually steel. Type 2 containers start to incorporate other materials with a metallic liner and an overwrapping of carbon fiber or fiberglass in a hoop wrapped pattern on the side walls of the cylinder. Type 3 containers are similar to type 2 containers, but the cylinder domes are also wrapped with the carbon fiber as well. A lesser amount of metal is used as the liner and the metal used switches to aluminum. In the latest type 4 category, there is no longer a metallic liner and the tank is fully wrapped using carbon fiber or fiber glass making this option the lightest of the four options [7].

With the improvement of the tank's weight being solved, other researchers are focusing on the placement of the tanks such as the subject of this thesis. Around the world, researchers are altering the shape and size of the CNG tanks to find ways to make them fit in other unused spaces in everyday vehicles. One example is developed by a group of researchers in the EU using a Fiat Grande Punto. The group decided to use the conventional cylindrical shape for the natural gas tanks, but found a way to place the tanks underneath the rear seat/ truck section. The group was able to develop and execute detailed finite element (FE) models, numerical analysis, experimental analysis and crashworthiness analysis on the vehicle, but they found that their concept still needed optimized brackets supporting the vessel and reinforce in potential critical areas such as crash zones [10].

In addition to this project, the United States Department of Energy's Advanced Research Project Agency-Energy (ARPA-e) has been funding a number of natural gas tank development projects to solve the challenge of CNG storage in a non-cylindrical tank with companies and universities. Some of these include Ford, Gas Technology Institute, OtherLab Inc., Pacific Northwest National Laboratory, United Technologies,

SRI International, and Texas A&M University ranging from tanks using internal porous adsorption materials to a low cost tank that resembles a human intestine filled with many small tubes [6]. One of the sponsored companies is REL Inc. in Calumet, Michigan that is developing the conformable tank that is being applied in this project.

REL's innovative tank design applies the efficient body structure of a sea urchin as the tank has two separate chambers and applies the sphere structure to withstand the high gas pressures. A cutaway of the tank is shown in Figure 1.3. By using this complex structure, the company is able to alter the shape of the tanks to conform to almost any desirable shape, so the tank is able to be shaped around vehicle components underneath the vehicle and optimize the available space. The usage of these tanks and their application to this project are explained in more detail in the following chapter as well as throughout this thesis.

Figure 1.2: An image of the REL matrix tank with a cutout.

With the use of REL's innovative tank, the goal of this project is to integrate CNG tanks that will hold at least 20-gasoline gallon equivalent (GGE) and refrain from taking up bed space. The term GGE assists the researchers or customers with understanding how much natural gas is required to equal the same energy content of gasoline. The complex goal requires collaboration from multiple University faculty, graduate students, REL Inc., and SWN. The structure of the overall team utilizes a finite element analysis (FEA) team, a material property development team, a tank development team, and an integration team. The FEA team uses FEA software to develop, test, and improve models for the matrix

tanks and brackets. The material property development team researches and tests different material alloys to determine the best material used to cast the matrix tanks. The tank development team, REL, manufactures the matrix tanks in house and makes adjustments to the manufacturing of the tank based on input from the rest of the teams.

The integration team is responsible for:

- Ordering and obtaining the test vehicle
- Developing and running the test procedures
- Ordering, obtaining, and installing instrumentation required for testing
- Integrating the matrix tanks onto the vehicle
- Communicating with other teams to simplify integration process

At the start of the project, the integration team ordered a 2015 Silverado 1500 4wd LS double cab standard box from Chevrolet. This vehicle was chosen because it is a common fleet pickup truck and the box size would allow for a large amount of space underneath to integrate the matrix tanks. However, the vehicle would be a conventional gasoline powered truck, so the vehicle needed to be converted to use natural gas before it was received. The company that was chosen to install the natural gas system was Carburetion and Turbo Systems Inc. (CTS), who installs IMPCO natural gas conversion kits. This company is based in Shakopee, MN, which is the closest CNG conversion company to Michigan Technological University. As a production vehicle, the Silverado uses direct injection to feed the gasoline into the engine. With this being the method of injection, CTS installed a dual-fuel CNG system. The term duel-fuel refers to a CNG system that always runs on gasoline, but the CNG is fed into the engine chamber with the gasoline if there is CNG available. The system never runs on CNG alone. Another available option is called bi-fuel, which is a system that is capable of running completely on CNG without any assistance of gasoline. The truck was then picked up from CTS once the conversion was completed.

Figure 1.3: A picture of the Silverado after the graphics were installed.

Chapter 2 Project Design Configurations

As mentioned previously, there are a total of four configurations for the SWN, REL Inc., and Michigan Technological University joint project. The four configurations include the Baseline, Quantum, Phase 1, and Phase 2. However, for the scope of this thesis, it will only include data from the first 3 configurations.

2.1 Baseline

The Baseline configurations can be classified as the 2015 Silverado 1500 4wd LS double cab standard box as if it were a traditional gasoline powered vehicle produced by Chevrolet without a CNG conversion. When the truck was first received, CTS had already converted the truck to run as a dual-fuel vehicle with the CNG tank installed in the bed of the truck with additional CNG required hardware to secure the tank and CNG components, and fuel lines to feed the alternative fuel into the engine.

The baseline/traditional system can be categorized as the truck being a production vehicle with the quantum tank removed. However, the fuel lines, brackets, regulator, and other components of the natural gas system were left in their same position because they are negligible and to simplify the transition between the Baseline and Quantum configurations.

2.2 Quantum

The Quantum configuration of the project is classified as how the truck was received from CTS after they completed the natural gas conversion on the truck. The main visual difference between the Baseline and Quantum configurations is that the Quantum configuration will have the 24 GGE type 4 natural gas cylinder in the bed of the truck. The actual internal volume of the cylinder is roughly 280.12 L (74 gallons), meaning that natural gas has an energy content that is close to 1/3 the amount of gasoline. At 24,821 kPa (3600 psi), the tank roughly adds 113 kg (250 lbs.) to the truck's overall weight when the tank is full of natural gas Figure 2.1 below include pictures of the Quantum configuration.

Figure 2.1: The truck as received from CTS with the quantum natural gas tank installed.

2.3 Phase 1

Phase 1 of the project is classified as utilizing the 4 cubic matrix tanks produced by REL Inc. Initially, the plan was to integrate 7 matrix tanks as seen in Figure 2.2. The rear tanks were installed once the spare tire was removed. A special bracket was fabricated to accommodate 3 tanks which attaches to the tow hitch and a stable rear chassis cross member above the back drive axle with a swinging motion. The three rear tanks have one valve that then routes the CNG flow to the main line that was described above. The installed rear bracket can be seen below in Figure 2.3. After further discussion and due to the low hanging nature of the bracket, it was decided to not include the back bracket and tanks for the Phase 1 design. Only the side tanks are being applied which will be about 92 L (24.3 gallons) of internal volume for all 4 tanks.

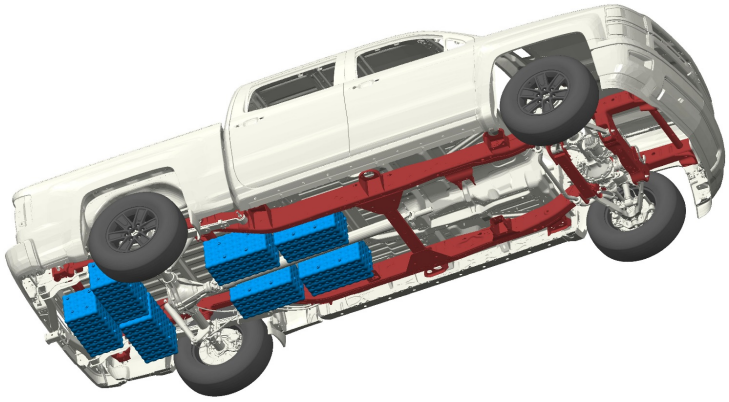

Figure 2.2: A model of seven matrix tanks positioned under the truck.

Figure 2.3: A picture of the truck after Phase 1 integration with the rear bracket and tanks.

2.4 Phase 2

Phase 2 is classified as the final phase of the truck having 2 conformable tanks installed underneath the vehicle instead of the 4 cubic matrix tanks as shown in Figures 2.4 & 2.5. This phase demonstrates the full capabilities of the matrix tank created by REL Inc. as the tank will achieve greater than 20 GGE. The design of the tanks is altered to specifically shape to the underbody of the truck to take advantage of areas that could not be accessed with the cubic tanks as seen in Figure 2.5. Furthermore, the spare tire is replaced in the Phase 2 design to make the truck a commercial option for company fleet vehicles. The Phase 1 plumbing will be altered to adapt the conformable tanks into the

existing natural gas lines for simplicity. As for the gasoline system, a custom liquid tank will be developed with the fill from the production location.

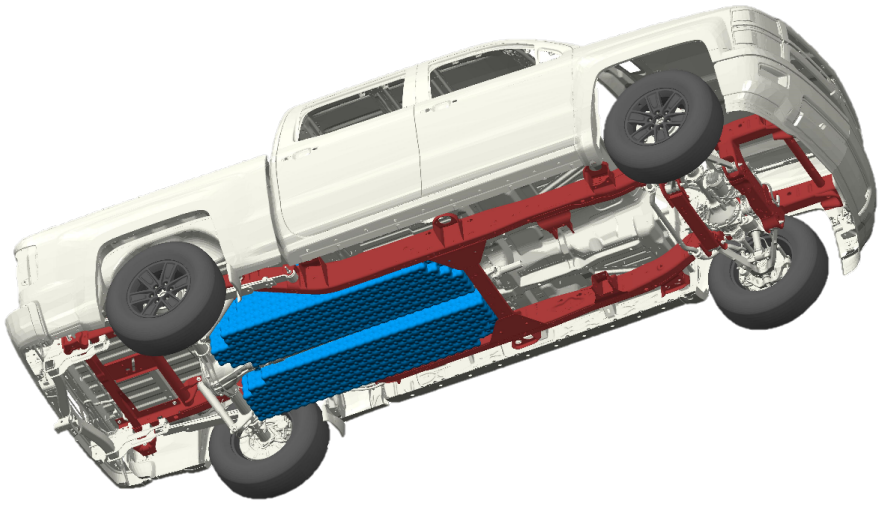

Figure 2.4: A model of two configurable matrix tanks positioned under the truck.

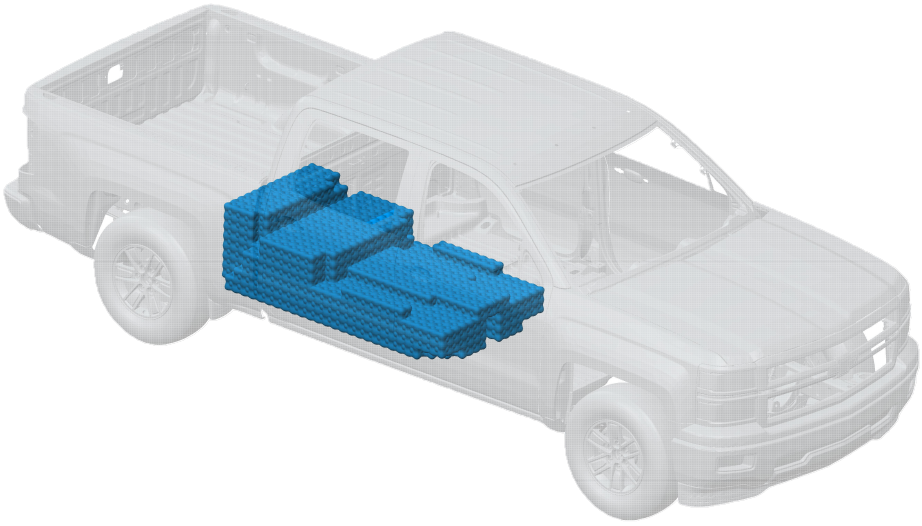

Figure 2.5: A model of two configurable matrix tanks positioned under the truck from an aerial view.

Chapter 3 Phase I Integration

3.1 Body Lift

The truck was lifted 7.6 cm (3”) to increase the space between the truck body and frame to allow space for the exhaust to be routed to the outside of the truck. This lift also provides benefit of more room for the matrix tanks to be installed safely above the lowest point of the truck’s frame. The body lift kit, a 2014 Chevy 1500 P/U Kit # 10293, was ordered from Performance Accessories, which includes spacers, bolts, washers, and hardware to raise the front and rear bumper to the original positions. The 2015 kit was not available when the kit was ordered, so minor modifications had to be made. Figure 3.1 displays some of the visible spacers that were installed to lift the body 7.6 cm (3”) off of the chassis. Figure 3.2 displays the truck after the lift was completed.

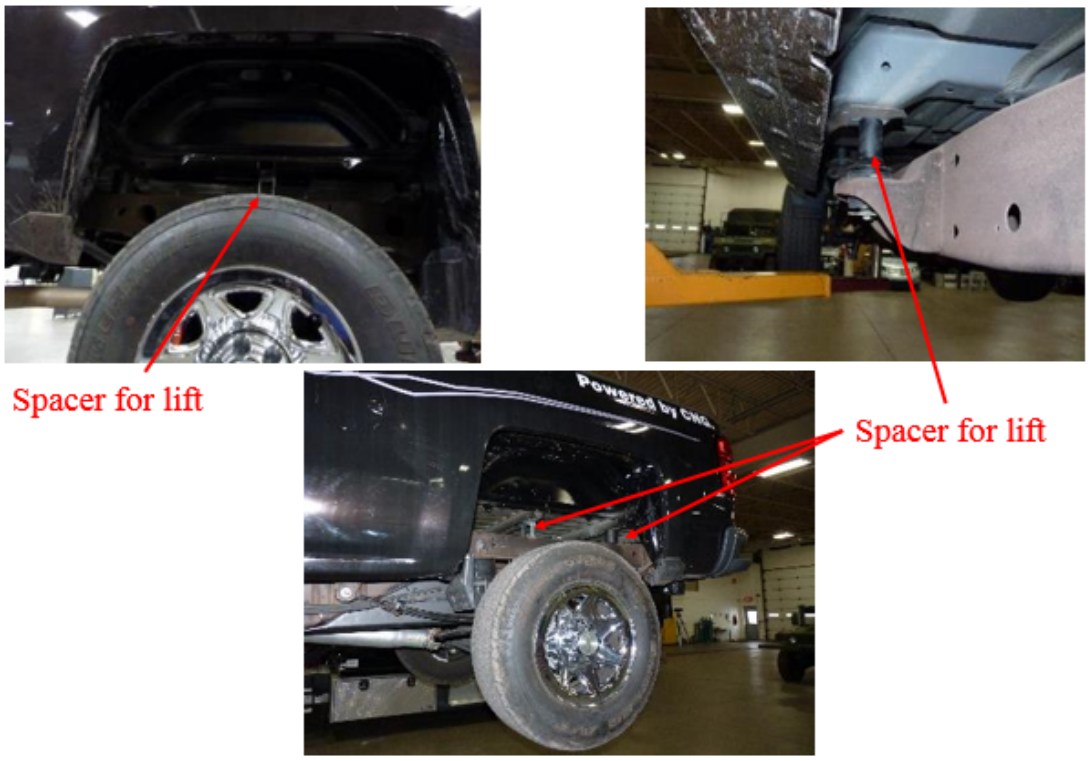

Figure 3.1: The location of some of the lift spacers that were applied to the vehicle for the 7.6 cm (3”) lift.

Before After

Figure 3.2: The vehicle before and after the 7.6 cm (3") lift was completed.

3.2 Removal of Exhaust and Liquid Tank

The existing exhaust needed to be rerouted and the gasoline tank needed to be removed to create package space for the left and right pairs of matrix tanks. The exhaust was cut closer to the engine after the first catalytic converter. This location was chosen to be able to simply reroute the exhaust to the outside of the vehicle through the space between the body and chassis that was created by the vehicle lift. The second catalytic converter is not actively diagnosed, so it was assumed that it is not needed for emissions testing in regards for this demonstration vehicle. However, for a full production saleable solution, a solution to reinstall the second catalytic converter will need to be investigated as well as an emissions test on the second catalytic converter to understand why it is not diagnosed. More information about the new exhaust installation will be discussed in the next section. Figures 3.3 and 3.4 display the space created by the removal of the exhaust.

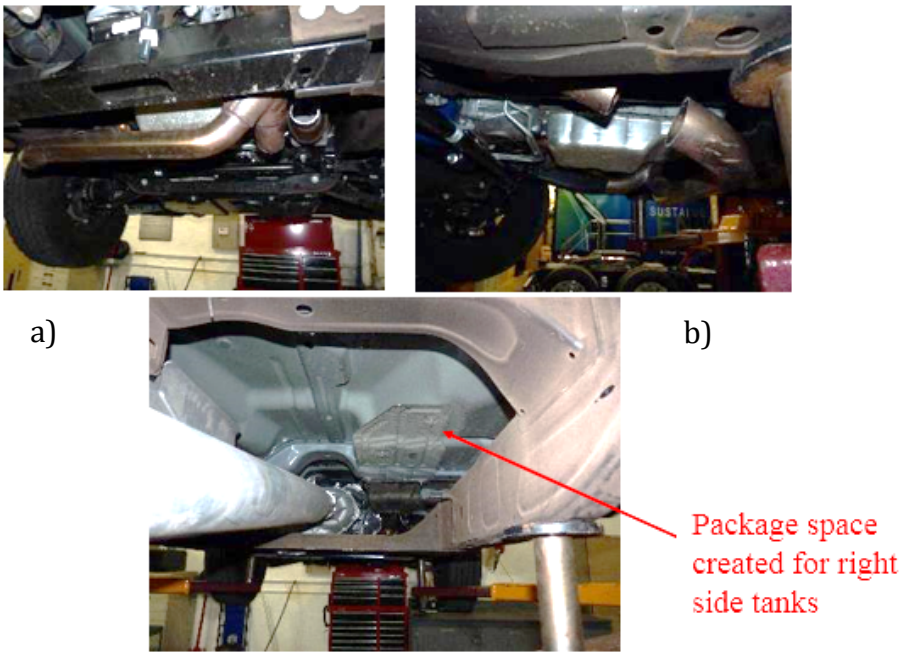

Figure 3.3: a) & b) Picture of the location where the exhaust was cut for Phase 1 integration. c) The package space that was created after the exhaust was removed.

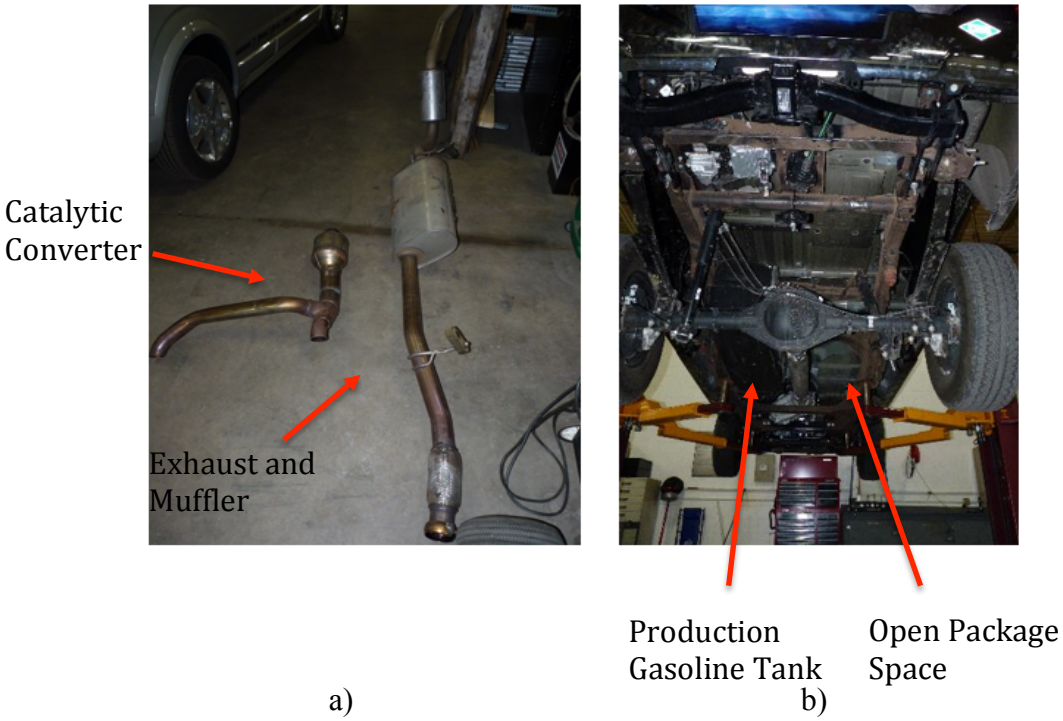

Figure 3.4: a) The production exhaust system after it was removed from the vehicle. b) A view of the space created by removing the exhaust.

The 98.4 L (26-gallon) gasoline tank on the left side of the vehicle was removed as well. Since the evaporation canister was installed next to the gasoline tank, it was also removed to reduce the amount of obstructions that could affect the placement of the Phase I tanks. For phase 1, a CAN BUS code occurs since the evaporation system is disconnected, but the system will be relocated and connected in Phase 2. Figure 3.5 shows the gasoline tank after it was removed from the vehicle, while Figure 3.6 gives a visual of the package space created after the tank was removed.

Figure 3.5: The production gasoline tank after it was removed for Phase 1 integration.

Figure 3.6: The package space created after the factory gasoline tank was remove.

3.3 Alternative Exhaust System Installation

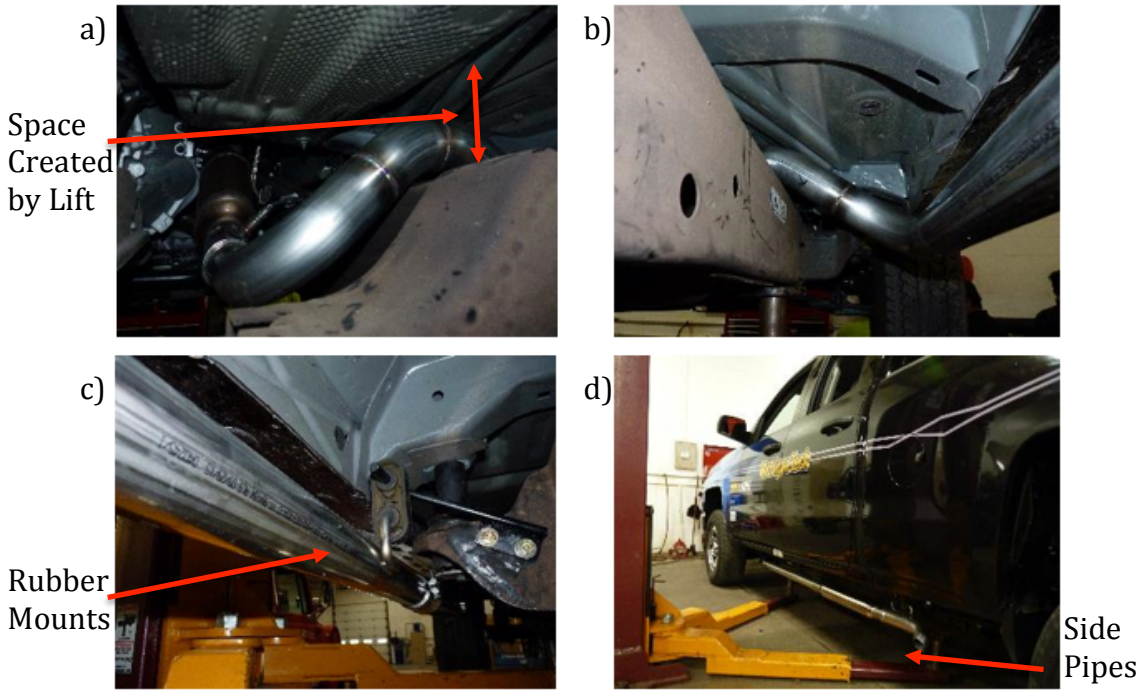

Figure 3.7: The installation of the new side pipe exhaust.

Figure 3.7 displays the alternative exhaust system that was installed by Great Lake Sound and Vibration in Houghton, MI. As described in the previous section, the space between the truck body and chassis was used to route the new exhaust system to the outside of the vehicle, which can be seen in Figure 3.7a & 3.7b. Rubber mounts, similar to the ones used to hold the previous exhaust system, were installed to help minimize vibration and movement when the vehicle is in motion. An example of these mounts can be seen in Figure 3.7c. Glass packs and straight pipe were chosen to give the side pipes a clean and stylish look as seen in Figure 3.7d. A glass pack is a muffler that allows the exhaust gas to pass through the center of the muffler and helps reduce back pressure. However, they are not very effective at muffling noise. The Great Lake Sound and Vibration also installed heat shields on the side pipes. This safety precaution is intended to protect passengers as they enter and leave the vehicle after the vehicle has been in use. It also adds an aesthetic touch to the side pipes, which can be viewed in Figure 3.8.

a)

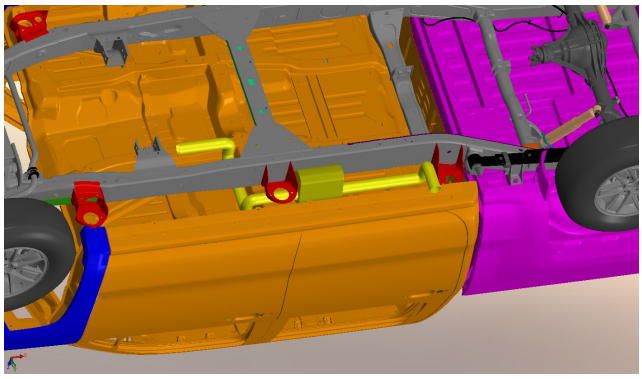

b)

Figure 3.8: a) A model of the initial side pipe idea. b) A picture of the custom side pipe heat shields installed on the finished side pipes.

3.4 Phase I Liquid Tank Installation

An 18.9 L (5-gallon) DOT approved gasoline tank was installed in front of the rear axle on the driver's side of the vehicle as a replacement for the production gasoline tank. An in-line fuel pump and regulator were installed. This location was chosen to simplify fuel routing to the gasoline fuel port as well as tapping into the previous fuel lines that route to the engine for delivery. In addition, the location was chosen to keep the truck bed clear of any components. However, this alternate gasoline system can be configured to have the 18.9 L (5-gallon) tank placed in the truck bed during testing to make delta mass measurements easier. Otherwise, the tank would have to be disconnected and lowered every time mass measurements are necessary. To accommodate this configuration, a fuel distribution system, with two sets of fuel lines and four ball valves, was developed that permitted the capability to have the tank in either location. One pair of fuel lines would

stay underneath the vehicle and the other pair of lines was routed to the bed of the truck for easy installation. In Figure 3.9, it can be seen that the distribution system has valves 1 and 2 open and valves 3 and 4 closed to allow gasoline flow from the tank in its current position. If the tank was in the truck bed, valves 1 and 2 would be closed and valves 3 and 4 would be opened. This system allows both configurations to have the same X-Y coordinates and only a change in Z coordinates to reduce the affect it as on the vehicle's COG. The fuel pump and regulator are also attached on top of the aluminum plate to keep both components rigid and safe from any road debris as seen in Figure 3.9.

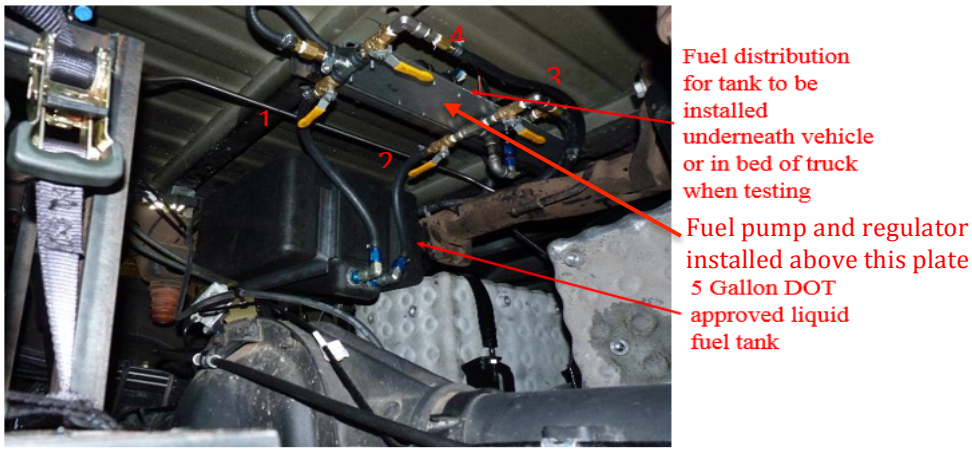

Figure 3.9: A picture of the 18.9 L (5-gallon) fuel cell and fuel distribution system.

3.5 Phase I Matrix Tank Installation

Once the exhaust and original gasoline tank were removed, there was enough space to start installing the four side matrix tanks. Original Equipment Manufacturer (OEM) tank brackets from General Motor's 1973-1987 full sized trucks and additional hardware were modified and utilized to fix tanks 1, 2, 6, and 7 to the inside of the truck frame. For modifications done by Tucker Alsup, the brackets were cut at the lower seams and re-welded to be shorter to not hit the drive shaft. The brackets can be seen in Figure 3.11 below.

By using the plumbing diagram presented in Figure 3.10, the tanks were plumbed using 0.9525 cm (3/8") SS tubing. To reduce the difficulty of creating new natural gas lines routed to the engine for the Phase 1 tanks, the Phase 1 plumbing feeds into the

existing IMPCO plumbing for the quantum tank right before the lines reach the natural gas filter. During the quantum phase, the filter was in the bed of the truck. The filter was relocated under the body the truck close to the gasoline and CNG fuel port to simplify the natural gas plumbing.

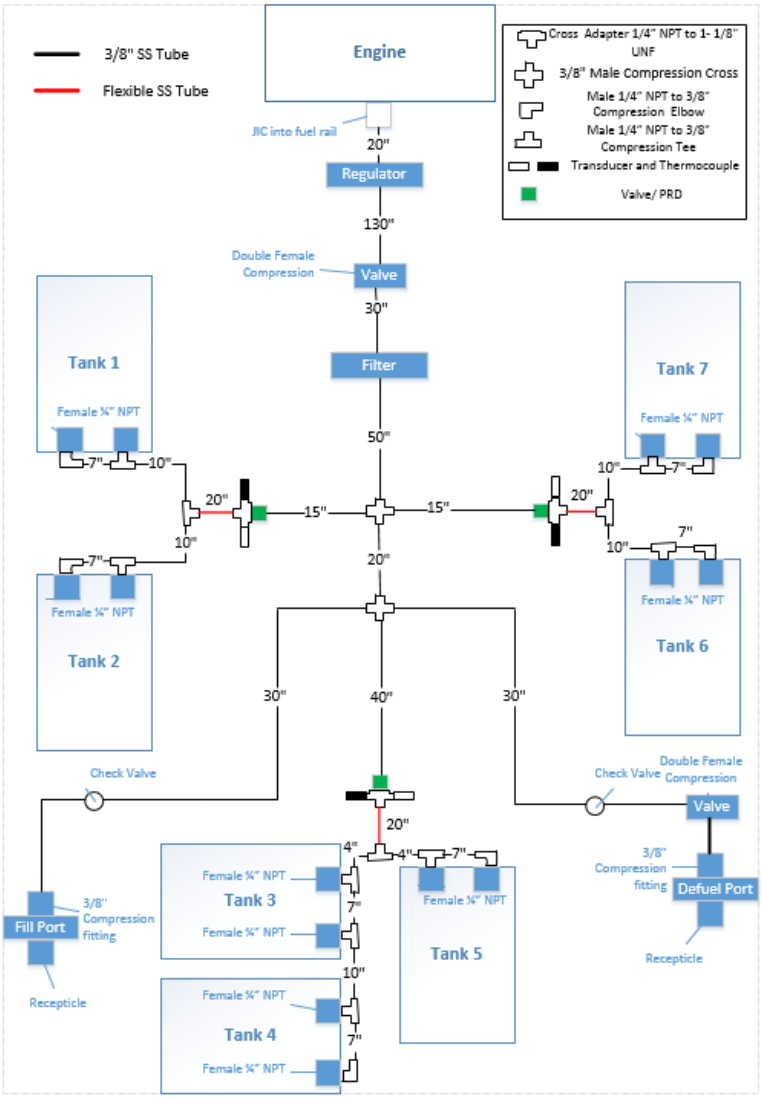

Figure 3.10: Phase 1 Plumbing Diagram underneath the truck.

A fixture was created and bolted to a chassis cross member to attach the adapters for the pressure relief devices (PRD) valves for each pair of tanks. These PRDs were ordered from Optimum. The purpose of the PRD valves is to ensure that the natural gas inside the tanks do not exceed a predetermined temperature and pressure and potentially burst. If so,

the PRD will activate and release the contents of the tank to reduce the temperature and pressure. This can be viewed in Figure 3.12. The aluminum adapters were developed to create a central location where the CNG flow from the pairs of tanks can be controlled using the valve as well as a location to evaluate the temperature and pressure of the pair using a K-type thermocouple and 350 bar transducer respectively. From the adapters, the CNG flow from the pairs is routed to a main line running to the back of the truck that also connects to the 3 rear matrix tanks and to the existing natural gas line that routes to the engine. The Solidworks design of the adapter can be seen in Figure 3.13. The plumbing between the pairs of tanks as well as the routing from the valves to the main line can be viewed in Figures 3.11 & 3.12.

a) b)

Figure 3.11: a) A picture of the side Phase 1 tanks installed. b) A picture of the PRD and adapter locations for the side tanks.

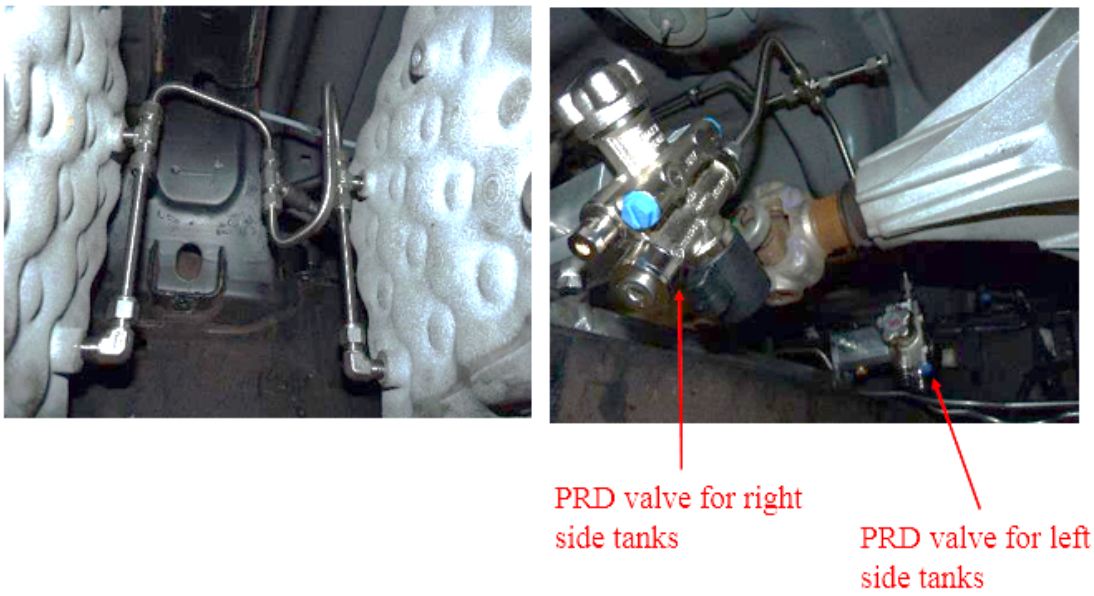

Figure 3.12: a) The plumbing installed between the side tanks. b) A close up picture of the PRD valves dedicated to each pair of side tanks.

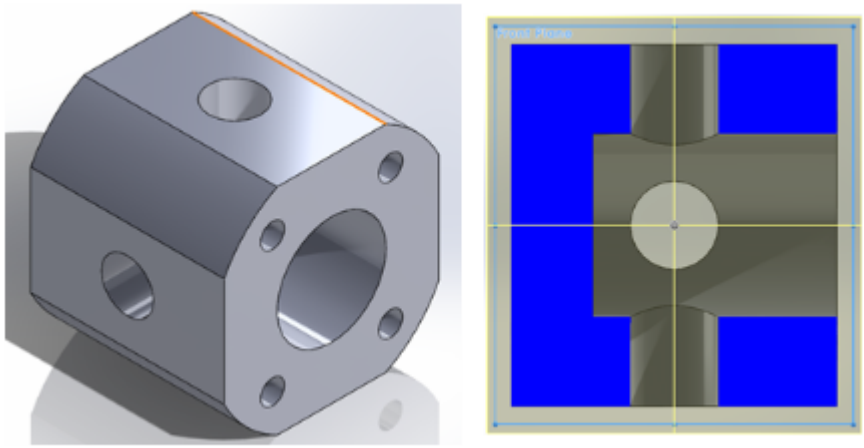

Figure 3.13: A model of the design of the adapters used to incorporate the PRD valve, pressure transducer and thermocouple.

Chapter 4 Experimental Setup

4.1 Test Procedure Development

The main purpose of the project is to move the location and change the number of CNG tanks on the vehicle, so these changes would affect the static and dynamic performance of the vehicle. Static performance relates to vehicle parameters that can be measured when the vehicle is stationary such as the vehicle weight, vehicle center of gravity, approach, break-over, and departure angles, and ground clearance. A majority of these tests can be measured using devices such as scales and tape measures. Dynamic performance relates to vehicle parameters that are measured when the vehicle is in motion such as the acceleration, fuel economy, drag and air resistance, understeer/oversteer, and suspension performance.

4.2 Test Instrumentation

At the beginning stages of the project, the parameters to be measured were defined in conjunction with a variety of vehicle performance tests. When relating to vehicle performance, the parameters that would be measured needed to cover every aspect of the vehicle that would be affected by the installation of the natural gas system. This would include observing the operation of the CNG system starting from the storage in the tank(s) to observing the natural gas flow being fed into the engine. Parameters such as the pressure and temperature inside of the natural gas tank(s), the strain of the tanks during filling and discharge, the pressure and temperature before and after the natural gas regulator, and the flow rate of the CNG entering the engine. To measure these parameters, one would need to use devices such as pressure transducers, thermocouples, and strain gages.

Each of these vehicle parameters requires its specific factors that need to be measured by different devices. All of the vehicle parameters require information from vehicle computer through the CAN BUS port such as vehicle speed, time, and steering wheel position. To record the vehicle acceleration, one measures the vehicle speed as well as the corresponding time stamp. The device required to measure these parameters would be a connection to the vehicle's CAN BUS. To record the fuel economy, one measures the

fuel consumption of the gasoline and CNG as well as the corresponding speed. The devices required to measure this parameter would be a flow meter or an alternative method of measuring fuel consumption such as changes in tank weight and a CANBUS connection to the vehicle's timing. To determine the drag and air resistance, one measures the vehicle speed as well as the corresponding time lapse. The device required to measure these parameters would be a CANBUS connection to the vehicle's speed and timing. To measure the understeer/oversteer, one measures the change in steering wheel position, vehicle speed, and the corresponding time lapse. The device required to measure these parameters would be a CANBUS connection to the vehicle's steering wheel position, speed, and timing. To measure the suspension performance, one measures the vehicle acceleration in the X, Y, and Z coordinate directions and corresponding time lapse as well as the displacement of the vehicle suspension. The devices required to measure these parameters would be a 3-way directional accelerometer, a CAN BUS connection to the vehicle's timing, and a ruler and Go-Pro camera to measure suspension displacement. All of the tests, static and dynamic, will be covered in more detail in Chapter 5.

4.2.1 DAQ System and LabVIEW

After the measured parameters and required devices were decided, there still needed to be a way to log all of the data in real time during the testing. This is where a data acquisition (DAQ) system and a LabVIEW program are utilized. A DAQ system consists of multiple modules that can connect to the previously mentioned devices including the pressure transducers, thermocouples, strain gages, accelerometers, and vehicle CAN BUS to process the data collected by the devices. Each device requires its own specific module that would then connect to a global cDAQ chassis that transfers all the data to a LabVIEW program on a laptop. The LabVIEW program provides the researcher(s) with real-time data of any data that the testers chooses as well as offers the researcher(s) the capability of saving the data being measured by all or selected devices.

The modules were determined for each device first before deciding which cDAQ chassis to order because the size of the chassis depends on how many modules are

required. To compare and select different modules, the number of channels, resolution, range, sample rate, and price were evaluated to narrow down the options. The company that was used was National Instruments. A list of the options that were decided for each of the main devices to cover all of the data logging that was needed can be viewed in Appendix D. For the pressure/fuel flow, temperature, strain, and accelerometer modules, the module with the most channels was chosen to reduce the number of chassis slots needed in addition to providing freedom to install extra devices in the future if needed. The CAN module was selected based on the cheapest price and the higher available range to allow for as much logging freedom as possible. The modules and chassis selected as well as the distribution to the modules are listed in Table 4.1. Due to the number of inputs required, two temperature modules, two strain modules, one pressure/flow rate module, two accelerometer modules, and two CAN module were ordered. One 8-slot and one 4-slot chassis were ordered to accommodate the 9 modules. In Appendix D, a spreadsheet of the terminal connections for the devices is given to demonstrate how the device wires were connected to the modules. A summary of all of the channels can be viewed in Table

Table 4.1: A list of the cDAQ chassis and the modules that are connected as well as the measurement that each module is dedicated to and its slot location in the cDAQ chassis.

Chassis Part #	Module Part #	Measurement Dedication	Module Chassis Slot Location
NI-cDAQ-9172 (8-slot)	NI 9213	Thermocouples	1
	NI 9205	Pressure/ Flow Rate	2
	NI 9219	Strain Gages	3
	NI 9219	Strain Gages	4
	NI 9234	Accelerometers	5
	NI 9234	Accelerometers	6
	NI 9213	Thermocouples	7
NI-cDAQ-9174 (4-slot)	NI 9862	CAN	1
	NI 9862	CAN	2

Table 4.2: A list of parameters that are logged during testing.

Parameter List Summary

Temperature	External & Internal (each tank)
	Discharge & Fill Line (each tank)
	Engine Inlet
	Exhaust Pipe & Floor Pan (multiple locations)
	Ambient
Pressure	Internal (each tank)
	Discharge & Fill Line (each tank)
	Each Regulation Stage & Fuel Rail
Flow	Liquid Fuel
	Gaseous Fuel
Strain	External Wall (each tank, each side)
	Mounting (each tank, each bracket)
Accel	Tank X,Y,Z (each tank)
	Seat Track
CAN Bus	Vehicle Speed
	Engine Speed
	Accelerator Pedal Position
	Throttle Position
	Intake Manifold Pressure
Other	Steering Wheel Position
	CNG Solenoid Valve PWM
	Mass @ Each Wheel (static only)
	Suspension Displacement

The requirements of DAQ chassis location were that it needed to be in a central location of the vehicle to make wiring simpler, it needed to be hidden from a normal passenger, and it needed to be easy to access by a researcher. With these requirements in mind, it was decided to install both chassis under the rear passenger seat. In this location, wires could be easily routed to the front of the vehicle under the cabin carpet, routed under the vehicle and the back through a conduit in the cabin back wall, the chassis are

non-visible by a normal passenger, and the tester is easily able to access the chassis by simply lifting up the rear passenger seat. Figures 4.1-4.5 give a visual of the chassis placements and the conduit to route the wires to their respective locations.

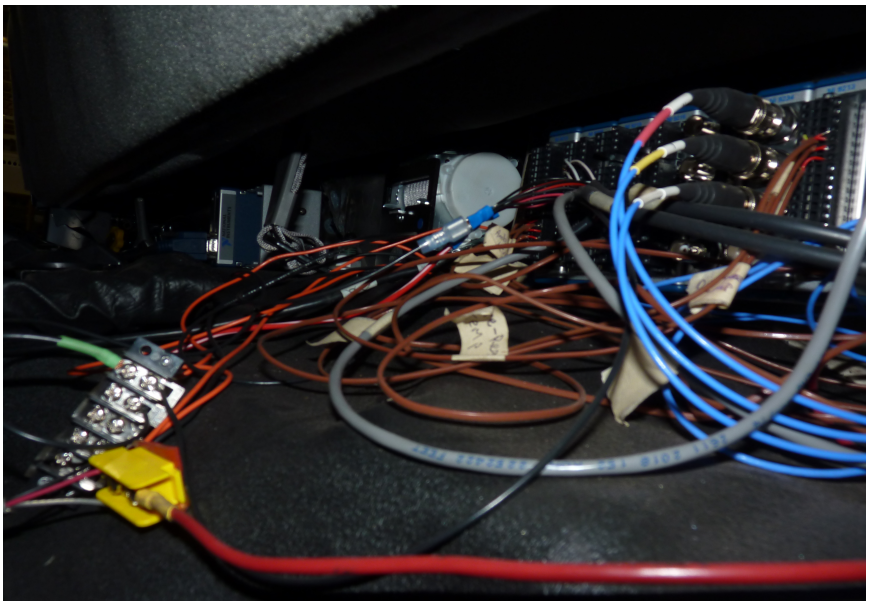

Figure 4.1: A picture of the two cDAQ chassis installed underneath the rear seat. The power strip can also be seen in the bottom left corner.

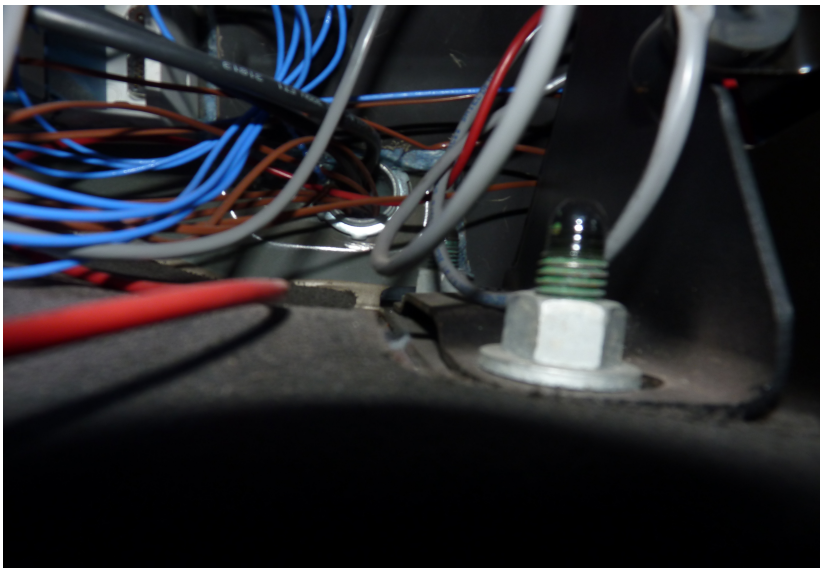

Figure 4.2: A picture of the conduit hole located to the right of the 8-slot cDAQ chassis. This hole leads to underneath the vehicle to route the devices to the designated areas.

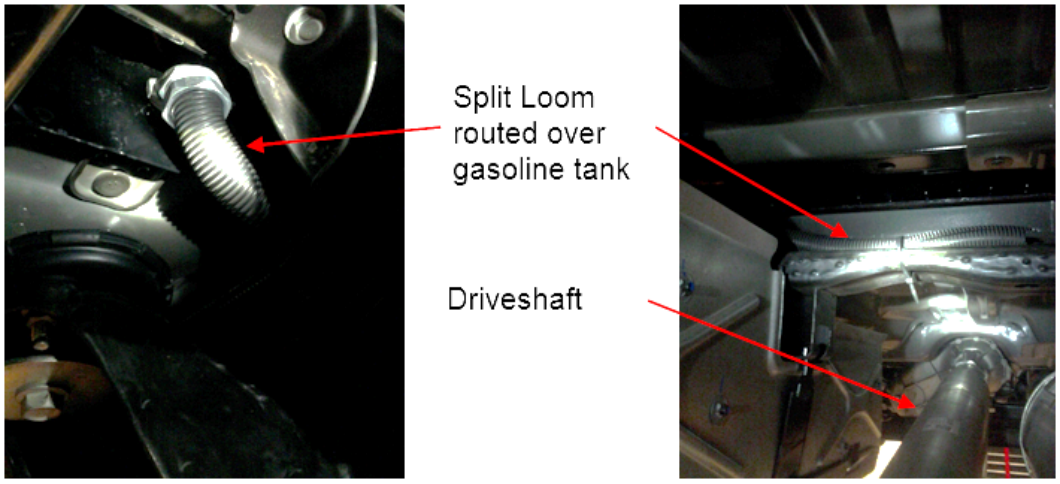

a) b)

Figure 4.3: a) The location of the conduit hole underneath the vehicle and the split loom installed to assist with routing and protecting the wires. b) The routing of the split loom over the drive shaft to disperse the wires at a central location.

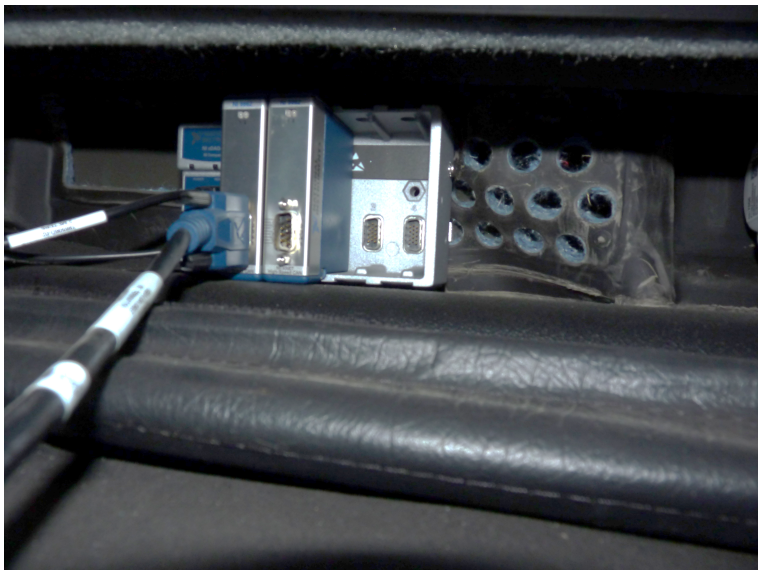

Figure 4.4: A close up picture of the 4-slot cDAQ chassis dedicated to the CANBUS data.

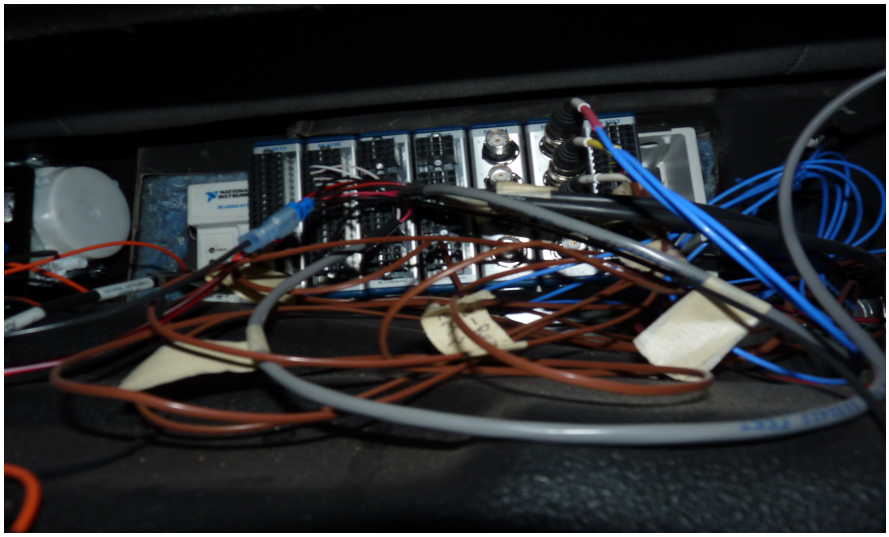

Figure 4.5: A close up picture of the 8-slot cDAQ chassis dedicated to rest of the parameter data such as temperature, pressure, acceleration and strain.

The LabVIEW Virtual Instrument (VI) code and display to log the data was developed by Tucker Alsup on the integration team. When developing the VI, he developed the different screens optimized for each of the dynamic tests that would be performed. For example, one would be able to view parameters such as vehicle speed, tachometer, gasoline fuel gage, CNG fuel gage, and the manifold absolute pressure (MAP). The VI can be seen below in Figure 4.6. The LabVIEW code can be viewed in Appendix C.

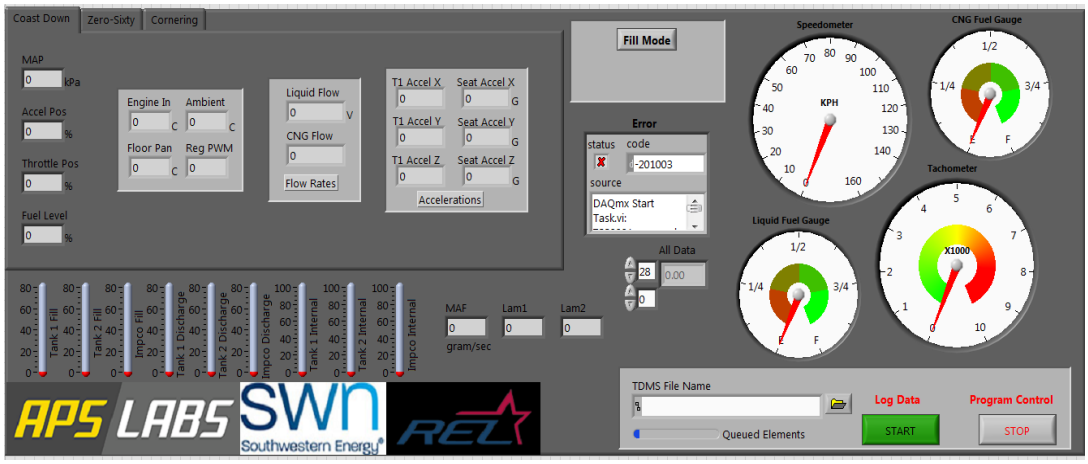

Figure 4.6: A snapshot of the Virtual Instrument used to record data during testing developed by Tucker Alsup.

4.2.2 Pressure Transducers

Omega pressure transducers were utilized to measure the CNG pressure throughout the CNG system. This knowledge is used to have a better understanding of how the system works, to quickly detect leaks in the system, and give the researcher a reference of how much CNG is left in the system at any given time. The criteria of the pressure transducers were that they needed to withstand the CNG system pressure, output 0-10V, be weatherproof and dustproof, and have a sealed cable. The CNG tanks when full are pressurized to 24,821 kPa (3600 psi), so transducers were chosen to be able to withstand this pressure with a factor of safety in the case that the system is pressurized above the normal limit. After the regulator, the pressure is greatly reduced to a maximum of 950 kPa (~138 psi). In this case, a transducer with a small range was selected to achieve the best resolution. The transducers depending on their location would be exposed to the environment, so it was necessary to ensure that the weather did not affect the readings in any way. The transducers ordered had a ¼ BSPP thread instead of an NPT thread, so ¼ BSPP female to ¼ NPT male stainless steel adapters and FKM seals were ordered to simplify the installation process. The respective part numbers for the adapters and seals from Omega are MTA4-1/4-1/4-SS and PXMW-4. The specific locations, type, and part numbers of the transducers installed are shown below in Table 4.2. Figures 4.7 & 4.8 also display visuals of the transducers after they were installed.

Table 4.3: A list of the pressure transducer locations, types, and part numbers used during testing.

Pressure Transducer Location	Transducer Type	Transducer Part #
Quantum Tank Internal Pressure	350 Bar (5076 psi)	PXM309-350G10V
Regulator Input Pressure	350 Bar (5076 psi)	PXM309-350G10V
Regulator Output Pressure	10 Bar (145 psi)	PXM309-10G10V
Left Side Matrix Tanks Pair Pressure	350 Bar (5076 psi)	PXM309-350G10V
Right Side Matrix Tank Pair Pressure	350 Bar (5076 psi)	PXM309-350G10V
Fill Pressure	350 Bar (5076 psi)	PXM309-350G10V

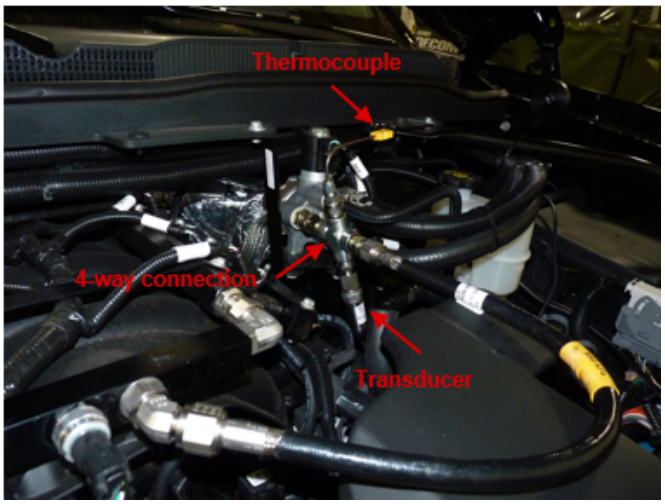

Figure 4.7: A picture of the thermocouples and pressure transducers installed after the regulator.

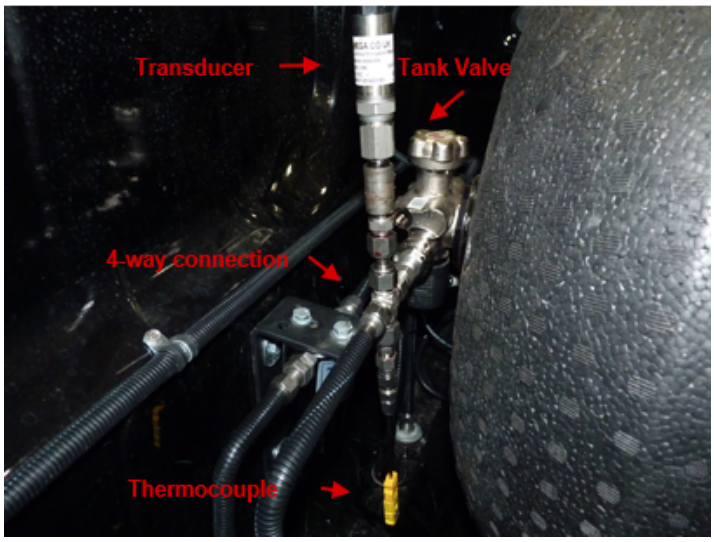

Figure 4.8: A picture of the thermocouple and pressure transducer installed to record internal tank pressure and temperature.

4.2.3 Thermocouples

Temprel thermocouples were used to measure a variety of temperatures around the vehicle, mostly pertaining to the CNG system. The temperature of the gas is important to know because it can cause the gas to expand in warmer environments and condense in colder environments. With the matrix tanks being cast out of aluminum, temperature changes from the environment could potentially affect the gas temperature inside the tanks since metals are conductors of heat. In addition to the CNG system, it was deemed necessary to also measure the ambient temperature and vehicle floor temperature. The purpose of the vehicle floor temperature measurement was to monitor how much heat would radiate from side pipes that are installed on the vehicle during Phase 1 and 2. The thermocouple is installed underneath the left rear passenger side door because of the easier wire routing from inside the cab.

Due to the wide range of temperatures that needed to be measured with a fast response rate, K-type thermocouples were ordered in different sizes and lengths based on its specific purpose. K-type thermocouples are known to have good flexibility, and temperature ranges from -67 up to 315 C [11]. These qualities make them the best choice for the project's application. Additional criteria for the thermocouples were that the connector needed to be a molded on mini plug for a simpler connection, the junction type

needed to be grounded, and the sheath material type needed to be 304 stainless steel to withstand any corrosion. Thermocouples that needed to be inserted in tanks were sheathed probes to help protect the thermocouple tips from any damage as well as provided simpler installation using thermocouple specific NPT compression fittings. For thermocouples that would be installed on the outside of tanks, a spool of solid Teflon thermocouple wire was ordered to also simplify the installation process. The thermocouple locations are listed in Table 4.3 and Figures 4.9-4.12 display the locations of the thermocouples that were installed. In all cases, wherever a pressure transducer was installed, a thermocouple was installed in the same location with an NPT cross compression fitting ensure the pressure and temperature correlate to the same place.

Table 4.4: A list of the thermocouple locations, size, length, and part numbers used during testing.

Thermocouple Location	Thermocouple Size	Thermocouple Length	Thermocouple Part #
Quantum Internal Tank Temperature	1/8” (0.3175 cm)	6” (15.24 cm)	T21-MG6KCS
Quantum External Tank Temperature	1/8” (0.3175 cm)	6” (15.24 cm)	T21-MG6KCS
Regulator Input Temperature	1/8” (0.3175 cm)	6” (15.24 cm)	T21-MG6KCS
Regulator Output Temperature	1/8” (0.3175 cm)	6” (15.24 cm)	T21-MG6KCS
Left Side Matrix Tanks Pair Temperature	1/8” (0.3175 cm)	6” (15.24 cm)	T21-MG6KCS
Right Side Matrix Tank Pair Temperature	1/8” (0.3175 cm)	6” (15.24 cm)	T21-MG6KCS
Fill Temperature	1/8” (0.3175 cm)	6” (15.24 cm)	T21-MG6KCS
Ambient Temperature	1/8” (0.3175 cm)	6” (15.24 cm)	T21-MG6KCS
Floor Pan Temperature	1/8” (0.3175 cm)	6” (15.24 cm)	T21-MG6KCS

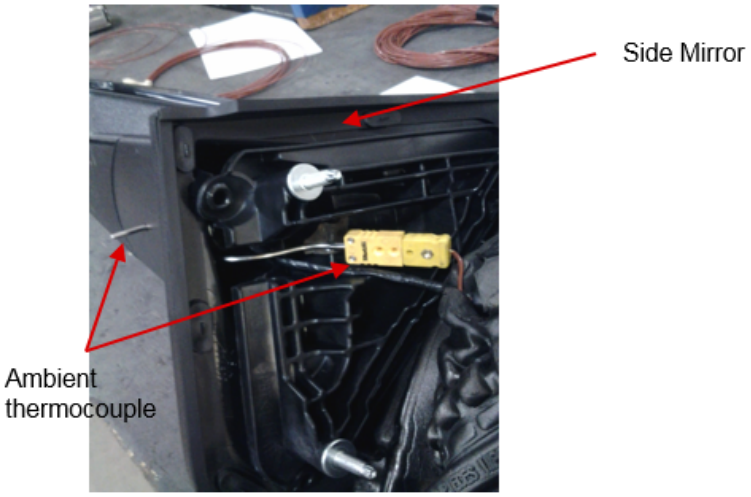

Figure 4.9: A picture of the ambient thermocouple being installed in the driver side mirror.

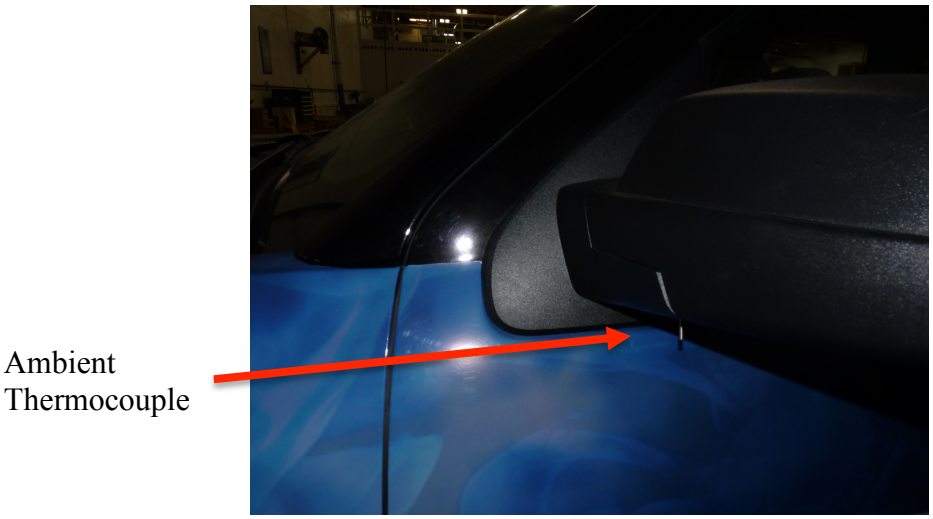

Figure 4.10: A picture of the ambient thermocouple after it was installed.

Figure 4.11: A picture of the floor temperature thermocouple installed underneath the left rear side door.

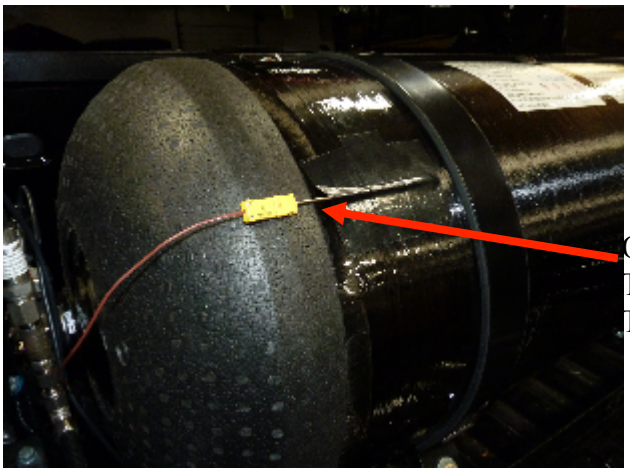

Figure 4.12: A picture of a thermocouple installed on the outside of the quantum tank to measure its external temperature.

4.2.4 Accelerometers

As described above, accelerometers were applied to measure the amount of acceleration that the vehicle and tanks experienced during the different performance tests. This measurement is necessary because it gives the researcher an indication of how the tank location and weight affects basic vehicle operation. Furthermore, when the accelerometer is applied to the matrix tanks, the experimental data can be compared with

the simulation data developed by the Finite Element Analysis (FEA) team to help validate the matrix tank brackets. It is crucial that the tank brackets do not fail at any point. The safety of the passengers and others are always top priority, so every precautionary measure is taken to complete the task.

Two accelerometers were ordered from PCB Piezotronics. One accelerometer is dedicated to the vehicle acceleration by installing it to the driver's seat track and the other is dedicated to the matrix tank acceleration. The criteria for the accelerometers were that they needed to have the capability to measure in X, Y, and Z directions (triaxial), high sensitivity, a maximum acceleration of 10 Gs, minimal signal noise, and a low frequency range. The triaxial feature is necessary to capture every aspect of acceleration that the vehicle and tank may experience during the tests because the acceleration will never just be in one direction. High sensitivity, minimal signal noise, and low frequency range assist with making the recorded data easier to understand and analyze during post processing. In general, a vehicle can experience up to about 1 G of lateral acceleration during a cornering test, so it was decided to incorporate a factor of safety to ensure that all of the data could be measured as well as guarantee that overshooting its range would not damage the accelerometer. After these requirements were given to a PCB representative, a ceramic shear ICP accelerometer with triaxial capability, high sensitivity, 100 mV/g resolution, 2 to 5k Hz frequency range, titanium housing, and 4-pin connector was recommended and ordered along with a 10-ft (3.05 m), 4-conductor, low noise, shielded FEP cable with a 4-socket plug to (3) BNC plugs that could easily connect to the accelerometer dedicated module on the DAQ chassis. Table 4.4 lists the installed accelerometer locations and part numbers and Figure 4.13 displays the installed locations. The tank accelerometer has not yet been installed.

Table 4.5: A list of the current and future accelerometer locations and part numbers.

Accelerometer Location	Accelerometer Part #	Cable Part #
Driver Seat Track	356A15	034G10
One of the 4 Matrix Tanks	356A15	034G10

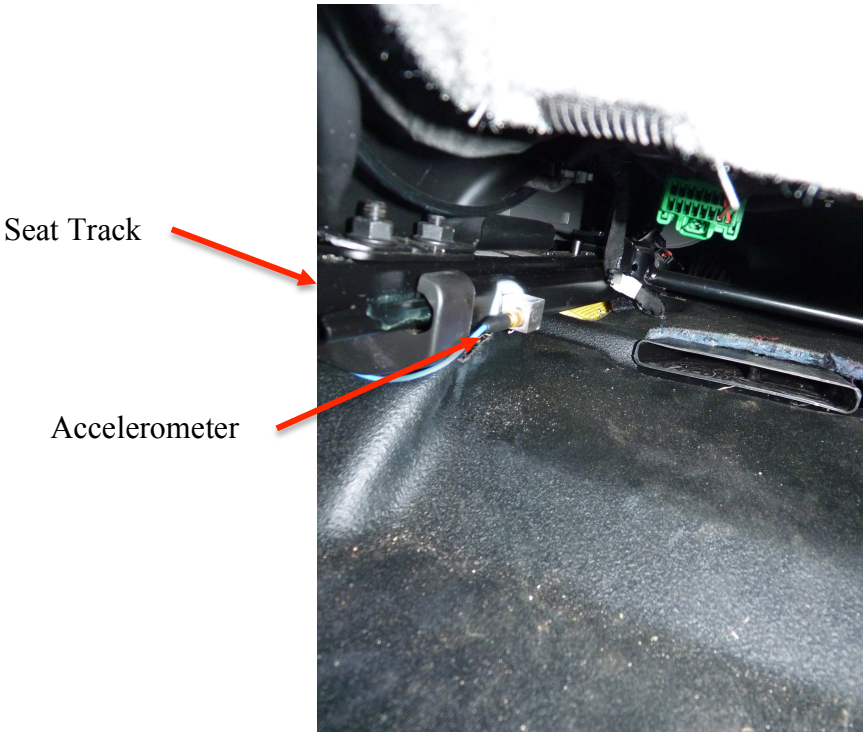

Figure 4.13: A picture of the accelerometer installed on the driver side seat track.

4.2.5 Strain Gages

The main purpose of the strain gages is to measure the strain of the tanks during filling and discharge and to measure the strain of the tank brackets during testing. As the tanks are being filled with natural gas, they will have a tendency to expand depending on the fullness of the tanks. This expansion will change based on the outside environment temperature and rate or filling, so the strain gages would serve as an indicator as to how much and how rapidly the tanks are expanding. Similar to the acceleration data, the strain information provided on the tank brackets can give the vehicle integration team and FEA team an indication of how well the brackets are designed and if there needs to be any additional reinforcement.

To minimize the number of manufactures used in this project as well as to ensure compatibility, the strain gages were ordered from Omega. The criteria required for the gages are that they need needed to have full bridge load cells, 2-wire ribbon leads, temperature compensation, an excitation voltage of 12 volts, and a large surface area. A full bridge is known to be the most accurate way to measure strain because it measures in

two directions and also incorporates temperature compensation [12]. The 2-wire ribbon leads and 13 volts are required due to the strain gage connection method to its dedicated module on the DAQ chassis and the voltage that can be supplied to the modules is restricted to the vehicle's 12 volt system. The larger surface area is essential to get the best strain average as the tank deforms. The model that best fit the requirements from Omega has a nominal resistance of 350 ohms, grid size of 2.5mm by 2.9mm, a Vrms of 13 volts, and ribbon leads. The strain gages have not been installed yet because the Phase 1 tanks have not been certified to be filled with CNG. The ordered strain gages are a one-time use, so the strain gages will be installed once the certified tanks are received. The preferred locations and part numbers are listed in Table 4.5 and the potential placements on the short side and long side of the matrix tanks can be referenced in Figure 4.14.

Table 4.6: A list of the future strain gage locations and part numbers.

Strain Gage Location	Strain Gage Part #
Matrix Tank Short Side	SGT-3G/350-FB13
Matrix Tank Longer Side	SGT-3G/350-FB13
Matrix Tank Bracket	SGT-3G/350-FB13

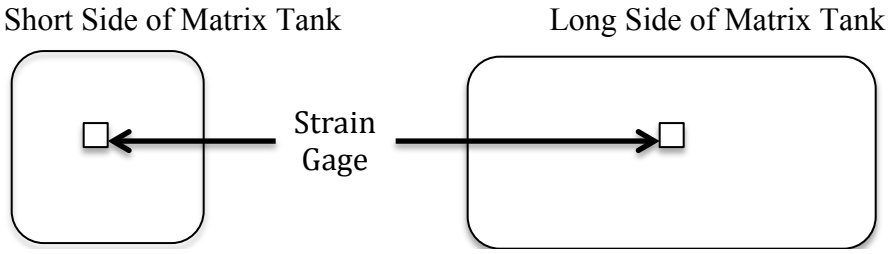

Figure 4.14: A diagram of the potential strain gage locations on the Phase 1 tanks.

4.2.6 Go-Pro Camera

A GoPro camera was attached to the frame underneath the vehicle to capture the compression of the rear passenger side suspension. This camera is only used during the pothole and speedbump tests to capture the suspension response. The suspension scale and the installed GoPro camera can be seen in Figure 4.15.

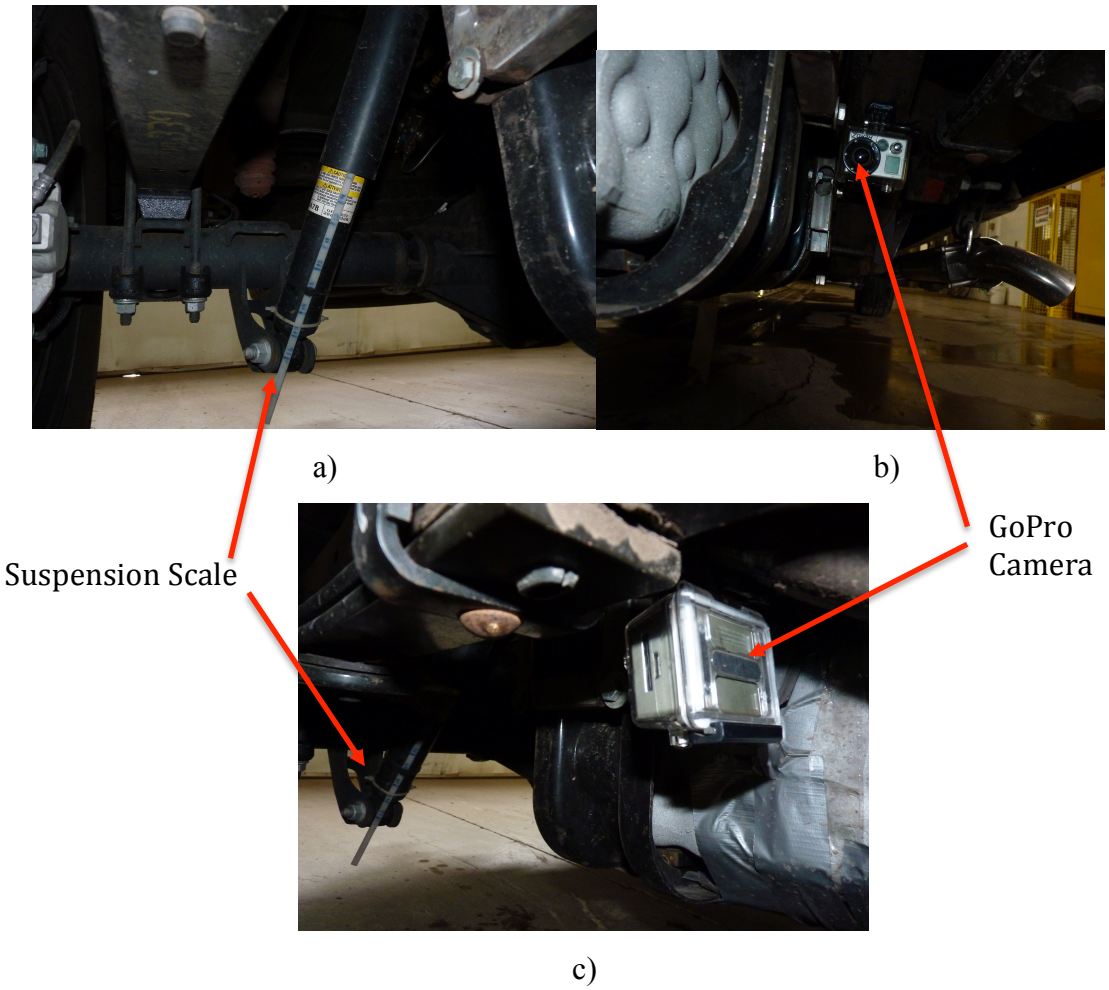

Figure 4.15: Pictures of the suspension scale and the GoPro camera installed.

Chapter 5 Testing

As described previously, static tests consist of tests that are completed when the vehicle is not in motion. These tests include weight, center of gravity, ground clearance, and approach, break-over, and departure angles. All of these tests are completed inside of the APSRC building. Dynamic tests consist of tests that are completed when the vehicle is in motion. These tests include ride quality performance, acceleration, fuel economy, drag and air resistance, and understeer/oversteer. A table of all the tests and their objectives can be viewed in Table 5.1.The static and dynamic tests are described in more detail in the following sections.

Table 5.1: A progress oriented table of the tests and objectives for the project.

	Test	Objective	Baseline	Quantum	Phase 1	Phase 2
Static Tests	4-corner weight; flat and inclined	Total Mass, Mass Distribution, & CG	Complete	Complete	Complete	Not Started, No Issues
	Wheelbase & heights	Ride Height, Min Ground Clerance, breakover angle, approach / departure angle	Complete	Complete	Complete	Not Started, No Issues
Dynamic Tests	Pothole	Validate Models w/ Tank and Bracket Strains. Assess impact to ride quality	Complete	Complete	Complete	Not Started, No Issues
	Speed Bump	Validate Models w/ Tank and Bracket Strains. Assess impact to ride quality	Complete	Complete	Complete	Not Started, No Issues
	Cornering & Understeer / Oversteer	Validate Models w/ Tank and Bracket Strains. Assess impact of mass & CG shift.	Complete	Complete	Complete	Not Started, No Issues
	Coastdown	Assess impact on Drag and Rolling Resistance	Complete	Complete	Complete	Not Started, No Issues
	Acceleration	Validate Models w/ Tank and Bracket Strains. Assess impact of mass & CG shift.	Complete	Complete	Complete	Not Started, No Issues

5.1 Weight and Center of Gravity

Measuring the weight and calculating the center of gravity of the truck during each phase indicates how the center of gravity changes with tank configuration. This test is important because center of gravity impacts the on road and off road stability as well as high speed stability with the effect of rolling over. These two factors have an effect on the other static and dynamic tests, so the data assists with understanding patterns in other test data. To measure the weight, 4 scales were used to determine the weight at each wheel as well as the total weight. A hydraulic car lift was used to lift the truck and place it on the scales that are placed underneath the middle of each tire to achieve the best accuracy. Each scale is rated to measure up to 1588 kg (3,500 lbs.) to also ensure that the readings were accurate.

A similar setup was used to obtain center of gravity measurements. In addition to the scales, one side was raised by 0.27 m to create an angle between the left and right side. The altered wheel weights, ramp height, wheelbase, track width, and tire radius were then used to determine the center of gravity of the truck in X, Y, and Z coordinates using Equations 5.1-5.4. Figures 5.1-5.3 display the center of gravity testing in progress during the Baseline Phase as well as the reference for Center of Gravity measurements. The center of gravity calculator in excel can be referenced in Appendix D.

Equation 5.1

$$Distance\ from\ Front\ Axle\ (X) = \frac{Wheelbase * Rear\ Axle\ Weight}{Total\ Weight}$$

Equation 5.2

$$Distance\ from\ Center\ (Y) = \frac{Left\ Side\ Weight}{Total\ Weight} * Track\ Width - \frac{Track\ Width}{2}$$

Equation 5.3

$$Height\ from\ Axle\ (Z) = \frac{Distance\ from\ Rear\ Axle - Wheelbase * Front\ Axle\ Weight(Inclined)}{Total\ Weight} * \frac{1}{\tan\left(arcsin\left(\frac{Incline\ Height}{Wheelbase}\right)\right)} + \frac{Tire\ Radius}{2}$$

Equation 5.4

$$Distance\ from\ Rear\ Axle = \frac{Wheelbase * Front\ Axle\ Weight}{Total\ Weight}$$

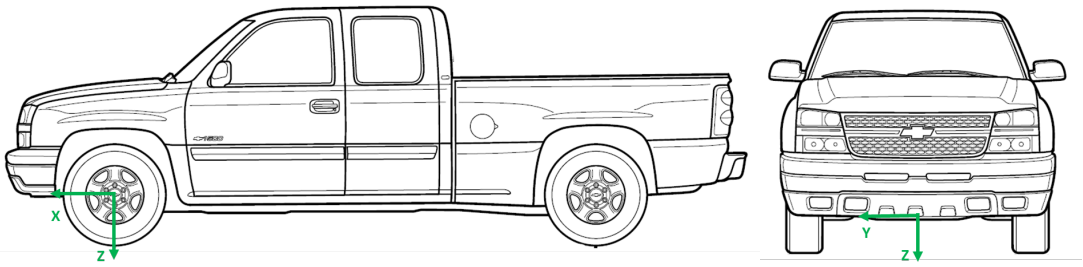

Figure 5.1: A diagram of the X, Y & Z orientation in relation to the vehicle based on SAE J670 standard coordinates[13]. The permission to use this figure is in Appendix E.

Figure 5.2: A picture of the truck during center of gravity testing.

5.2 Ground Clearance

The ground clearance of the truck during the different phases will help us determine how the weight of the different natural gas tanks effects the ride height to optimize the tank locations underneath the truck. This test is important because the vehicle will need to drive over objects, such a speedbumps, so the ground clearance needs to be high enough to refrain hitting common objects on road and off road. The tanks will be place above the bottom of the truck frame. As more weight is added to the truck, the ground clearance will decrease as the truck suspensions compress. For each phase, the distance from the ground to the bottom of the truck frame underneath both back passenger doors is measured using a tape measure to ensure one side is not lower than the other.

5.3 Approach, Departure, & Break-over Angles

The approach, departure, and break-over angles allow the researcher to determine how the weight & weight distribution of the tanks impacts ride height, and usability of

the truck. Changes in sprung mass (or a low hanging tank) will affect these angles. The approach angle can be visualized as the steepest slope/ramp that the truck would be able to climb without damaging the front bumper if the driver were to climb an incline. The departure angle is the same concept of the approach angle, but refers to the limits when leaving an incline/ramp. The break-over angle is the maximum supplementary angle the truck can drive over an object without the tip of the angle touching the object with the wheels still having continuous contact with the ground [14]. An example of these angles can be seen in Figure 5.4.

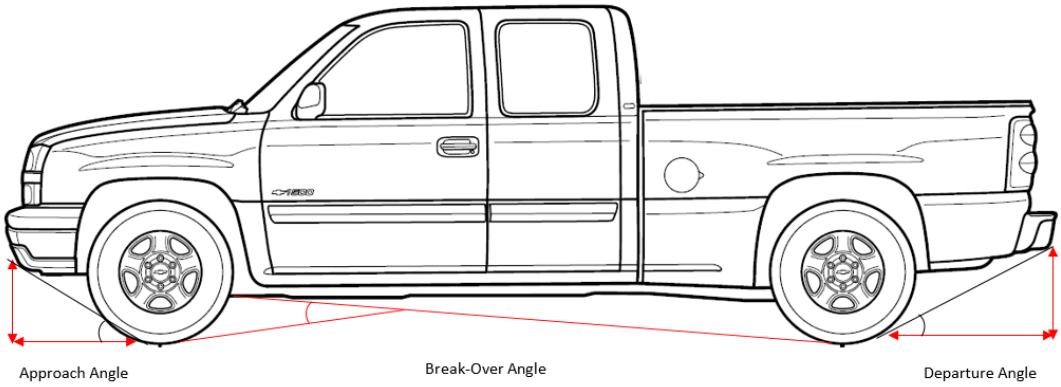

Figure 5.3: A diagram of how the approach, break-over, and departure are measured for a typical vehicle. The permission to use this figure is in Appendix E.

The approach angle was measured using a metal sheet to emulate a ramp. The sheet was placed in front of the left front wheel and was lifted until the sheet touched the bottom of the front bumper. A tape measure was then used to measure the height of the ramp based on the contact point with the front bumper and the distance from the contact point with the air dam to the contact point with the front tire. The departure angle was measured with the same process, but with the left rear tire and rear bumper. Since the truck has a tow hitch, the departure angle was measured with and without a towing hitch in the situation that the tow hitch was ever removed. Alternatively, the break over angle was approximated using Equation 5.5. Equation 5.6 was used to calculate the approach and departure angles.

Figure 5.4: A picture of the actual points where the approach and departure angles were measured.

Equation 5.5

$$Break\ over\ Angle_{approximate} = 2 * \arctan\left(\frac{2 * ground\ clearance}{wheelbase}\right)$$

Equation 5.6

$$Approach(Departure)Angle = \arctan\left(\frac{Height}{Distance}\right)$$

5.4 Pothole and Speed bump

The pothole and speed bump test was implemented to assess ride quality. The test also provides boundary conditions and validation for bracket design as well as quantifies changes in vehicle suspensions. According to the National Association of City Transportation Officials (NACTO), there are specific dimensions for speed bumps, but not for potholes. The height of a standard speed bump ranges from 7.62 - 15.24 cm (3 – 6 in.) and the width ranges from 0.3048 - 0.9144 m (1 - 3 ft.) [15]. Based on this information, two speed bumps were fabricated using a log that was sawn lengthwise to

make two different heights. One speed bump has a height of 6.35 cm (2.5 in.) and length of 0.304 m (1 ft.) and the second has a height of 6 in. (15.24 cm) and length of 0.304 m (1 ft.). After initial tests with both speed bumps, it was noticed that the15.24 cm bump was very rough on the truck suspensions and could potentially damage the vehicle and data logging equipment, so it was decided to only use the 6.35 cm (2.5 in.) bump for the remaining tests. Both speed bumps can be seen in Figure 5.5a. Without a standard to follow for potholes, one was developed using a car rim to simulate a fixed hole in ground. The steel car rim was used instead of digging a hole for two main reasons. One, the dimensions of the pothole would remain consistent and be robust to erosion from repeated use and rain. Two, this method ensures that the test can be easily duplicated. A majority of the tire of an unused wheel was removed using a razor and the rim was buried in the ground to create a pothole that is 11.43 cm (4.5 in.) deep with a radius of 20.32 cm (8 in.). The pothole can be seen in Figure 5.5b.

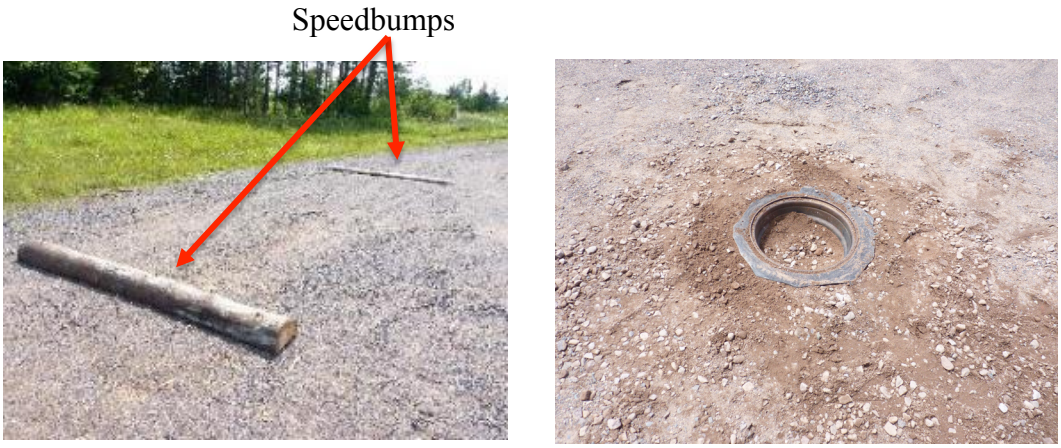

Figure 5.5: a) A picture of the speedbumps installed on the side of the APSRC driveway. b) A picture of the pothole which is located to the right of the speedbumps when facing the entrance of the driveway.

The test procedure for the speed bump test consists of driving the truck over the 6.35cm (2.5 in.) speed bump, while sweeping speeds (8 - 40 kph) in 8-kph increments. As the required speed increased for each run, the start distance from the speed bump was increased to provide ample time for the tester to reach the required speed. A minimum of three trials was completed at each speed to ensure accurate results. The data for the seat

track accelerometer, to capture the X, Y, and Z acceleration experienced, time, and the speed of the truck were recorded using the LabVIEW program as the tester drove over the speed bump. The data logging was started when the vehicle was at rest before each test trial and was terminated after the vehicle was brought back to rest after driving over the speed bump. The GoPro camera videos were separated by speed, so there would be a total of 5 videos for each phase with each video capturing all of the runs for the respective speed. Since the camera, captures the displacement of the shock and not the suspension, the shock displacement had to be converted to suspension displacement. Equation 5.7 below was used to make the conversion.

Equation 5.7

Length of Shock= 52.1 cm (20.5 in.)

Height of Suspension= 45.7 cm (18 in.)

$$Suspension\ Displacement = Shock\ Displacement * \frac{Height\ of\ Suspension}{Lenght\ of\ Shock}$$

The test procedure for the pothole test is very similar to the speed bump test. The only difference is that the researcher would drive over the pothole on the left side of the vehicle since the accelerometer is attached to the driver's seat track. This procedure allows the accelerometer to detect the acceleration fluctuations more accurately. The tests were completed in the parking lot of the APSRC building as shown in Figure 5.6 below.

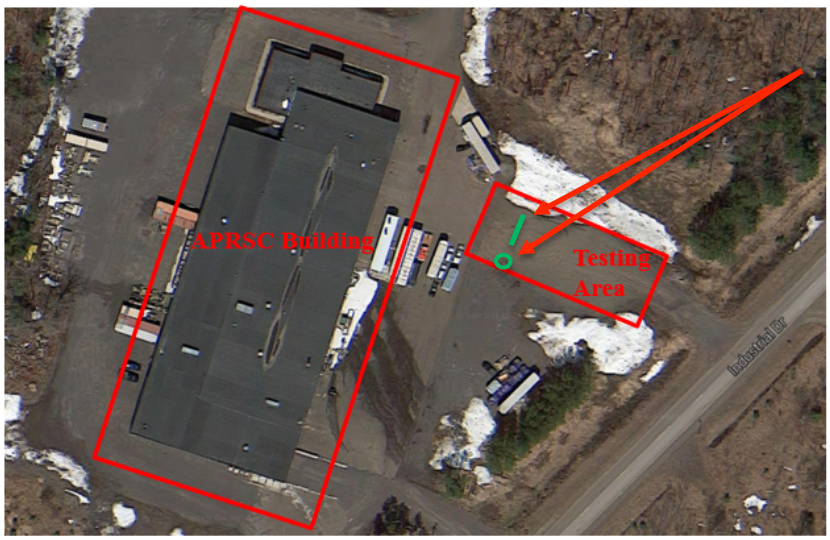

Figure 5.6: Arial view of the pothole and speedbump test location and approximate location of the pothole and speed bump (Image retrieved from Google Maps March 2016 and permission granted in Appendix E).

5.5 Acceleration

The acceleration of the truck is tested to determine how the change in weight and CG affects the acceleration / deceleration and examine force / strain on tanks and brackets during quick accelerations. The tanks need to remain secure during rapid accelerations and decelerations. This test is most commonly known as the zero to sixty test. As the name suggests, the vehicle is started from rest and full load acceleration is applied until the vehicle reaches 96.6-kph (60 mph). However, in order to receive accurate results, the tester must not allow any wheel spin during launch. Wheel spin occurs when the tires do not have traction with the ground, so the wheels will spin in place until the wheels regain traction with the road to begin moving the vehicle.

Using the LabVIEW program developed, the time elapsed and the vehicle's speed is recorded during each test trial. On average, the tester performed a total of 10 runs to gather sufficient data. The program would be started before each test when the vehicle is at rest and terminated after the tester reached the required speed of 96.6-kph (60 mph). After each run, the tester would allow the truck to rest for roughly 5 minutes to refrain from overheating the transmission as this tests requires a great deal of effort from the transmission. The location of the test was on Shortcut Road, which is a 0.48 km (0.3

mile) straight portion of a road near by the APSRC building with latitude/longitude coordinates of 47.167601°/-88.514442°. The road consists of light traffic, so the tester would only test when the road was clear and would wait in a safe location near by the test road if there was any traffic on the road. Figure 5.7 shows where the test site is located in relation to the APSRC building.

Figure 5.7: Arial view of the acceleration test location (Image retrieved from Google Maps March 2016 and permission granted in Appendix E).

5.6 City and Highway Fuel Economy

Fuel economy tests were executed to determine how the placement and weight of the tanks underneath the vehicle and the type of fuel affect the fuel consumption of the truck. The tests were completed using only liquid gasoline to observe any changes in the overall fuel economy of the vehicle. This test is important because the achievable fuel economy of the vehicle will be a major selling factor for most customers in the future.

The vehicle speed and time were recorded using the LabVIEW program for post-processing to calculate the city and highway fuel economy for each phase and fuel choice. The tester would begin the recording log while at rest before starting the test and would terminate the recording at the end of each run after coming to a complete stop. The fuel consumption was also recorded, but was based on the weight changes of the 18.9 L

(5-gallon) gasoline fuel cell. At the beginning of each fuel economy test, the fuel cell was filled with the maximum amount of fuel and weighed using an Ohaus Ranger RD35 scale, with a resolution scale of 0.1g, which was placed in the bed of the truck during testing. The weight after each run was also recorded to find the delta mass of the tank to determine how much gasoline was consumed during each run. Before weighing the tank, the tester verified that the scale was level with a leveler to ensure accurate weight measurements each time. On average, 5 runs were completed for each phase and for each cycle (city and highway) to reassure dependability in the data.

The truck was driven through a predetermined city and highway cycle shown in Figures 5.8 & 5.9. As seen in Figure 5.8, the city cycle started at point A on the map and ended at A to complete one test run with a route distance of 4.18 km. To promote uniformity throughout the test runs, the driver would stop at every stop sign for 5 seconds. The route was strategically chosen to have almost no traffic to minimize test to test variability. As for the highway cycle seen in Figure 5.9, the test began at the red marker on the map and the tester would drive clockwise around the 22.5 km route and end the test run back at the red marker. The tester would follow the speed limit displayed in the routes along with a route with no traffic to also promote uniformity in the tests.

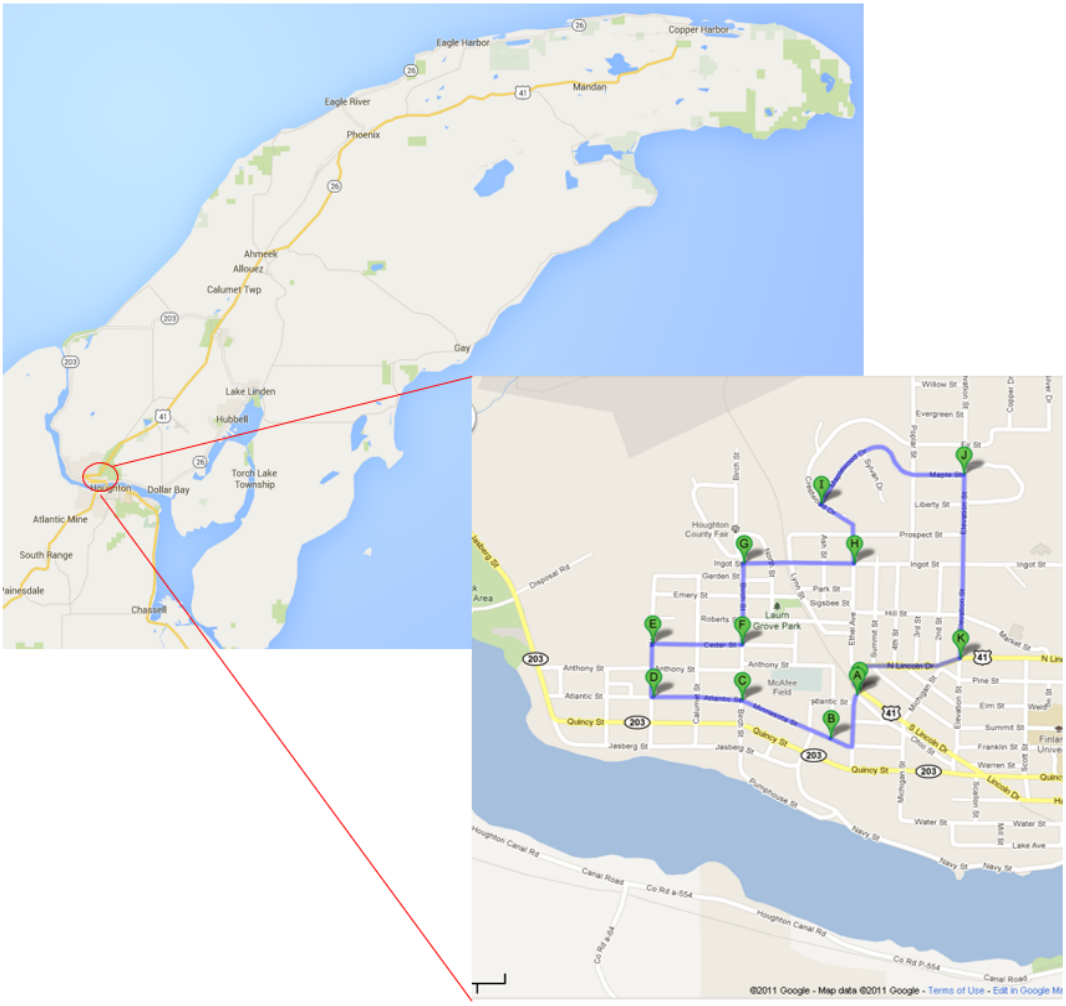

Figure 5.8: Arial view of the city fuel economy cycle test location (Image retrieved from Google Maps March 2016 and permission granted in Appendix E).

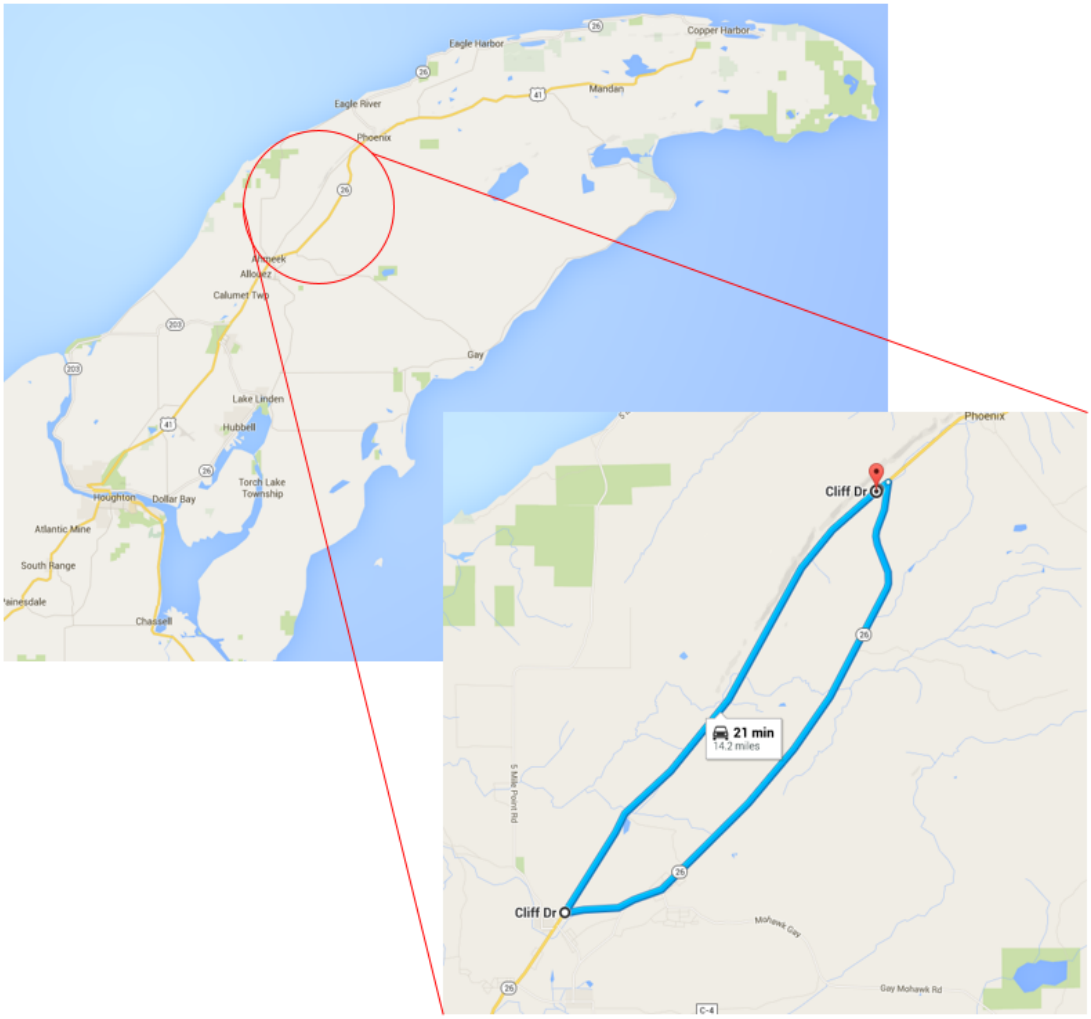

Figure 5.9: Arial view of the highway fuel economy cycle test location (Image retrieved from Google Maps March 2016 and permission granted in Appendix E).

5.7 Coast Down

Coast down tests were performed to determine how the placement of the tanks underneath the vehicle affect the aerodynamics and rolling resistance of the truck. Aerodynamics can be affected by the slightest changes in the shape of the vehicle whether that being the main body of the vehicle or even how components are placed underneath the vehicle. For rolling resistance, it would be more affected by the weight change of the vehicle more than how the shape of the overall vehicle body changes since it is affected by the relationship between the tires and the ground. Depending on how the matrix tanks are installed underneath the vehicle and the overall weight of the matrix, the

aerodynamics and rolling resistance of the truck could change for each phase of the project.

The testing procedure that was referenced when completing this section of the testing is SAE J1263 [16]. This Society of Automotive Engineers (SAE) article provides the process to conduct a proper and accurate coast down test for all vehicles. For a coast down test, the truck is coasted in neutral from 113-kph to 32-kph (70 – 20 mph) on a level and straight road without any interruptions. To cancel out environmental effects such as road slope or wind, the test in performed in both directions. Prior to the experiment, the wind speed parallel and perpendicular to the road and ambient temperature are recorded using a 6 in 1 Multifunction CE Digital Environment Multimeter. This data is collected to ensure that the vehicle is tested in similar conditions during the phases to accurately compare and contrast the data.

Contrary to the previous dynamic tests, the data log in the LabVIEW program is started when the vehicle is already in motion. Similarly to previous tests, only the vehicle speed and the time were recorded during this test. Two testers are required to be in the vehicle to complete this test safely. One tester focuses on the driving, while the other tester controls the data logging of the test. As soon as the driver has reached the 113-kph and has kept the speed constant, the second tester would begin the data log and the driver would then shift the truck's gear from drive to neutral and remove his or her foot from the accelerator and brake pedal. Once the vehicle's speed has dropped to 32-kph, the second tester would terminate the data logging and the driver would then shift the truck's gear back into drive and bring the vehicle to an appropriate speed to navigate to a turnaround point to repeat the experiment in the opposite direction. A pair of tests in both directions is seen as one test run and a total of 10 runs were completed for each phase. The location of the test was on Armheim Road which is approximately 2.25 km (1.4 miles) long as shown below in Figure 5.10 with latitude/longitude coordinates of 46.917324°/-88.499851°. During the post-processing of the data, a 2^{nd} order polynomial fit is correlated to the vehicle's equation of motion to determine the approximate drag coefficient and rolling resistance for each phase.

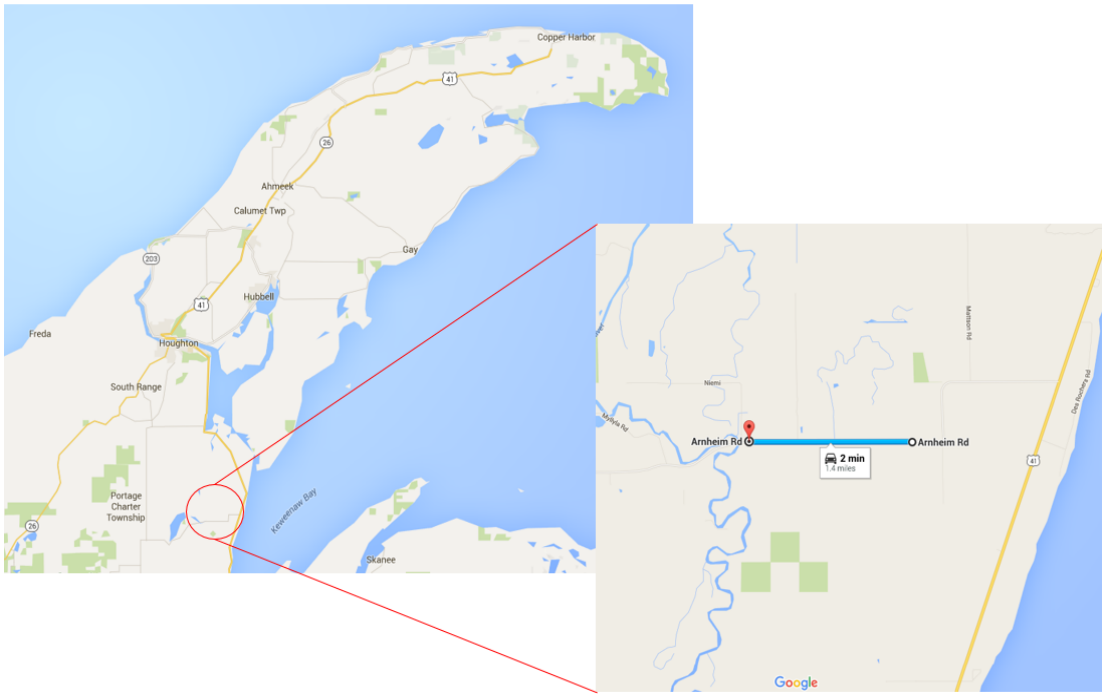

Figure 5.10: Arial view of the coastdown test location (Image retrieved from Google Maps March 2016 and permission granted in Appendix E).

5.8 Cornering & Understeer / Oversteer

Weight and weight distribution impact vehicle handling. Therefore, a cornering test was conducted to quantify the impact of tank configurations on vehicle handling as well as determine force / strain / acceleration on tanks and brackets during hard cornering. When conducting a cornering test, the two factors that one is trying to observe are understeer and oversteer. Understeer occurs when the front wheels lose traction before the rear wheels, so it will cause the entire vehicle to push to the outside of the road when going around a turn or a curve. On the other hand, oversteer occurs when the rear wheels lose traction before the front wheels, so it will cause the back of the vehicle to push toward the outside of the road making the entire vehicle spin inwards towards the curve or turn [17].

The testing procedure that was referenced when completing this section of the testing is SAE J266 [17]. This SAE article depicts and explains the process to conduct a proper and accurate tests and analysis procedures for assessing vehicle steady-state handling response. Since the article describes multiple ways to test understeer and oversteer,

Method 1, the constant radius test was chosen based on the simplicity of the procedure. Due to the limitations of the testing area, the truck was driven on an 18 m radius circular path, instead of a 30 m radius as recommended in J266, over a range of 12 to 55 kph while the steering wheel theta, vehicle speed, and time were recorded using the LabVIEW program. This test requires a total of three testers; one as the driver, another to control the data logging, and another outside of the vehicle to supervise the test site area and notify the other two testers if a pedestrian or another vehicle was entering or leaving the test area. The location of this test was in a Michigan Technological University parking lot as shown in Figure 5.11, so there would be light traffic moving into and out of the lot that needed to be supervised to guarantee the safety of the three testers as well as others.

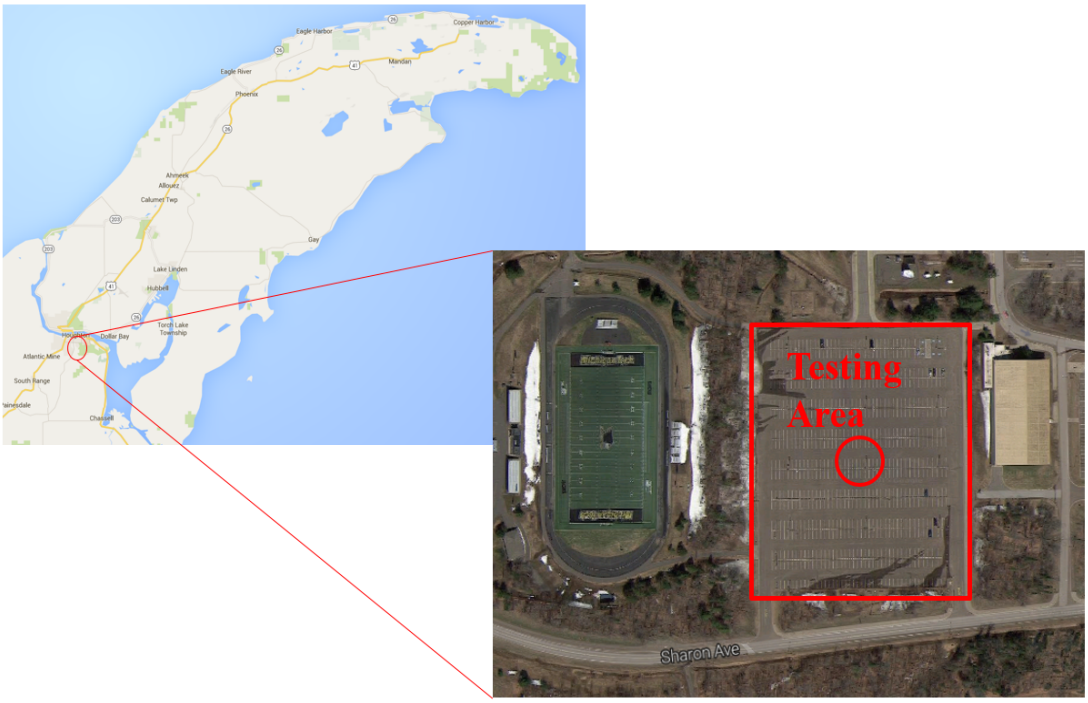

Figure 5.11: Arial view of the cornering test location (Image retrieved from Google Maps March 2016 and permission granted in Appendix E).

5.9 Truck Ballasting

The number of testers and fuel capacity add variability to the curb weight of the truck, which can impact the results. Therefore, test weights were established for each of the tank configurations to uphold uniformity through all of the phases to confidently compare the data. The baseline test weight is set at slightly more than the weight of the vehicle with two testers, full instrumentation, and maximum fuel. With this process, the only difference in test weights is the actual delta from that tank configuration. A table of the ballasted weights for each phase can be seen below in Table 5.1 Ballast weights are located as close as possible to the CG in the bed of the truck and is added or removed as needed to achieve the test weight as shown in Figure 5.12. If there is only one tester performing a test, then ballast weights are also placed in the front passenger seat to emulate another passenger based on the average male weight, being 81.6 kg (180 lbs.) [18]. The weights are in 9.1 kg (20 lb.) increments, so the ballast targets can be achieved within +/- 9.1 kg (20 lbs.)

Table 5.2: A chart of the ballasted weights used for each testing phase.

Phase	Baseline	Quantum	Phase 1
Ballasted Weight	2721.6 kg (6000 Lbs.)	2834.9 kg (6250 Lbs.)	2902.9 kg (6400 Lbs.)

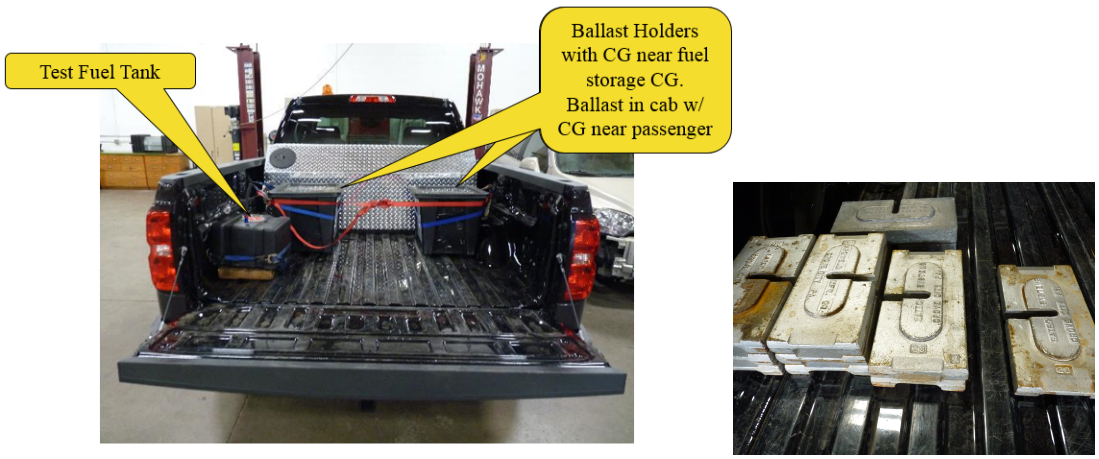

a) b)

Figure 5.12: a) A picture of the location of the ballast weight boxes and test fuel tank installed in the bed of the vehicle. b) A picture of the weights.

In addition to truck ballasting, the fuel density, heating value, and C/H/O ratio are critical for volumetric fuel consumption measurements, and acceleration testing. Thus, two 55 gallon drums of fuel was procured at the beginning of the testing, so there would be enough for the duration of all the tests.

Chapter 6 Results & Discussion

6.1 Static Test Results

The static data for the first three configurations can be viewed and compared in Table 6.1. This table gives the researcher and the reader a better understanding of how each of the phases relate to one another based on their configuration. As expected, the baseline phase has the lowest total weight than the quantum configuration and phase 1. In addition, phase 1 has a higher weight than the quantum configuration, but only by 61 kg (135 lbs.) which is a smaller margin compared to the 172 kg (380 lb.) difference between phase 1 and the baseline configuration. The weight of the phase 1 tanks integrated on the vehicle weighs around 181 kg (400 lbs.) when full of natural gas, but items were removed to integrate the matrix tanks such as the original gasoline tank and some of the quantum hardware that was located in the bed of the truck to reduce the weight of the truck. A list of the items and their estimated weights that were altered on the vehicle from the baseline configuration to phase 1 are included in Table 6.2.

The added weight during each phase correlates to the ground clearance, approach angle, break-over angle, and departure angle. With the increase in vehicle weight, the data shows that there is an indirect relationship with ground clearance even with the addition of the body lift in phase 1. The additional weight causes the vehicle suspension to compress more which will lower the overall height of the vehicle. In relation to the approach angle, the data demonstrates that the angle increases through the different configurations. This increase is due to where the natural gas tank is integrated in each configuration. With both tanks installed in the back portion of the vehicle, the added weight in the back enhances the amount of forces on the back vehicle suspensions which will cause the back to dip down and the front of the vehicle to lift up slightly. The reason that phase 1 has a higher angle than the quantum configuration is because of the larger quantity of added weight and the lower placement of the phase 1 matrix tanks. This same concept can be applied to the departure angle, but with the opposite effect. With the additional weight being applied to the back end of the vehicle, the back portion of the vehicle will get lower with more weight and in turn decrease the departure angle. The

break-over angle is directly related to the ground clearance when referencing Equation 5.5, so it is expected for the break-over angle to decrease as the ground clearance decreases.

Table 6.1: A table comparing the static data for the baseline configuration, quantum configuration, and phase 1.

Parameter	Baseline	Quantum	Phase 1
Total Weight	2479 kg (5465 lbs.)	2590 kg (5710 lbs.)	2651 kg (5845 lbs.)
Center of Gravity (X)	-1.48 m (- 58.29 in.)	-1.55 m (-61.1 in.)	-1.53 m (-60.34 in.)
Center of Gravity (Y)	-1.59 cm (-0.625 in.)	-1.1 cm (-0.435 in.)	-1.03 cm (-0.407 in.)
Center of Gravity (Z)	-66.4 cm (-26.14 in.)	-59.94 cm (-23.6 in.)	-21.74 cm (-8.56 in.)
Ground Clearance	31.75 cm (12.5 in.)	30.48 cm (12 in.)	29.21 cm (11.5 in.)
Approach Angle	18.14°	18.58°	20.77°
Break-Over Angle	19.7°	18.99°	18.21°
Departure Angle (hitch)	23.63°	23.03°	22.72°

Table 6.2: A list of the items installed and removed from the baseline configuration to phase 1.

Item Added or Removed	Weight (kg)	Weight (lbs.)
Remove Gasoline Tank	-81.65	-180
Remove Production Exhaust	-9.07	-20
Remove Catalytic Converter	-9.07	-20
Remove Quantum Brackets	-4.54	-10
Install Phase 1 Fuel Cell	22.68	50
Install Lift Kit	13.61	30
Install Phase 1 Plumbing	18.14	40
Install Phase 1 Tanks and Brackets	204.12	450
Install Side Pipes	18.14	40
Total	172.36496	380

A visual of the center of gravity (COG) data for the three configurations can be viewed in Figure 6.1 below. The COG markers in the figure are to an approximate scale. The placement of the tanks strongly correlates to how the vehicle COG changes in the phases. In the X-direction, the data indicates that the COG moves towards the back of the vehicle for the quantum configuration since the quantum tank is installed in the bed of the truck. The X-direction COG moves back towards the front of the vehicle during phase 1 because the tanks are then placed more towards the center of the vehicle and the weight is distributed from behind the transmission to the rear axle. In the Y-direction, the COG moves towards the center of the vehicle through the phases. The addition of the quantum tank centered in the bed of the truck caused the total weight distribution to shift slightly to the middle. The total weight shifts more to the middle during phase 1 as the original gasoline tank and exhaust are removed and replaced with pairs of phase 1 matrix tanks and dual side pipes to make the vehicle weight more symmetrical. The Z-direction COG has the greatest change of the three directions. The installation of the quantum tank in the bed of the truck caused the COG to drop by about 7.62 cm (3 in.), but the phase 1 installation caused the COG to drop by about 45.72 cm (18 in.) with the tanks being installed underneath the vehicle. This evaluation of the static data should assist with the understanding of the dynamic test data.

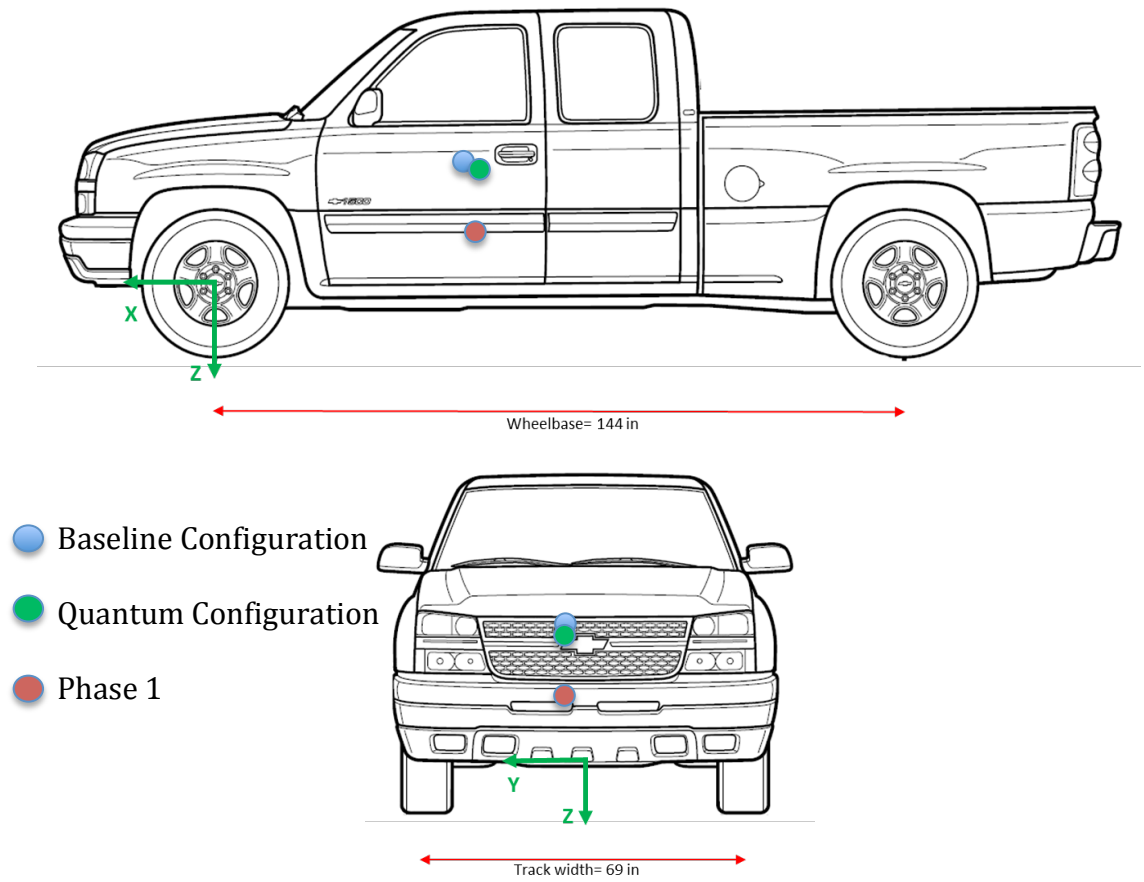

Figure 6.1: A comparison visual of the center of gravity for the baseline configuration, quantum configuration, and phase 1. The permission to use this figure is in Appendix E

6.2 Dynamic Test Results

The pothole data for the three configurations shows different relationships based on the perspective that is chosen. Figure 6.2 illustrates the perspective of observing the maximum and minimum acceleration experienced in the Z-direction for all three configurations. According to the data, phase 1 on average experiences the highest and lowest acceleration of the three configurations. On the other hand, the quantum phase tends to encounter the lowest maximum and highest minimum of the three phases. This correlation can be connected back to the location of the natural gas tanks for the quantum configuration and phase 1. When the quantum tank is installed in the bed of the truck above the suspensions, it seems to dampen the acceleration experienced by the vehicle. When the matrix tanks are installed underneath the vehicle around the same height as the

suspensions, the added weight seems to enhance the acceleration that the vehicle experiences when driving over a pothole at increasing speeds.

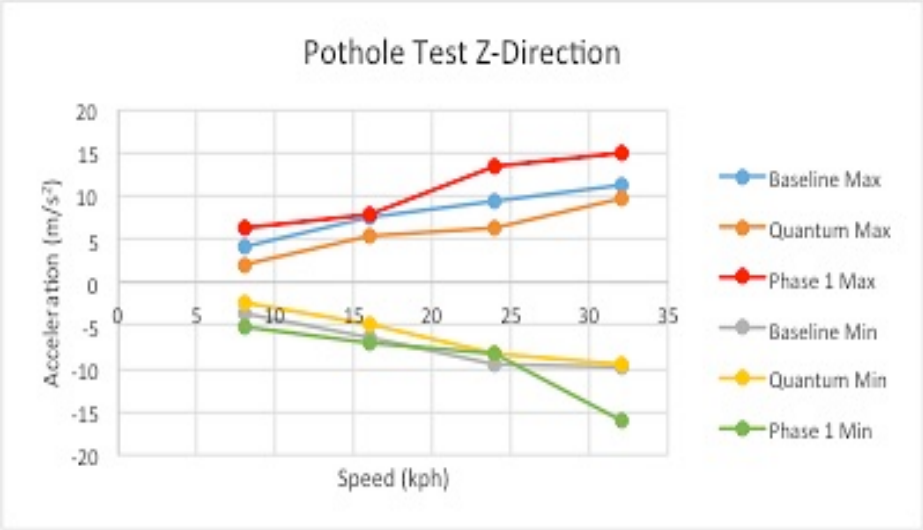

Figure 6.2: A graph comparing the maximum and minimum pothole seat track acceleration for all three configurations.

The next perspectives to view are the cycles and time for the seat track acceleration to decay once the maximum acceleration is encountered. These perspectives can be viewed in Figures 6.2 & 6.3. For the cycles to decay, the quantum configuration and phase 1 have similar decreasing trends until 40-kph. This trend could be due to the additional weight of the tanks acting as a source for the acceleration to be absorbed and mitigated. This trend can also be coupled with the reasoning that the increase in vehicle speed causes a decrease in the amount of time that the vehicle tire spends in the pothole. This analysis can also be applied to the time to decay for the quantum configuration and phase 1 since they still have a decreasing trend with speed. The baseline configuration has a constant trend with an exception for 8-kph for cycles to decay and 24-kph for time to decay. It is also noticed that baseline configuration and phase 1 have shorter time to decay than the quantum configuration. This increase in time to decay for the quantum configuration could be due to the higher location of the natural gas tank.

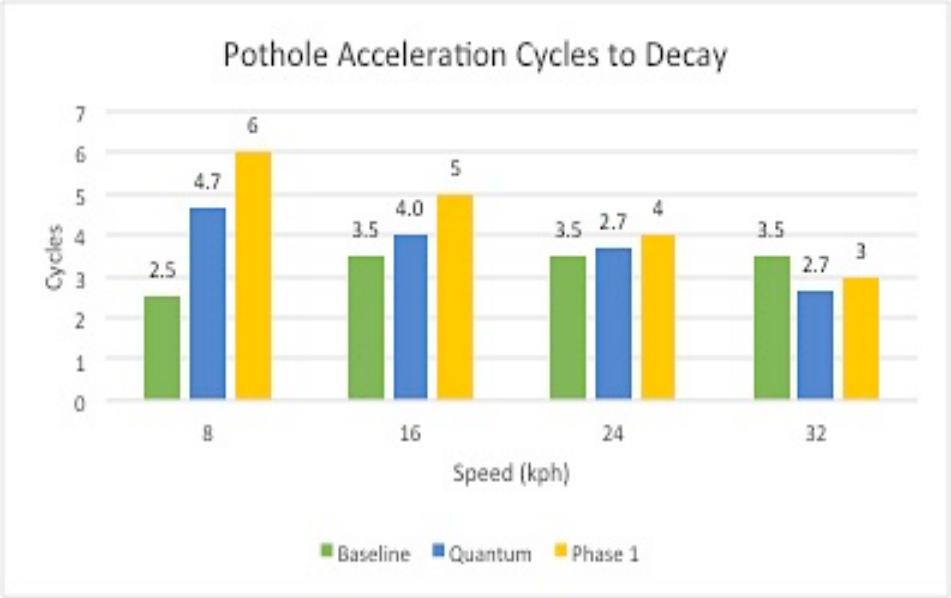

Figure 6.3: A graph comparing the pothole suspension cycles to decay for all three configurations.

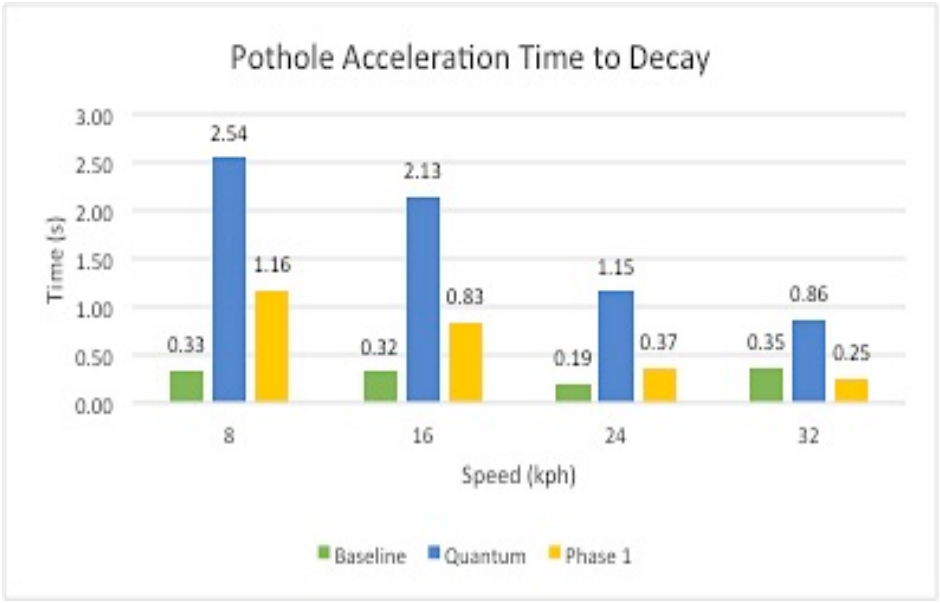

Figure 6.4: A graph comparing the pothole suspension time to decay for all three configurations.

The last perspective to observe the effect of the pothole is the suspension's expansion and compression as seen in Figures 6.5 &6.6. This compression data on average experienced greater displacement than the expansion because the maximum compression occurs once the wheel actually drops into the pothole. The expansion occurs afterwards

as the wheel comes back out of the pothole; the vehicle suspension reacts to the compression to return back to equilibrium. Similar to the seat track acceleration data, phase 1 faced the largest displacement for both expansion and compression, while the quantum configuration experienced the smallest displacement of the three phases. In general, the phases tend to follow a parabolic like trend, but the peak is not always the middle speed, 24-kph. For the baseline phase, the expansion displacement peaks at 24-kph, but the compression displacement peaks at 32-kph. For the quantum configuration, the expansion stays relatively constant for the first three speeds and then reduces for the last two speeds, while the compression displacement peaks at 16-kph. Phase 1 seems to follow a non-traditional trend that is neither constant, linear, or a parabolic for all speeds. For the expansion, the displacement has a slight parabolic trend starting at 16-kph with a peak at 32-kph. The compression, in contrast, has a parabolic shape ending at 32-kph, but the displacement peak is at 40-kph.

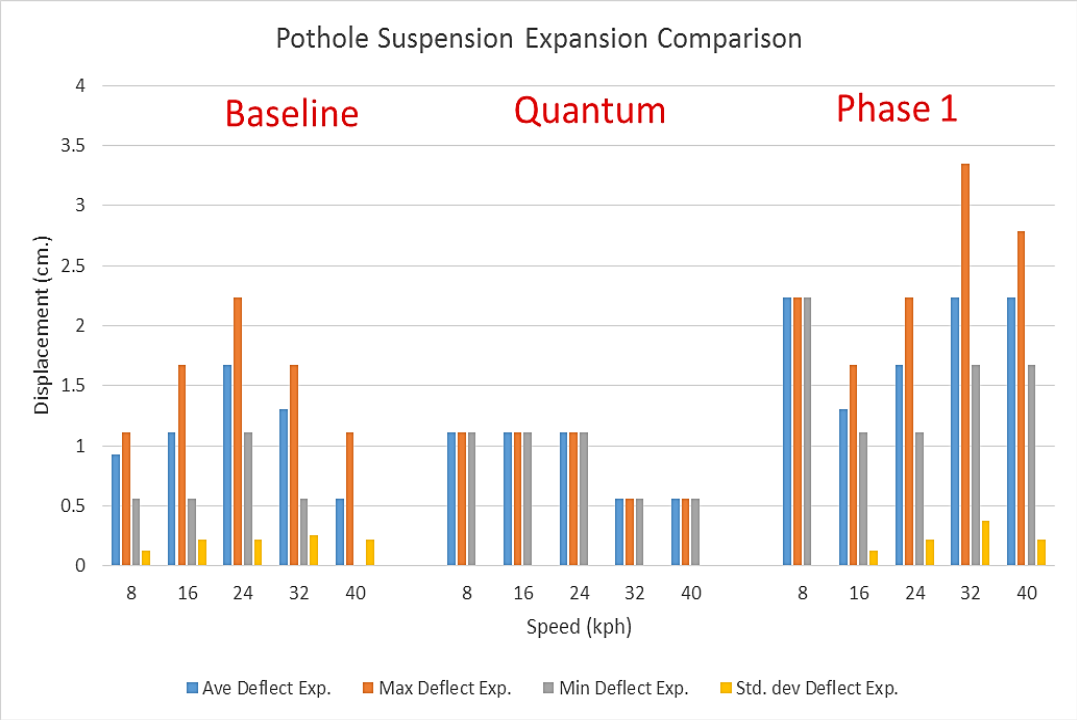

Figure 6.5: A graph comparing the rear suspension expansion pothole data for all three configurations.

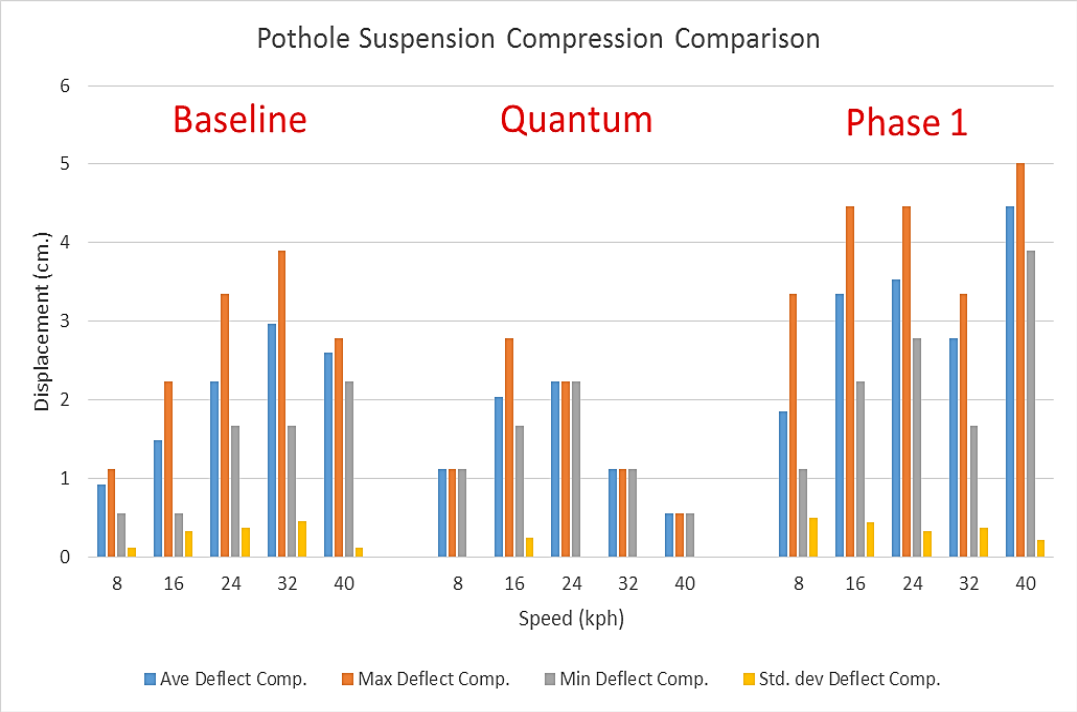

Figure 6.6: A graph comparing the rear suspension compression pothole data for all three configurations.

The speedbump data portrays different trends than the pothole tests. Based on Figure 6.7, one can see the seat track acceleration is similar for all of the configurations up until 24-kph. For each speed starting at 24-kph, each phase peaks at a specific speed. The baseline configuration experiences the highest maximum and lowest minimum of the three phases at 24-kph. The quantum configuration experiences the highest maximum and lowest minimum of the three phases at 40-kph and phase 1 experiences the highest maximum and lowest minimum of the three configurations at 32-kph. Of the three phases, the quantum configuration is the only phase that is constantly increasing with the speed. The other two configurations peak at a particular speed and then the acceleration experienced starts to decrease with higher speeds.

Figure 6.7: A graph comparing the maximum and minimum speedbump seat track acceleration for all three configurations.

The seat track acceleration cycles to decay and time to decay have different trends based on the configuration. For cycles to decay seen in Figure 6.8, the quantum configuration and phase 1 follow a parabolic trend with both configuration peaking at 16-kph.They also share similar acceleration values at all speeds with the maximum difference between the two phases being 2 cycles at 40-kph. On the contrary, the baseline configuration cycles to decay increases with the increasing vehicle speed. This information implies that the weight of the natural gas tanks act as a source for the acceleration to be absorbed and mitigated similar to the same effect discussed with the pothole tests. This deduction can also be supplemented by the time of decay also decreasing with increasing vehicle speed as seen in Figure 6.9. The time to decay greatly decreases from the lowest vehicle speed to the top speed for the quantum configuration and phase 1, while the baseline configuration time to decay remains relatively constant over the different speeds.

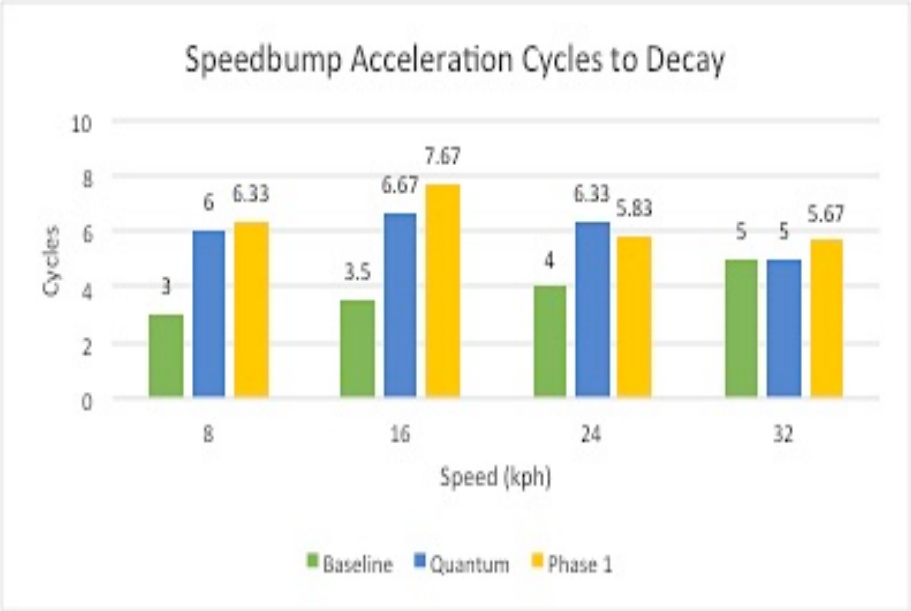

Figure 6.8: A graph comparing the speedbump suspension cycles to decay for all three configurations.

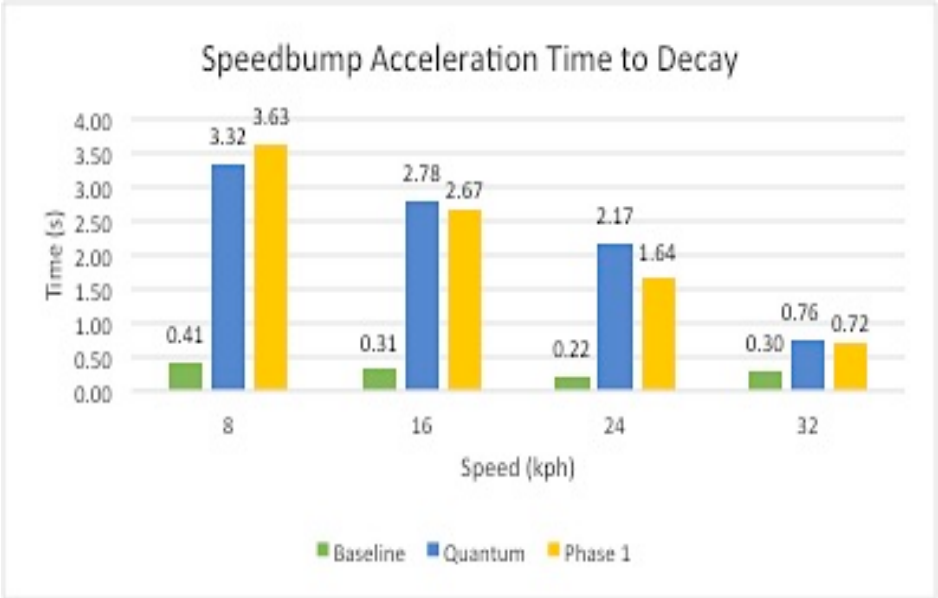

Figure 6.9: A graph comparing the speedbump suspension time to decay for all three configurations.

Unlike the pothole test data, the speedbump suspension data experienced greater displacement during expansion than compression on average. The difference between the expansion and compression is not as large as the pothole tests though. The rear suspension experiences its greatest compression as the wheels are coming onto the speedbump as the change in road height and the truck's gravity cause the suspension to

compress to compensate for this quick change. The expansion is then experienced as the wheels are coming off of the speedbump because the truck body is still ascending from the speedbump, but the wheels are coming back down to the road before the vehicle body causing the rear suspension to expand. All of the configurations seem to follow a linear increasing trend with suspension compression as the vehicle speed increases as shown in Figure 6.11. As the vehicle hits the speedbump at higher speeds, the wheels hit the bump with a greater force causing the suspension to compress more to compensate for the greater forces. The suspension expansion follows different trends for each of the configurations as can be viewed in Figure 6.10. The baseline configuration follows a rough parabolic trend with a peak at 16-kph. The quantum configuration expansion decreases with increasing vehicle speed which implies that the weight of the tank has a greater effect on the suspension expansion at higher speeds. This is also observed at 24 and 32-kph during phase 1. The weight of the tanks seems to decrease the displacement experience by the suspensions while the vehicle is coming off of the speedbump.

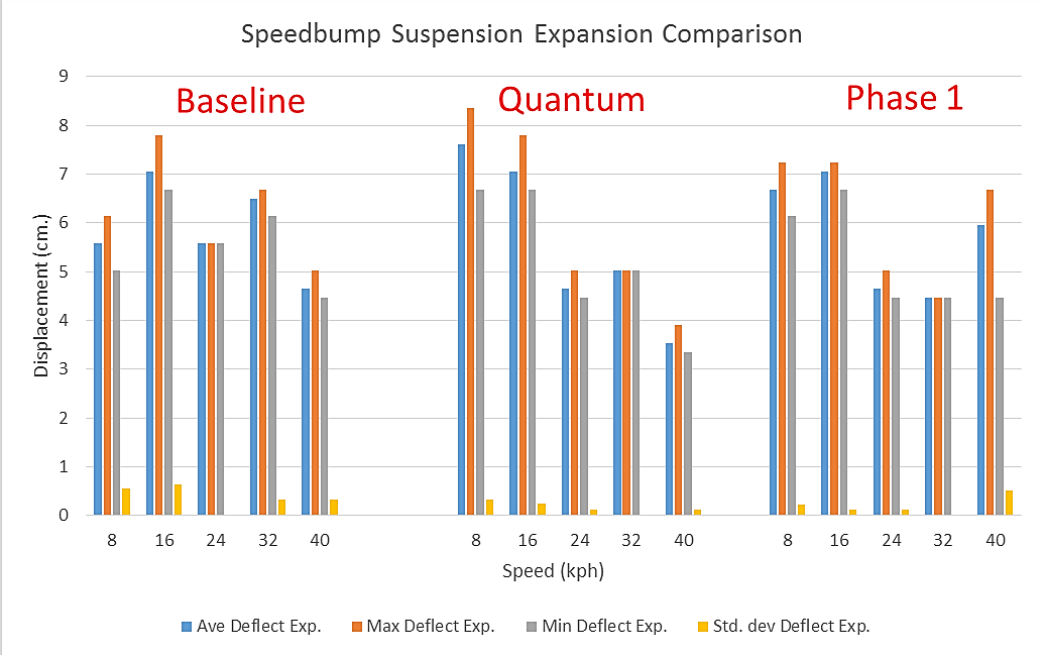

Figure 6.10: A graph comparing the rear suspension expansion speedbump data for all three configurations.

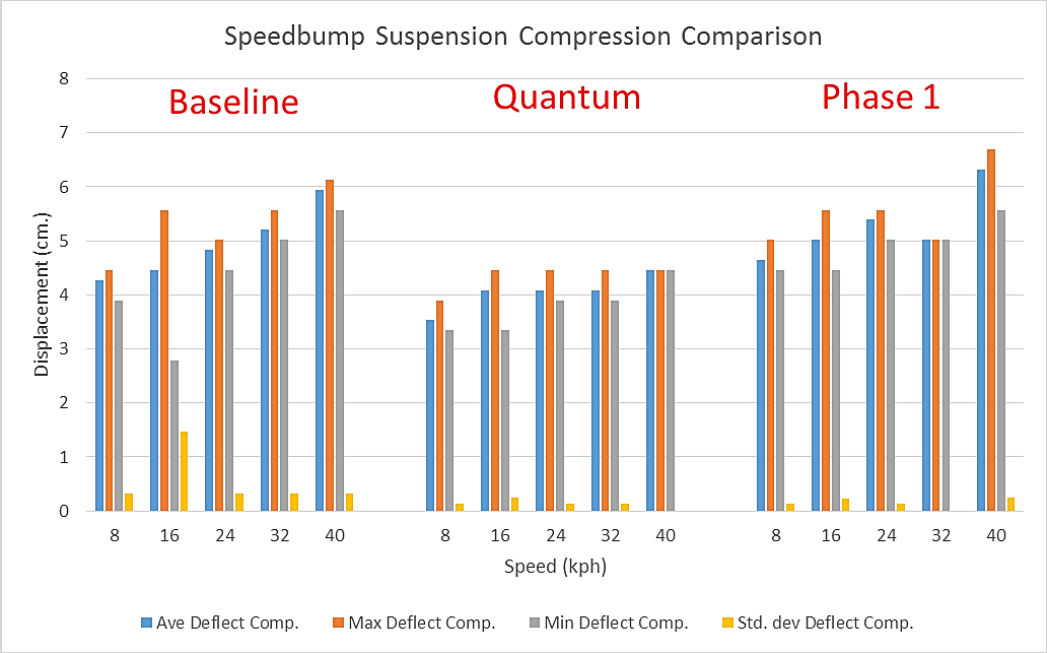

Figure 6.11: A graph comparing the rear suspension compression speedbump data for all three configurations.

The vehicle acceleration data from the 0 to 60 tests of all three configurations can be viewed and compared in Figure 6.12. In general, the acceleration time is only changed slightly by the addition of the natural gas tank weight. The biggest time difference that is observed is during the quantum configuration when the CNG was utilized as fuel. CNG is known to produce less engine power, so it was expected for the acceleration time to increase in this situation. The quantum configuration and phase 1 utilizing only gasoline fuel have slight increases in the acceleration times due to the increased weight, but the slight increase is not something that would be noticed by a normal vehicle owner. It can also be observed that phase 1 has a lower average time than the quantum configuration. This drop in time can be attributed to the placement of the CNG tanks. In the theoretical sense, Equation 6.1 could be referenced when attempting to determine how the placement of the tanks affects the maximum tractive force that the vehicle can encounter [19]. In this equation, μ is the friction coefficient, W is the weight, b is the distant from the center of gravity to the front axle, L is the wheelbase, and h is the height to the center of gravity.

Equation 6.1

$$F_{xmax} = \frac{\mu * \frac{Wb}{L}}{1 - \left(\frac{h}{L}\right)\mu}$$

One would be able to determine the maximum tractive force of the vehicle by changing the W, h and b parameters with all of the other parameters constant. However, μ is constantly changing since it includes factors such as tire temperature, ambient temperature, and humidity, so it is difficult to predict this parameter as it will affect the overall tractive force and the vehicle acceleration.

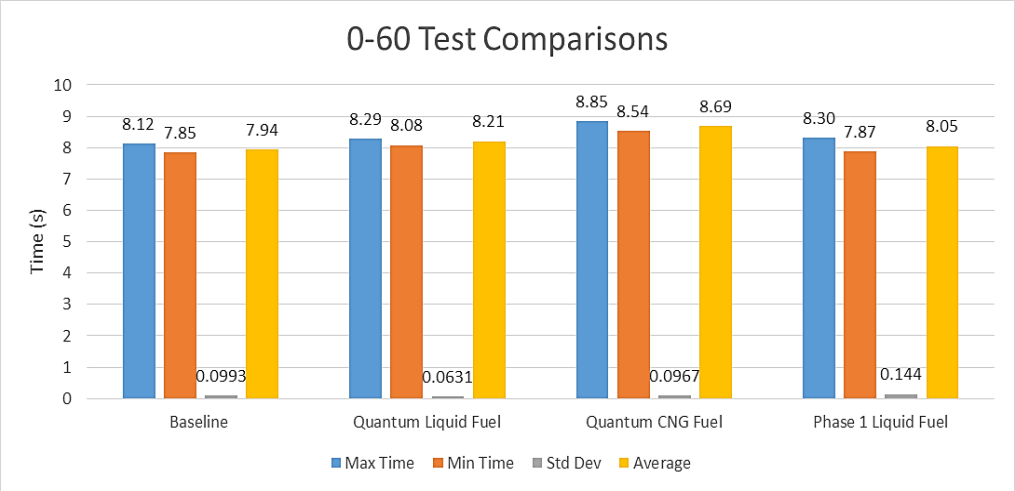

Figure 6.12: A graph comparing the acceleration data for the first three configurations.

The city and highway fuel economy data follow slightly different patterns as seen in Figures 6.13 & 6.14. However, the fuel economy tests were only tested using liquid gasoline. The average city fuel economy increased by 0.4 L/100 km from the baseline to quantum configuration, but increases by a larger margin of 1.5 L/100 km during phase 1. This data proves that the added weight of the natural gas tanks changed as expected and has an effect on the vehicle's city fuel economy. However, the highway fuel economy is more affected by the addition of the CNG tanks. The fuel economy improved during the quantum configuration, but the fuel economy diminished during phase 1. This change in the highway fuel economy is affected by the placement of the tanks more than the weight of the tanks. When the quantum configuration tank is installed in the bed of the truck

covered with the diamond plate, the diamond plate allows the passing wind above the vehicle to flow smoothly over the quantum tank while the vehicle is in motion. Alternatively, when the phase 1 tanks are underneath the truck and not covered, the passing wind going underneath the vehicle hits the phase 1 tanks creating another force that the vehicle has to fight against while in motion. This then translates to the vehicle having to consume more fuel to overcome this additional force.

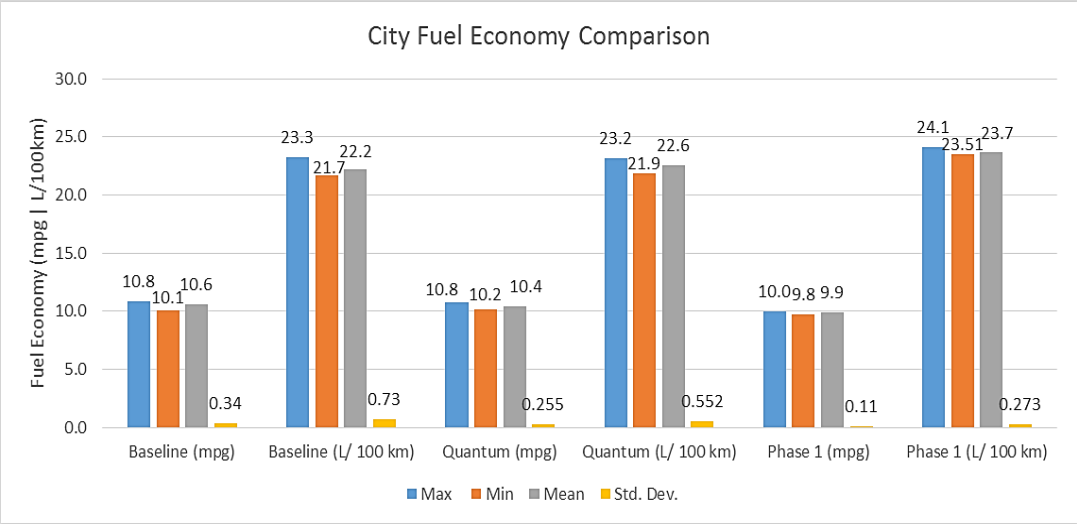

Figure 6.13: A graph comparing the city fuel economy data for all three configurations.

In addition, these fuel economy values are affected by the elevation changes for both cycles as changes in elevation will affect the vehicle acceleration with more mass. In general, city fuel economy will be affected by changes in mass due to the stop and go tendencies. The highway fuel economy will be affected by aerodynamic changes, but mass changes will have an affect with changes in elevation.

Initially, the intention was to utilize flow meters to measure the liquid gasoline and CNG flow into the engine to get precise measurements of fuel consumption and to also observe the liquid gasoline/CNG ratio of fuel being fed into the engine. However, when the liquid gasoline flow meter was installed, high-pressure pulses from the high-pressure pump for the production gasoline system affected the meter. These pulses caused the flow meter to output incorrect gasoline flow data, which is when it was decided to utilize delta mass measurements.

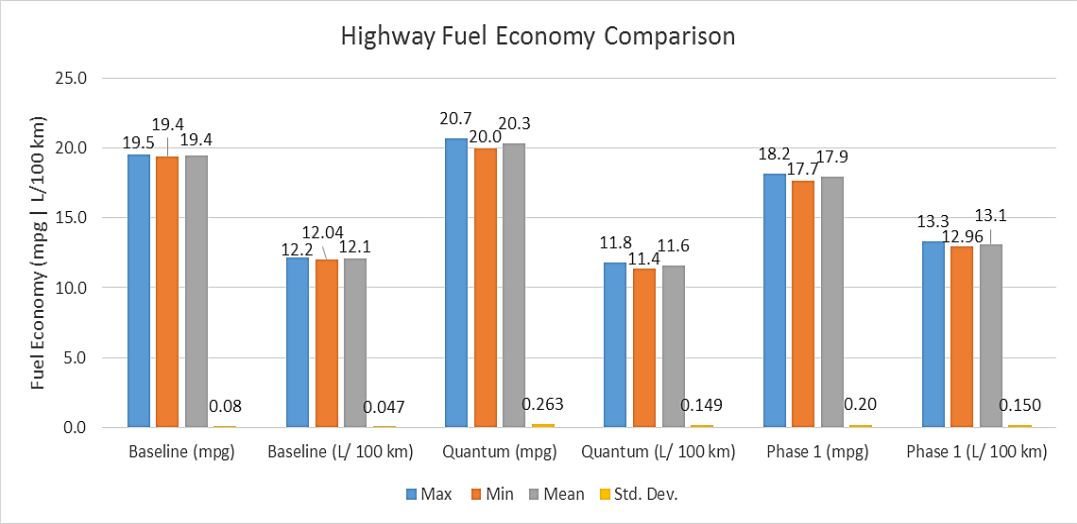

Figure 6.14: A graph comparing the highway fuel economy data for all three configuration.

The data from the coastdown test for all three configurations can be compared and contrasted in Figures 6.15 & 7.16 and Table 6.2. Nonetheless, the coastdown data does have correlations to the highway fuel economy data with both tests undergoing high speeds. As seen in Table 6.3, the quantum phase has the longest coast time and phase 1 has the shortest coast time of the three configurations. The explanation that was provided for the highway fuel economy results can be applied to this data as well. The aluminum plate over the quantum tank improved the aerodynamics as well as the added additional weight contributes to the vehicle's momentum causing the vehicle to coast further. With the wind pushing against the phase 1 tanks underneath the vehicle and not having the engine to combat this additional resisting force, the vehicle aerodynamics are diminished causing the vehicle to decelerate at a greater rate as can be seen in Figure 6.16. The average speed standard deviation of the runs that were completed for each configuration can be seen in Table 6.4.

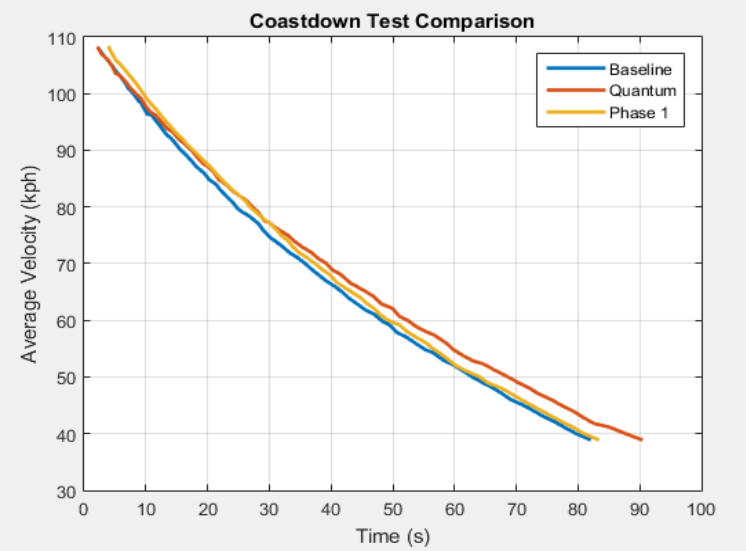

Figure 6.15: A graph comparing the average velocity coastdown data for all three configurations.

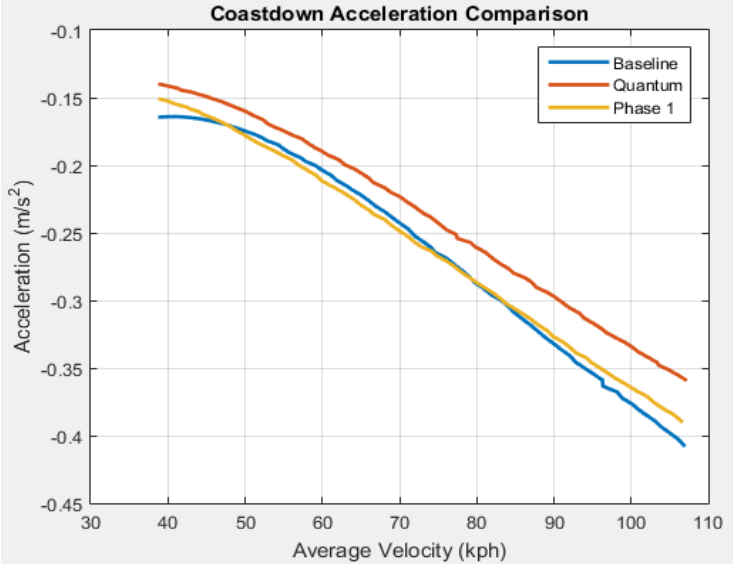

Figure 6.16: A graph comparing the average velocity against the acceleration for all three configurations.

Table 6.3: A table of the average coast times for all three configurations from 108 to 39 kph (67 to 24 mph).

Average Coast Time		
Baseline	**Quantum**	**Phase 1**
79.4 s	88.15 s	79.06 s

Table 6.4: A table of the average speed standard deviation for all three configurations from 108 to 39 kph (67 to 24 mph).

Average Speed Standard Deviation		
Baseline	**Quantum**	**Phase 1**
0.204	0.282	0.235

The cornering data below, in Figure 6.17, displays the effects of integrating the CNG tanks to the vehicle. The quantum configuration at minimum requires the steering wheel to be turned an additional 50 degrees compared to the baseline configuration in the same speed range. Likewise, phase 1 requires on minimum of about 60 additional degrees to the baseline configuration. In comparison of the quantum configuration and phase 1, phase 1 on average requires higher average steering theta values, but not by a large margin. This small margin could be due to the heavier overall vehicle weight and lower tank placement of the phase 1 tanks. The speed and steering wheel theta variability can be seen in Figures 6.18 & 6.19 respectively. Overall, the additional weight of the CNG tanks and the placement have a large impact on the cornering characteristics of the vehicle. In the future, it may be beneficial to repeat the cornering tests while also measuring the steer angle of the actual wheel along with the steering wheel theta.

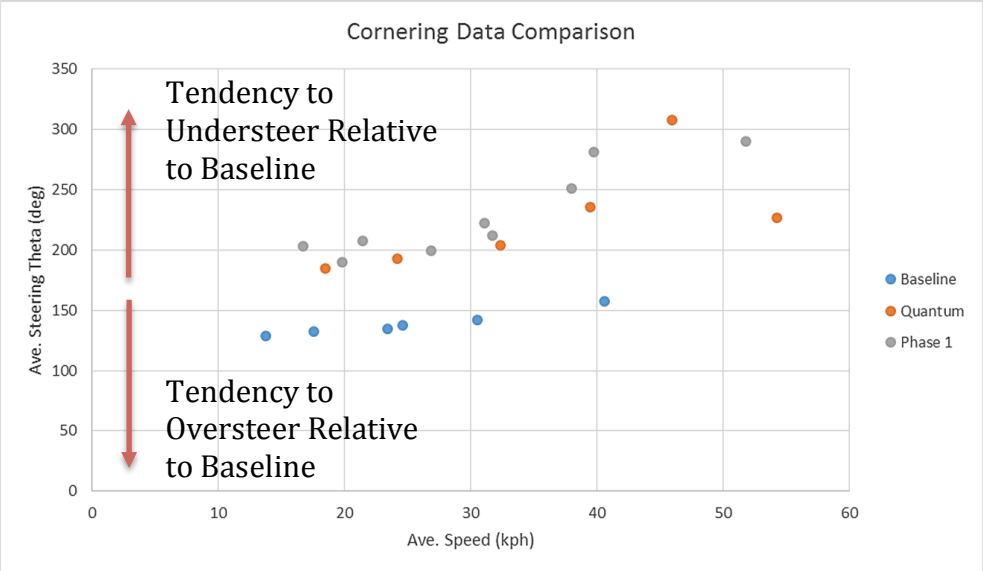

Figure 6.17: A graph of the average speed against average steering theta data for all configurations during the cornering test.

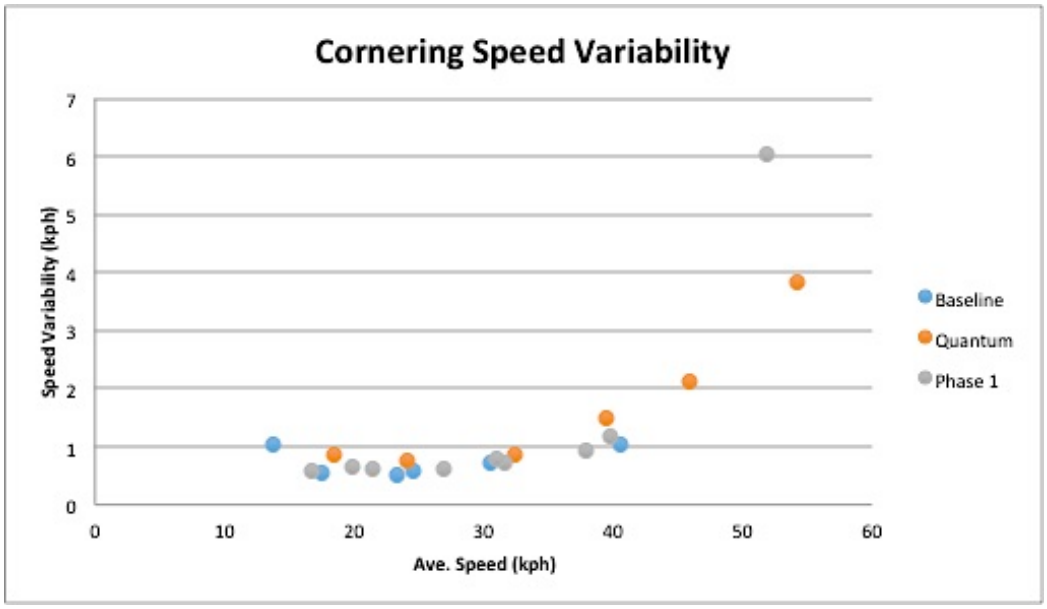

Figure 6.18: A graph of the average speed variability for all configurations during the cornering test.

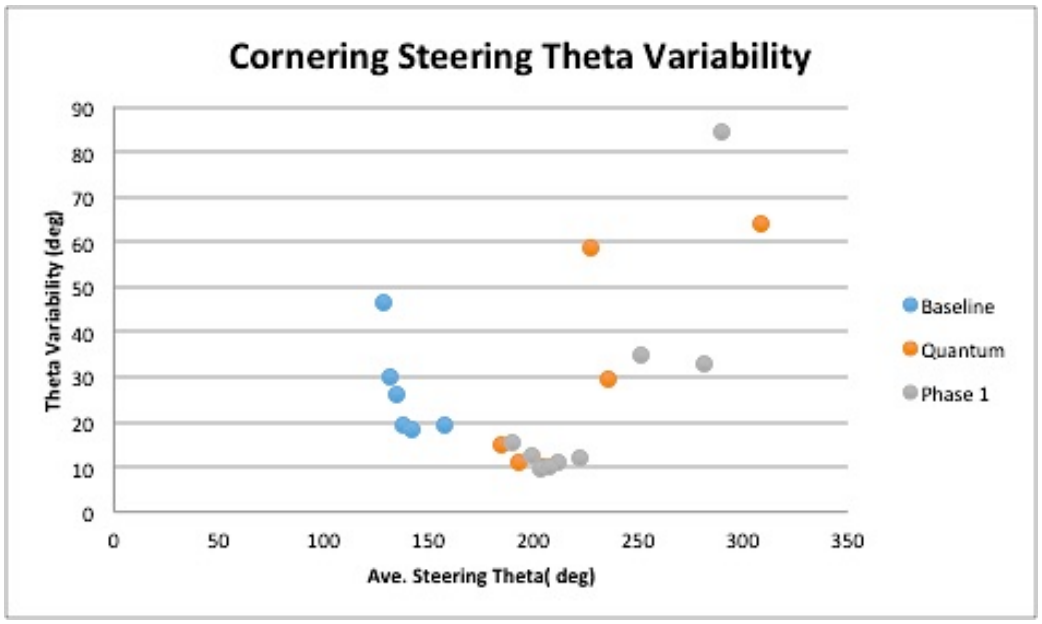

Figure 6.19: A graph of the average steering theta variability for all configurations during the cornering test.

Chapter 7 Conclusions

In conclusion, the integration of natural gas tanks does have an impact on the performance of a full-sized light-duty pickup for both static and dynamic parameters. The additional weight of the tanks increases the overall weight of the vehicle and lowers the center of gravity and ground clearance of the vehicle. The placement and weight of the tanks causes an increase in the approach angle and a decrease in the break-over angle and departure angle. The addition of the CNG tanks seem to act as a source for the vertical acceleration to be absorbed and mitigated in the pothole and speedbump tests, but the inconsistent data trends cause the data to be inconclusive. The vehicle acceleration time increases as the natural gas tanks are implemented, but the phase 1 tanks have a shorter time than the quantum configuration. As for the fuel economy, the integration of the natural gas tanks has a greater impact on the highway fuel economy compared to the city fuel economy. The coast time of the vehicle is greatly affected by the weight and placement of the tanks as it increases the coast time during the quantum configuration and decreases the coast time during phase 1. Lastly, the installed CNG tanks will cause the required average steering wheel theta to increase compared to the baseline configuration.

Chapter 8 Future Work

As this thesis only covers 3 of the 4 configurations of the project, there are some remaining tasks and testing that still need to be completed for the future of this project. At the current state of the project, the phase 1 tanks are not certified to be filled with CNG, so the Phase 1 results provided only show the effect of the phase 1 tanks based on the tank weight and placement. However, the fuel economy and acceleration tests will need to be repeated with natural gas being the primary fuel when the tanks are approved to document how the engine performance changes based on the fuel intake. This procedure will also apply during the phase 2 testing once the tanks are approved as well. In addition, it would be beneficial to find a better way to measure both the liquid gasoline and CNG flow rates to have a better understanding of the engine consumption.

With the certification of the tanks, the strain gages can be applied to the Phase 1 tanks to measure the ballooning of the tanks during filling and discharging. Due to the inconclusive nature of the pothole and speedbump data, the data will need to be analyzed further to gain better understanding of the trends. After phase 1 testing is fully completed, the group will be able to move into phase 2 integration and testing. The phase 2 brackets are currently being designed by Tucker Alsup and will need to be fabricated before phase 2 integration begins. All of the tests will be completed as described in Chapter 5.

With the completion of the phase 2 testing, the researchers can then develop a control algorithm to optimize and improve the CNG system efficiency. The PRD valves that were ordered for each pair of tanks can be opened and closed based on a developed algorithm to test various filling and discharging schemes. Ideally, this algorithm would be executed on a different laptop than the data collection laptop to have the capability of implementing different algorithms while testing.

A fast-fill system is being developed to expedite the time required to fill the natural gas tanks for the project and for any future projects. The current slow-fill system can require up to a couple days for a complete fill, while a fast-fill system can reduce that time to a couple hours or less. This system will be installed at the APSRC to simplify the refueling process. Other benefits of tis system will also be examined.

In the future, it would be beneficial to conduct all of the phase 1 test with an aluminum skid plate installed. This aluminum cover would have a slight effect on the static tests depending on its weight, but it would have a larger effect on the dynamic tests. Specifically, the acceleration, fuel economy, and coastdown tests due to the effect of skid plates on theses test parameters.

There is also some future work that can be completed to further understand data, improve safety, and looking at the far future of the project. The fuel economy data for all of the configurations can be extrapolated to CAFÉ type predictions to compare and contrast. The removed catalytic converter can be emission tested and/or added to the under floors back into the side pipes. One can investigate the importance of flowing liquid through the injectors and if there should be an on-board diagnostics (OBD) check for the PRDs. As a safety precaution, a guardrail can be installed for the drive shaft to protect the matrix tanks in the event that the drive shaft breaks. A bill of materials with approximate costs to make this an aftermarket kit will also need to be developed.

Lastly, an AVL Cruise Model can be developed for the vehicle to simulate tests, such as acceleration. This model could then be used to validate the actual vehicle testing data to ensure that the data collected is reasonable and following similar trends to those found in the AVL Cruise model.

Bibliography

1. Saidur, R., et al. *Analysis of exhaust emissions of natural gas engine by using response surface methodology*. Journal of Applied Sciences, 2008. **8**, 3328-3339.
2. Naber, J.D. and J.J. Worm, *6 Application of biomass derived fuels for internal combustion engines with a focus on transportation*. Renewable Energy from Forest Resources in the United States. Vol. 10. 2008: Solomon,B.D. and V.A. Luzadis.
3. Administration, U.S.E.I., *March 2016 Monthly Energy Review*. 2016.
4. Das, L.M., R. Gulati, and P.K. Gupta *A comparative evaluation of the performance characteristics of a spark ignition engine using hydrogen and compressed natural gas as alternative fuels*. International Journal of Hydrogen Energy, 2000. **25**, 783-793 DOI: http://dx.doi.org/10.1016/S0360-3199(99)00103-2.
5. Geok, H.H., et al. *Experimental investigation of performance and emission of a sequential port injection natural gas engine*. European Journal of Scientific Research, 2009. **30**, 204-214.
6. Ashley, S. *Improved natural gas fuel tanks and pumps for autos*. Automotive Engineering, 2012.
7. Zalosh, R. *CNG and hydrogen vehicle fuel tank failure incidents, testing, and preventive measures*. in *Proceedings of the Affichee Spring National Meeting, New Orleans, USA*. 2008.
8. Committee, V.A.F.S.T., *NFPA 52: VEHICULAR GASEOUS FUEL SYSTEMS CODE*. 2013.
9. Gallman, P.G., *Green alternatives and national energy strategy: the facts behind the headlines*. 2011: JHU Press.
10. Storer, D.M., et al. *The Development of an innovative on-board CNG storage system for methane-fuelled cars conducted within the FP7 EU project „InGAS"*. in *Transport Research Arena (TRA) 5th Conference: Transport Solutions from Research to Deployment*. 2014.
11. *Temprel Product Information*. [cited 2015; Available from: http://www.temprel.com/products/info.aspx.
12. *Basic Strain Measurements*. SCM Consultancy and Engineering Services [cited 2015; Available from: https://sites.google.com/site/scmces/media-center/blog-newsletter-articles/basicstrainmeasurementsandstraingauges.
13. International, S., *Surface Vehicle Recommended Practice*, in *Vehicle Dynamics Terminology*. 2008, SAE International. p. 8.
14. Matoussevitch, E. *2008 HUMMER H3 ALPHA*. AutoReview 2007 [cited 2016 20/3/2016]; Available from: http://autoreview.belproject.com/wp/2007/03/2008-hummer-h3-alpha/.
15. Parkhill, M., R. Sooklall, and G. Bahar. *Updated guidelines for the design and application of speed humps*. in *ITE 2007 Annual Meeting and Exhibit. Pittsburgh PA*. 2007.

16. Chapin, C., *Road load measurement and dynamometer simulation using coastdown techniques*. 1981, SAE Technical Paper.
17. Committee, S.V.D.S., *Steady-state directional control test procedures for passenger cars and light trucks.* SAE Standard J, 1996. **266**.
18. Halls, D. *Feelin Fine Chart*. Moose & Doc 2016 [cited 2016 May 4]; Available from: http://halls.md/average-weight-men/.
19. Gillespie, T.D., *Fundamentals of vehicle dynamics*. 1992, SAE Technical Paper.

Appendix A (Bill of Materials)

Table A. 1: A list of the bill of materials for the Phase 1 plumbing.

Phase 1 Plumbing					
Part Description	**Supplier**	**Part #**	**Individual Cost**	**Quantity**	**Total Cost**
Receptacle	Hylok	QCCB-6-S316 CNG	87.15	2	174.3
3/8" SS Lift Check Valve (1 psi cracking)	Hylok	CVH2-H-6T-1-S316	58.19	2	116.38
Lyra CV Valve/PRD	Optimum/OMB	-	163	6	1013
Male 1/4" NPT to 3/8" Compression Elbow	Tylok/Galloup	6-DME-4	16.7	8	133.6
Male 1/4" NPT to 3/8" Compression Tee	Tylok/Galloup	6-DTTM-4	29.15	13	378.95
3/8" Male Compression Cross	Swaglock	SS-600-4	50.9	3	152.7
Custom Cross Adapter 1/4" NPT to 1 1/8"	REL	-		3	-
3/8" Manual Ball Valve	Ty-Flo/Galloup	SS-6-DTT-6-6-K	100.35	2	200.7
3/8" (4800 psig) 304-.049 thick	Ty-Flo/ Galloup		1.627/ft	60 ft	97.62
Male to Female 1/4" NPT Flexible Metal Hose	Ty-Flo/Columbia		43/2 ft.	6 ft	129
SS 9/16-18 UNF adapters to 3/8" Compression	Swagelok	SS-600-1-6STCE	14.4	5	72
SS 9/16-18 UNF Plug	Ty-Flo/Columbia		20	5	100
3/8" Front & Back ferrule set	Swagelok	SS-600-SET	2.36	10	23.6
3/8" Tube Caps	Swagelok	SS-600-C	7.7	10	77
1/4" NPT Plugs	CarQuest	-	1.374	5	6.87
1/2" Loop Clamps(SS/EPDM Cussion Clamps)	CarQuest	-	0.58	30	17.4
Self-tapping Screws(No 14 zincplated 1/2" long)	McMaster	90190A310	8.99/ 100 screws	100	8.99
SS 1/8" Female NPT to 1/4" Male NPT adapter	Tylok/Galloup	4-1RBMF-2	5.723	5	28.615
1/8" Male NPT to 3/8" Compression Straight SS	Tylok/Galloup	6-DMC-2	8.55	3	25.65
				Plumbing Total=	2756.375

Table A.2: A list of the bill of materials for the DAQ and thermocouple instrumentation.

Instrumentation					
DAQ					
Part Description	**Supplier**	**Part#**	**Individual Cost**	**Quantity**	**Total Cost**
TC module	National Instruments	NI9213	1066.5	2	2133
Accelerometer Module	National Instruments	NI9234	1640.7	2	3281.4
Strain Gauge Module	National Instruments	NI9219	988.2	2	1976.4
Analog Input Module	National Instruments	NI9205	792.9	1	792.9
CAN Bus Module	National Instruments	NI9862	657	1	657
8-slot Enet Chassis	National Instruments	cDAQ-9188	1588.5	1	1588.5
4-slot Enet Chassis	National Instruments	cDAQ-9174	829	1	829
				Total	11258.2
Thermocouples					
Part Description	**Supplier**	**Part #**	**Individual Cost**	**Quantity**	**Total Cost**
24 gauge teflon, solid spool (250ft)	Temprel	K24-2-507	0.60 per ft	250	166.4
304 SS sheathed, grounded probe w/ mini connector / size: 1/16" length: 6"	Temprel	T21-MG6KAS	14.35	4	57.4
304 SS sheathed, grounded probe w/ mini connector / size: 1/8" length: 6"	Temprel	T21-MG6KCS	14.35	18	258.3
304 SS sheathed, grounded probe w/ mini connector / size: 0.04" length: 6"	Temprel	T21-MG6KAAS	16.85	10	168.5
304 SS sheathed, grounded probe w/ mini connector / size: 1/8" length: 18"	Temprel	T21-MG18KCS	18.52	4	74.08
1/8" x 1/8" SS NPT compression fitting	Temprel	18FS-125	8.14	20	162.8
1/8" x 1/16" SS NPT compression fitting	Temprel	18FS-062	9.21	8	73.68
24 gauge mini-connecters	Temprel	MP500-K	2.9	30	87
				Total	1048.16

TableA.3: A list of the bill of materials for the remaining instrumentation.

Pressure Transducers					
Part Description	**Supplier**	**Part#**	**Individual Cost**	**Quantity**	**Total Cost**
350 Bar Industrial Pressure Transducers	Omega	PXM309-350G10V	200	5	1000
70 Bar Industrial Pressure Transducers	Omega	PXM309-70G10V	200	1	200
10 Bar Industrial Pressure Transducers	Omega	PXM309-10G10V	200	1	200
				Total	1400
Accelerometers					
Part Description	**Supplier**	**Part#**	**Individual Cost**	**Quantity**	**Total Cost**
Triaxial Accelerometer	PCB Piezotronics	356A15	1035	2	2070
Four Conductor Shielded Cable	PCB Piezotronics	034G10	162	2	324
				Total	2394
Strain gages					
Part Description	**Supplier**	**Part#**	**Individual Cost**	**Quantity**	**Total Cost**
Full Wheatstone Bridge Strain Gages	Omega	SGT-3G/350-FB13	101	3	303
Lift					
Part Description	**Supplier**	**Part#**	**Individual Cost**	**Quantity**	**Total Cost**
2014-2015 Silverado 3 " Body Lift Kit	Performance Accessories	10293	447.12	1	447.12
Fuel Cell					
Part Description	**Supplier**	**Part#**	**Individual Cost**	**Quantity**	**Total Cost**
Return style 4-port fuel pressure regulator	Summit Racing	SUM-220059	84.97	1	84.97
In-line Electric Fuel Pump	Summit Racing	SUM-G3138	84.97	1	84.97
5-gallon Fuel Cell	Summit Racing	SUM-290101	109.97	1	109.97
				Total	279.91
Side Pipes					
Part Description	**Supplier**	**Part#**	**Individual Cost**	**Quantity**	**Total Cost**
Side Pipe Installation	Great Lakes Sound and Vibration	-	-	-	4300
Dynomax 24240 - Thrush Glasspack Mufflers	Jegs	289-24240	99.99	2	199.98
				Total	4499.98
Flow Meters					
Part Description	**Supplier**	**Part#**	**Individual Cost**	**Quantity**	**Total Cost**
Omniflo Turbine Flowmeter 0.02-.6 GPM (gasoline)	Flow Technology	FTO-3NIXSRLHA-1	1445	1	1445
Linear Link	Flow Technology	LA-5-C-V1B6	815	1	815
10 Foot long interconnect cable	Flow Technology	19-60381-104	130	1	130
Mass Flow Meter 10 SLPM	Omega	FMA-1607A-V2	1345	1	1345
				Total	3735
Other					
Part Description	**Supplier**	**Part#**	**Individual Cost**	**Quantity**	**Total Cost**
Heavy Capacity 3500 lb Scales	Longacre Racing Products	72663	3549	1	3549
			Instrumentation Total:		28914.37
			GRAND TOTAL:		**31670.7**

Appendix B (MATLAB Code)

Coded and developed by myself, Yomi Famuyiwa.

Pothole and Speedbump Code

```
%% Yomi Famuyiwa 9/11/15
%% Parse Pot Hole/Speed Bump TDMS data

clc

test='Phase1_4152016_PH_5mph_0';

eval(['Time=', test, '.Values(:,5)/1000;']);
basetime= min(Time);
atime= Time - basetime;


eval(['X_Accel=', test, '.Values(:,1);']);
eval(['Y_Accel=', test, '.Values(:,2);']);
eval(['Z_Accel=', test, '.Values(:,3);']);


eval(['XMax=max(',test,'.Values(:,1));']);
eval(['XMin=min(',test,'.Values(:,1));']);
eval(['XAve=mean(',test,'.Values(:,1));']);

eval(['YMax=max(',test,'.Values(:,2));']);
eval(['YMin=min(',test,'.Values(:,2));']);
eval(['YAve=mean(',test,'.Values(:,2));']);

eval(['ZMax=max(',test,'.Values(:,3));']);
eval(['ZMin=min(',test,'.Values(:,3));']);
eval(['ZAve=mean(',test,'.Values(:,3));']);



test2='Phase1_4152016_PH_5mph_2';

eval(['Time2=', test2, '.Values(:,5)/1000;']);
basetime2= min(Time2);
atime2= Time2 - basetime2;
```

Figure B. 1: A partial snapshot of parsing the speedbump and pothole data.

```
eval(['X_Accel2=', test2, '.Values(:,1);']);
eval(['Y_Accel2=', test2, '.Values(:,2);']);
eval(['Z_Accel2=', test2, '.Values(:,3);']);

eval(['XMax2=max(',test2,'.Values(:,1));']);
eval(['XMin2=min(',test2,'.Values(:,1));']);
eval(['XAve2=mean(',test2,'.Values(:,1));']);

eval(['YMax2=max(',test2,'.Values(:,2));']);
eval(['YMin2=min(',test2,'.Values(:,2));']);
eval(['YAve2=mean(',test2,'.Values(:,2));']);

eval(['ZMax2=max(',test2,'.Values(:,3));']);
eval(['ZMin2=min(',test2,'.Values(:,3));']);
eval(['ZAve2=mean(',test2,'.Values(:,3));']);



test3='Phase1_4152016_PH_5mph_4';

eval(['Time3=', test3, '.Values(:,5)/1000;']);
basetime3= min(Time3);
atime3= Time3 - basetime3;

eval(['X_Accel3=', test3, '.Values(:,1);']);
eval(['Y_Accel3=', test3, '.Values(:,2);']);
eval(['Z_Accel3=', test3, '.Values(:,3);']);

eval(['XMax3=max(',test3,'.Values(:,1));']);
eval(['XMin3=min(',test3,'.Values(:,1));']);
eval(['XAve3=mean(',test3,'.Values(:,1));']);

eval(['YMax3=max(',test3,'.Values(:,2));']);
eval(['YMin3=min(',test3,'.Values(:,2));']);
eval(['YAve3=mean(',test3,'.Values(:,2));']);

eval(['ZMax3=max(',test3,'.Values(:,3));']);
eval(['ZMin3=min(',test3,'.Values(:,3));']);
eval(['ZAve3=mean(',test3,'.Values(:,3));']);
```

Figure B.2: A second partial snapshot of parsing the speedbump and pothole data.

```
%% 3 Runs
aveX_max=(XMax + XMax2 + XMax3)/3;
aveX_min=(XMin + XMin2 + XMin3)/3;
aveX_ave=(XAve + XAve2 + XAve3)/3;

aveY_max=(YMax + YMax2 + YMax3)/3;
aveY_min=(YMin + YMin2 + YMin3)/3;
aveY_ave=(YAve + YAve2 + YAve3)/3;

aveZ_max=(ZMax + ZMax2 + ZMax3)/3;
aveZ_min=(ZMin + ZMin2 + ZMin3)/3;
aveZ_ave=(ZAve + ZAve2 + ZAve3)/3;
```

```
%% Plot Data

[TIME ia ic] = unique(atime,'stable');
[TIME2 ia2 ic2] = unique(atime2,'stable');
[TIME3 ia3 ic3] = unique(atime3,'stable');

Z_A = Z_Accel(ia);
Z_A2 = Z_Accel2(ia2);
Z_A3 = Z_Accel3(ia3);

figure(1)
plot(TIME,Z_A);
 grid on;
    title('Z-Acceleration 1');
    xlabel('Time (s)');
    ylabel('Acceleration (G)');

figure(2)
plot(TIME2,Z_A2);
 grid on;
    title('Z-Acceleration 2');
    xlabel('Time (s)');
    ylabel('Acceleration (G)');
```

Figure B.3: A partial snapshot of averaging and plotting the speedbump and pothole data.

```
figure(3)
plot(TIME3,Z_A3);
 grid on;
    title('Z-Acceleration 3');
    xlabel('Time (s)');
    ylabel('Acceleration (G)');
```

```
 %% Print stats
fprintf('The max X-Accel was %d G. \r', aveX_max)
fprintf('The ave X-Accel was %d G. \r', aveX_ave)
fprintf('The min X-Accel was %d G. \n\r', aveX_min)
fprintf('The max Y-Accel was %d G. \r', aveY_max)
fprintf('The ave Y-Accel was %d G. \r', aveY_ave)
fprintf('The min Y-Accel was %d G. \n\r', aveY_min)
fprintf('The max Z-Accel was %d G. \r', aveZ_max)
fprintf('The ave Z-Accel was %d G. \r', aveZ_ave)
fprintf('The min Z-Accel was %d G. \r', aveZ_min)
```

Figure B.4: A partial snapshot of plotting and summarizing the speedbump and pothole data.

Acceleration Code

```
%% Yomi Famuyiwa 9/11/15
%% Parse 0-60 TDMS data
clc
%% Step 1: Extract data, correct time, & theoretical gas consumed
test='QSixty11_1106';
eval(['Speed=', test, '.Values(:,1);']);
eval(['Time=', test, '.Values(:,2)/1000;']); %55

basetime= min(Time);
atime= Time - basetime;
i=1;
j=1;

%% Step 2: Get rid of steps, convert speed
[cuttime ia ic] = unique(atime,'stable');
cutspeed = Speed(ia);
Speed_mph=cutspeed*0.621371; %kph to mph

%% Step 3: Find 0mph and 60mph section
start_index =find(Speed_mph == 0,1,'Last');
end_index =find(Speed_mph >=60,1,'First');

speed=Speed_mph(start_index:end_index);
ttime=cuttime(start_index:end_index);
CUTspeed(1:length(speed))=speed;
CUTtime(1:length(ttime))=ttime;

%% Step 4: Find time between 0 and 60 and plot
deltaT= max(ttime)-min(ttime);
ptime=ttime-min(ttime);
figure(1)
    plot(ptime,speed,'o','LineWidth',1)
    grid on;
    title('0-60 mph Test Run 7 -7.87s');
    xlabel('Time (s)');
    ylabel('Speed (mph)');

    %% Print stats
fprintf('The zero to sixty time was %d seconds. \n\r', deltaT)
```

Figure B.5: A snapshot of parsing, plotting, and summarizing the acceleration data.

Fuel Economy Code

```
%% Yomi Famuyiwa 7/28/15
%% Parse Fuel Economy TDMS data

%% Step 1: Extract data, correct time, & theoretical gas consumed

test='maf2';

eval(['Speed=', test, '.Values(:,45)']);
eval(['Time=', test, '.Values(:,55)']);
eval(['Fuel_Cons=', test, '.Values(:,29)']);
eval(['MAF=', test, '.Values(:,51)']);
eval(['Lambda1=', test, '.Values(:,52)']);
eval(['Lambda2=', test, '.Values(:,53)']);

basetime= min(Time);
atime= Time - basetime;
j=1;
m=1;

%% Step 2: Get rid of steps, convert speed and fuel consumption

[cuttime ia ic] = unique(atime,'stable');
cutspeed = Speed(ia);

Speed_mph=cutspeed*0.621371; %kph to mph
Speed_kps=cutspeed/3600; %kph to kps

Fuel_Cons_gps=Fuel_Cons/60; %gal/min to gal/s

G=Fuel_Cons_gps(ia);
G2 =trapz(cuttime,G);
%% Step 3: Integrate the fuel consumption and speed to calculate feul economy

int_fuel_cons=trapz(atime,Fuel_Cons_gps); %gal
position_km=trapz(cuttime,Speed_kps); %km
position_miles=position_km*0.621371; %miles

FE_mpg = position_miles/int_fuel_cons ;
FE_lpkm =FE_mpg*235.214583; %L/100km
```

Figure B.6: A snapshot of parsing and trimming the fuel economy data.

```
%% Step 5: Get MFF from MAF

AFR=14;
gas_density=2708; %g/gal
cutMAF=MAF(ia); %g/s
MFF=cutMAF/AFR; %g/s

F_cons_g=trapz(cuttime,MFF); %g
F_cons_gal=F_cons_g/gas_density; %gal


%% Step 4: Plot the data
figure(1);
subplot(2,1,1)
plot(cuttime,(MFF/gas_density)*60,'LineWidth',1)
grid on;
title('FE Hwy Test');
xlabel('Time (s)');
ylabel('MAP');

subplot(2,1,2)
plot(atime,Fuel_Cons,'LineWidth',1)
grid on;
xlabel('Time (s)');
ylabel('Fuel consumption (gal/min)');

figure(2);
subplot(3,1,1)
plot(cuttime,MFF,'LineWidth',1)
grid on;
xlabel('Time (s)');
ylabel('Fuel consumption (gal/s)');

subplot(3,1,2)
plot(atime,Lambda1,'LineWidth',1)
grid on;
xlabel('Time (s)');
ylabel('Lambda');

      subplot(3,1,3)
      plot(atime,Lambda2,'LineWidth',1)
      grid on;
      xlabel('Time (s)');
      ylabel('Lambda');
```

Figure B.7: A snapshot of plotting and summarizing the fuel economy data.

Coastdown Code

```
%% Yomi Famuyiwa 7/21/15
%% Parse Coastdown TDMS data Part 1

%% Step 1: Extract data, convert to mph, get max and min values, correct time
for i= 1:10
eval(['Speed=qcoastdown',num2str(i),'_0918.Values(:,1)']);
eval(['Time=qcoastdown',num2str(i),'_0918.Values(:,2)/1000']);

Speed=Speed*0.621371;

eval(['CD_MaxSpeeds(i)=max(qcoastdown',num2str(i),'_0918.Values(:,1))']);
eval(['CD_MinSpeeds(i)=min(qcoastdown',num2str(i),'_0918.Values(:,1))']);
eval(['CD_BaseTimes(i)=min(qcoastdown',num2str(i),'_0918.Values(:,2)/1000)']);

atime = Time - CD_BaseTimes(i);

%% Step 2: Get rid of steps
[SPEED ia ic] = unique(Speed,'stable');
TIME = atime(ia);

%% Step 3: Find 20mph and 70mph section & put data into an array
start_index = find(SPEED >= 67,1,'Last');
end_index =find(SPEED >=24,1,'Last');

cutspeed =SPEED(start_index:end_index);
cuttime= TIME(start_index:end_index);

CD_Speeds(1:length(cutspeed),i)=cutspeed;
CD_Times(1:length(cuttime),i)=cuttime;

end

CD_MaxSpeeds=CD_MaxSpeeds*0.621371;
CD_MinSpeeds=CD_MinSpeeds*0.621371;

CD_Speeds = CD_Speeds(1:77,:);
CD_Times = CD_Times(1:77,:);
```

Figure B.8: A snapshot of parsing and trimming the coastdown data.

```
%% Yomi Famuyiwa 7/22/15
%% Parse Coastdown TDMS data Part 2

veh_mass_kg = 2721.55; %6000 lbs
air_rho_kgpm3 = 1.255;
height = 72*.0254;
width = 77*.0254;
veh_area_m2 = .8*height*width;

%% Step 4: Averaging

avespeed = mean(CD_Speeds,2); %2 is to average rows
avetime = mean(CD_Times,2);

coasttime =max(avetime)- min(avetime);

max_ave_speed = max(avespeed);
min_ave_speed = min(avespeed);

%% Step 5: Find curve fit coefficients

avespeed_ms=avespeed*.44704; %mph to mps

p = polyfit(avetime,avespeed,3);
fit = polyval(p,avetime);

p_ms=polyfit(avetime,avespeed_ms,3);
fit_ms = polyval(p_ms,avetime);

a_mps2=diff(fit_ms)./diff(avetime);

coeff = polyfit(avespeed_ms(2:end),a_mps2,2);
FIT=polyval(coeff, avespeed_ms);

Cd = 1*coeff(1)*veh_mass_kg*2/(air_rho_kgpm3*veh_area_m2);
fd = 1*coeff(2)/9.81;
fs = 1*coeff(3)/9.81;

      %% Step 6: Plot the data with curve fits
      figure(1)
      plot(avetime,avespeed,'o','LineWidth',1)
      hold on
      plot(avetime,fit,'g','LineWidth',3);
      hold off
      grid on;

      title('Quantum Coastdown Test');
      xlabel('Time (s)');
      ylabel('Average Velocity (mph)');
      legend('Actual Data', 'Curve Fit');

      figure(2)
      plot(avespeed_ms(2:end),a_mps2,'o','LineWidth',1);
      grid on;
      title('Quantum Coastdown Acceleration');
      xlabel('Average Velocity (m/s)');
      ylabel('Acceleration (m/s^2)');
      hold on
      plot(avespeed_ms,FIT,'g','LineWidth',3);
      legend('Actual Data', 'Curve Fit');
      hold off

      %% Print stats
      fprintf('Your ave Cd coefficient is %d\n', Cd)
      fprintf('Your ave fd coefficient is %d\n', fd)
      fprintf('Your ave fs coefficient is %d\n', fs)
      fprintf('The max ave speed is %d mph. \n', max_ave_speed)
      fprintf('The min ave speed is %d mph. \n', min_ave_speed)
      fprintf('The ave coast time is %d seconds. \n', coasttime)
```

Figure B.9: A snapshot of averaging, plotting, and summarizing the coastdown data.

Cornering Code

```
%% Yomi Famuyiwa 7/22/15
%% Parse Cornering TDMS data

%% Step 1: Extract data, convert to mph, correct time
test='corn0_25_0913';

eval(['Speed=', test, '.Values(:,1)']);
eval(['Time=', test, '.Values(:,3)/1000;']);
eval(['Steering_theta=', test, '.Values(:,2)']);

basetime= min(Time);
atime= Time - basetime;

Speed=Speed*0.621371;

j=1;
m=1;

%% Step 2: Get rid of steps, align data, get mean and max values & put data into an array
[TIME ia ic] = unique(atime,'stable');
SPEED = Speed(ia);

Steer_T=Steering_theta(ia);

mean_speed= mean(SPEED);
mean_theata= mean(Steer_T);

%% Step 3: Plot the data
subplot(2,1,1)
plot(TIME,Steer_T);
ylabel('Steering Theta(degrees)');
xlabel('Time(s)');
grid on;
title('Cornering 25 mph Test');

subplot(2,1,2)
plot(TIME,SPEED);
ylabel('Speed(mph)');
xlabel('Time(s)');
grid on;
```

Figure B.10: A snapshot of parsing, plotting, and summarizing the cornering data.

Appendix C (LabVIEW Code)

Written and programmed by Tucker Alsup.

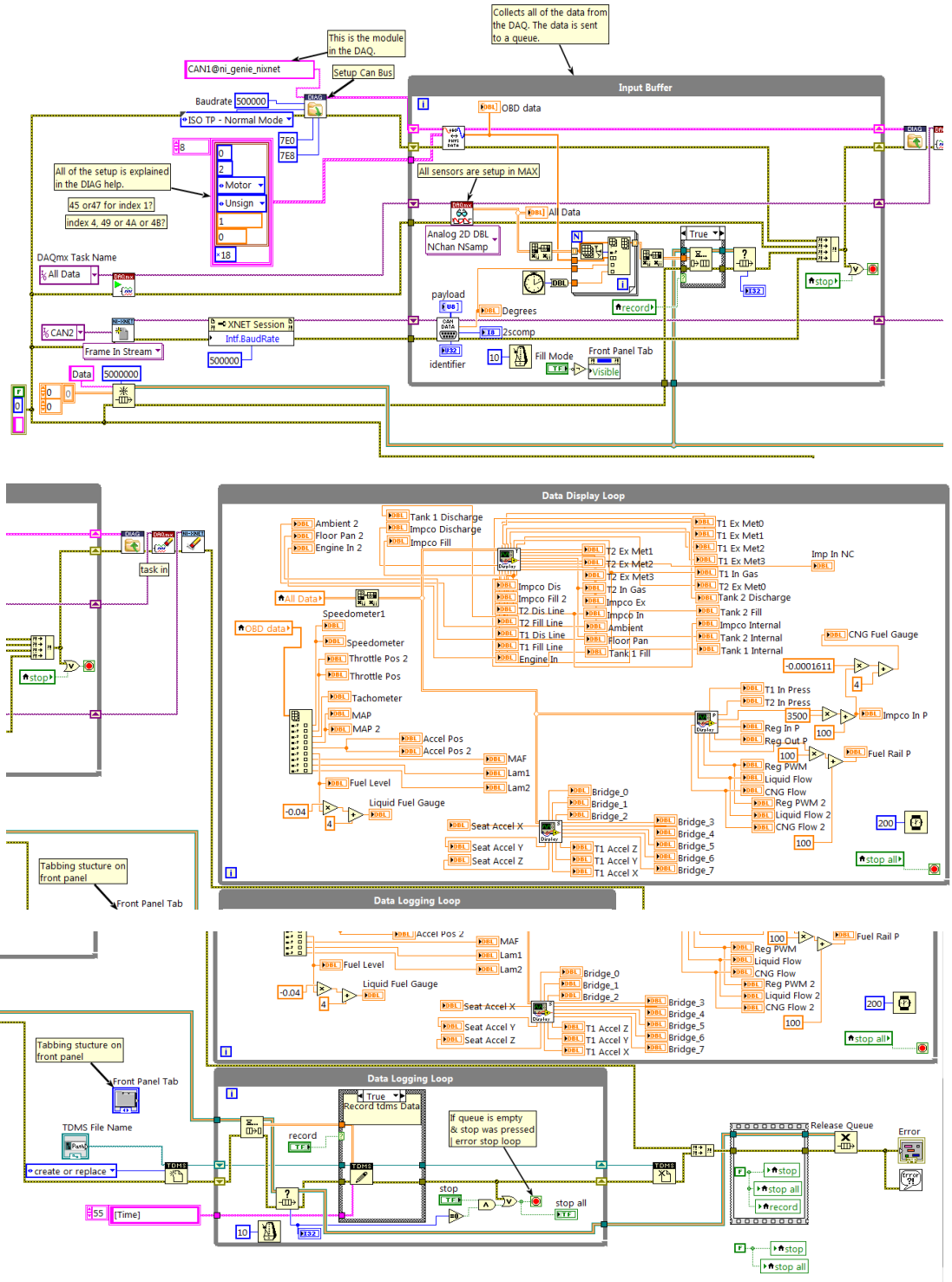

Figure C.1: A snapshot of the LabVIEW code developed by Tucker Alsup to log and save the data.

Appendix D (Miscellaneous)

Terminal Connections

Table D.1: A list of the terminal connections between the testing devices and the DAQ.

What Is Being tested?	Parameter Name	Priority (1=high, 3=low)	Type	I/O	NI Slot	NI Module	NI Terminal
CNG Tank 1 External Metal Temperature 1	Tank1 Extern Metal0	1	TC	I	1	9213	0
CNG Tank 1 External Metal Temperature 2	Tank1 Extern Metal1	1	TC	I	1	9213	1
CNG Tank 1 External Metal Temperature 3	Tank1 Extern Metal2	1	TC	I	1	9213	2
CNG Tank 1 External Metal Temperature 4	Tank1 Extern Metal3	1	TC	I	1	9213	3
CNG Tank 1 Internal Gas Temp	Tank1 Intern Gas	1					4
CNG Tank 2 External Metal Temperature 1	Tank2 Extern Metal0	1	TC	I	1	9213	5
CNG Tank 2 External Metal Temperature 2	Tank2 Extern Metal1	1	TC	I	1	9213	6
CNG Tank 2 External Metal Temperature 3	Tank2 Extern Metal2	1	TC	I	1	9213	7
CNG Tank 2 External Metal Temperature 4	Tank2 Extern Metal3	1	TC	I	1	9213	8
CNG Tank 2 Internal Gas Temp	Tank2 Intern Gas	1	TC	I	1	9213	9
IMPCO External tank temperature	Impco Extern	1	TC	I	1	9213	10
IMPCO Internal Tank Temperature	Impco Intern	1					11
Ambient Temperature	Ambient	1	TC	I	1	9213	12
Floor Pan Temperature near new exhaust	Floor Pan Side Pipes	3	TC	I	1	9213	13
CNG tank 1 line temperature	Tank1 Fill Line	1	TC	I	1	9213	14
	Tank1 Discharge Line	1	TC	I	1	9213	15
CNG tank 2 line temperature	Tank2 Fill Line	3	TC	I	7	9213	0
	Tank2 Discharge Line	3	TC	I	7	9213	1
IMPCO Tank Fill Temp	Impco Fill Line	1			7	9213	2
IMPCO Tank Discharge Temp	Impco Discharge Line	1			7	9213	3
Engine Inlet Temperature	Engine Inlet Temp	1	TC	I	1	9213	4
CNG tank 1 internal pressure	Tank1 Intern Press	1	Analog Voltage	I	2	9205	0
CNG tank 2 internal pressure	Tank2 Intern Press	1	Analog Voltage	I	2	9205	1
IMPCO tank pressure	Impco Intern Press	1	Analog Voltage	I	2	9205	2
fuel rail pressure	Fuel Rail Press	1	Analog Voltage	I	2	9205	3
pressure at regulator input	Reg In Press	3	Analog Voltage	I	2	9205	4
pressure at regulator output	Reg Out Press	3	Analog Voltage	I	2	9205	5
CNG flow	CNG Flow	1	Analog Voltage	I	2	9205	6
Liquid Fuel flow	Liquid Flow	1	Analog Voltage	I	2	9205	7
strain 1	Bridge_0	1	Analog Voltage	I	3	9219	0
strain 2	Bridge_1	1	Analog Voltage	I	3	9219	1
strain 3	Bridge_2	1	Analog Voltage	I	3	9219	2
strain 4	Bridge_3	1	Analog Voltage	I	3	9219	3
strain 5	Bridge_4	3	Analog Voltage	I	4	9219	0
strain 6	Bridge_5	3	Analog Voltage	I	4	9219	1
strain 7	Bridge_6	3	Analog Voltage	I	4	9219	2
strain 8	Bridge_7	3	Analog Voltage	I	4	9219	3
tank 1 acceleration X	Tank1 Accel X	1	Analog Input	I	5	9234	0
tank 1 acceleration Y	Tank1 Accel Y	3	Analog Input	I	5	9234	1
tank 1 acceleration Z	Tank1 Accel Z	3	Analog Input	I	5	9234	2
Seat Track acceleration X	Seat Accel X	1	Analog Input	I	6	9234	0
Seat Track acceleration Y	Seat Accel Y	1			6	9234	1
Seat Track acceleration Z	Seat Accel Z	1			6	9234	2

Center of Gravity Calculator (inspired by Chris Davis)

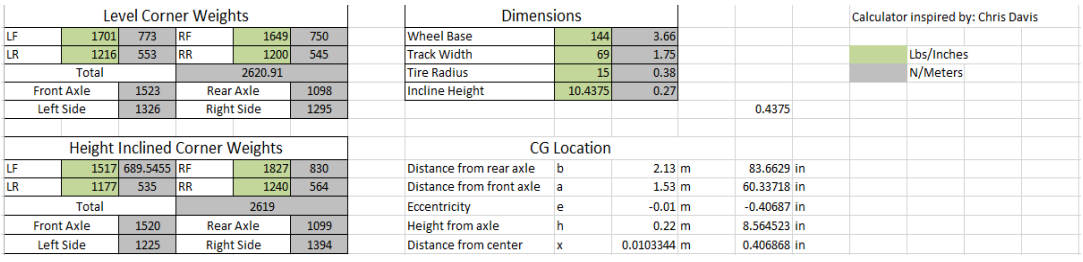

Level Corner Weights					
LF	1701	773	RF	1649	750
LR	1216	553	RR	1200	545
Total				2620.91	
Front Axle		1523	Rear Axle		1098
Left Side		1326	Right Side		1295

Dimensions			
Wheel Base	144	3.66	
Track Width	69	1.75	
Tire Radius	15	0.38	
Incline Height	10.4375	0.27	
			0.4375

Calculator inspired by: Chris Davis

Lbs/Inches

N/Meters

Height Inclined Corner Weights					
LF	1517	689.5455	RF	1827	830
LR	1177	535	RR	1240	564
Total				2619	
Front Axle		1520	Rear Axle		1099
Left Side		1225	Right Side		1394

CG Location					
Distance from rear axle	b	2.13	m	83.6629	in
Distance from front axle	a	1.53	m	60.33718	in
Eccentricity	e	-0.01	m	-0.40687	in
Height from axle	h	0.22	m	8.564523	in
Distance from center	x	0.0103344	m	0.406868	in

Figure D.1: A snapshot of the excel calculator that was used to calculate the center of gravity.

Appendix E (Permissions)

Permission to use virtual instrument images in Figure 4.6 and Figure C.1

7/5/16

Tucker Alsup

Dear Tucker Alsup:

I am currently putting my thesis together for publication and I would like your permission to use and reference the LabVIEW virtual instrument. The virtual instrument used to record data during testing and the code can be viewed in the figures below.

Figure 4.6

Figure C.1

The publication information is as follows:

Integration and Testing of an Advanced Conformable CNG Tank in a Full-sized Light-duty Pickup
Master's Thesis
ProQuest

I am requesting a non-exclusive license for world rights in all languages and for the life of the thesis.

Please indicate your consent by signing this letter and returning it to me through email. If you need any additional information about the thesis or the use of the virtual instrument, please feel free to contact me at aafamuyi@mtu.edu.

Sincerely,
Abayomi Famuyiwa

Permission granted for the use of the material as described above:

Agreed to: [redacted] Name & Title: [redacted]

Permissions to use logo images in Figure 4.6

7/14/16

Southwestern Energy Company ("SWN")

Dear John Gargani:
I am currently putting my thesis together for publication and I would like your permission to use the SWN logo (the "Logo"). The Logo is included in the virtual instrument used to record data during testing. The figure can be seen below.

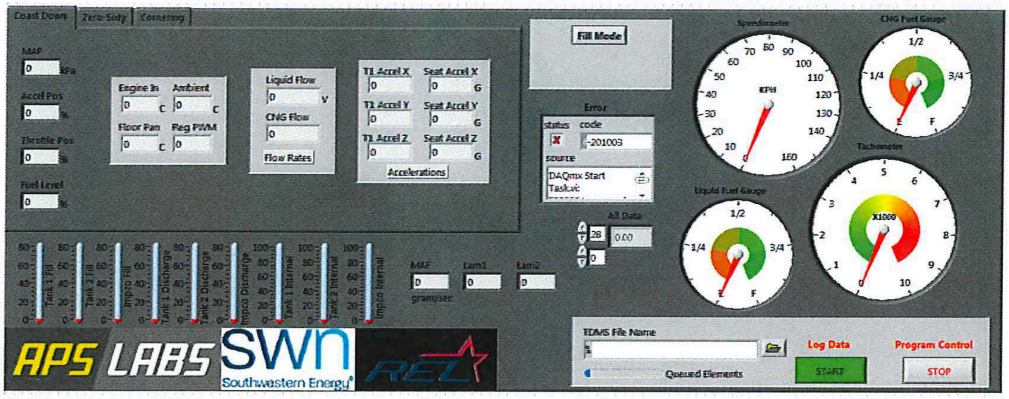

Figure 4.6: A snapshot of the Virtual Instrument used to record data during testing developed by Tucker Alsup.

The publication information is as follows:

Integration and Testing of an Advanced Conformable CNG Tank in a Full-sized Light-duty Pickup
Master's Thesis
ProQuest

I am requesting a limited, revocable, non-exclusive, non-sublicensable, non-transferable, non-assignable license for the sole purpose of including the Logo in Figure 4.6 of my Master's thesis. SWN retains ownership of all right, title and interest in the Logo and in all intellectual property rights therein.

Please indicate your consent by signing this letter and returning it to me through email. If you need any additional information about the thesis or the use of the Logo, please feel free to contact me at aafamuyi@mtu.edu.

Sincerely,
Abayomi Famuyiwa

Permission granted for the use of the Logo for the limited purpose as described above:

Agreed to: [redacted] Name & Title: [redacted] VP

7/4/16

REL Inc.

Dear Adam Loukus:

I am currently putting my thesis together for publication and I would like your permission to use the REL Inc. logo. The logo is included in the virtual instrument used to record data during testing. The figure can be seen below.

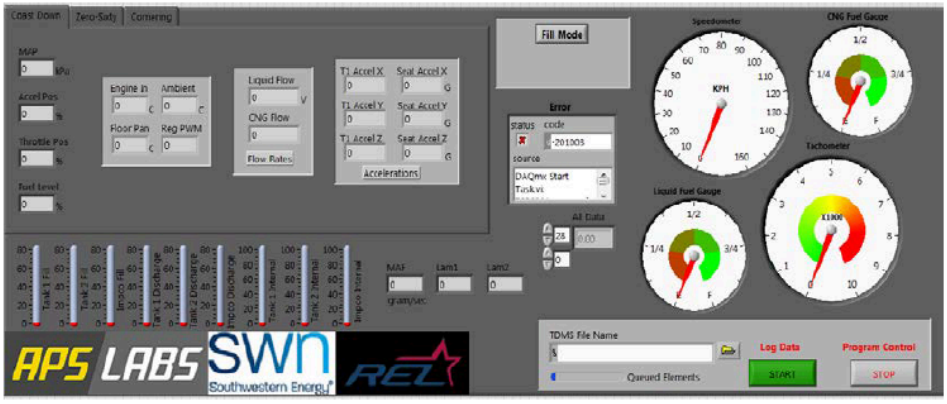

Figure 4.6: A snapshot of the Virtual Instrument used to record data during testing developed by Tucker Alsup.

The publication information is as follows:

Integration and Testing of an Advanced Conformable CNG Tank in a Full-sized Light-duty Pickup
Master's Thesis
ProQuest

I am requesting a non-exclusive license for world rights in all languages and for the life of the thesis.

Please indicate your consent by signing this letter and returning it to me through email. If you need any additional information about the thesis or the use of the logo, please feel free to contact me at aafamuyi@mtu.edu.

Sincerely,
Abayomi Famuyiwa

Permission granted for the use of the material as described above:

Agreed to: [redacted] Name & Title: Adam Loukus, PhD; Vice President

Jul 6,2016

Jeremy Worm

to me, Adam, Jeffrey, Christina

Yomi,

You are permitted to use the APS LABS Logo in your MS Thesis.

Let me know if you need anything else.

Jeremy Worm, P.E.
Director, Michigan Tech Mobile Lab
Advanced Power Systems Research Center
Department of Mechanical Engineering - Engineering Mechanics
Michigan Tech

Permission for blueprints used in Figure 5.1, Figure 5.3, and Figure 6.1

2006 Chevrolet Silverado GMT800 Pickup Truck blueprints free
https://getoutlines.com/blueprints/904/2006-chevrolet-silverado-gmt800-pickup-truck-blueprints
License: Creative Commons

You are free to:

- **Share** — copy and redistribute the material in any medium or format
- **Adapt** — remix, transform, and build upon the material for any purpose, even commercially.

- The licensor cannot revoke these freedoms as long as you follow the license terms.

Under the following terms:

- **Attribution** — You must give **appropriate credit**, provide a link to the license, and **indicate if changes were made**. You may do so in any reasonable manner, but not in any way that suggests the licensor endorses you or your use.

- **No additional restrictions** — You may not apply legal terms or **technological measures** that legally restrict others from doing anything the license permits.

Notices:

- You do not have to comply with the license for elements of the material in the public domain or where your use is permitted by an applicable **exception or limitation**.
- No warranties are given. The license may not give you all of the permissions necessary for your intended use. For example, other rights such as **publicity, privacy, or moral rights** may limit how you use the material.

Changes done to figure: Only the side and front views are used. Measurements of the test vehicle were applied to the figures.

Permission for Figure 5.6, Figure 5.7, Figure 5.8, Figure 5.9, Figure 5.10, Figure 5.11 from Google

Using Google Maps, Google Earth and Street View
https://www.google.com/permissions/geoguidelines.html
Last Modified: December 17, 2015

Thanks for considering Google Maps, Google Earth and Street View for your project! These guidelines are for non-commercial use except for the limited use cases described below; if you want to use Google Maps, Google Earth, or Street View for other commercial purposes, please contact the Google Maps for Work sales team.
"Commercial purposes" means "use for sale or revenue-generating purposes".

We created this page to clarify questions we've received from users over the years regarding uses of our mapping tools in everything from marketing and promotional materials, films, television programs, books, academic journals, and much more.

Generally speaking, as long as you're following our Terms of Service and you're attributing properly, we're cool with your using our maps and imagery; in fact, we love seeing all of the creative applications of Google Maps, Google Earth and Street View! But we know you're looking for more specifics to ensure you're using our maps and imagery correctly.

As you dive into the information below, we suggest starting with the general guidelines at the top, as these will apply to all projects. Then feel free to click directly to the section that applies to you.

GENERAL GUIDELINES

The Basics

Google Maps and Google Earth's "Content" (as defined in the Google Earth/Google Maps Additional Terms of Service) includes everything you'd find in these products: map and terrain data, imagery, business listings, traffic, reviews and other related information provided by Google, its licensors, and users.

These guidelines cover your use of the Content—with one exception. There are some particular guidelines regarding your use of Street View imagery available from both Google Maps and Google Earth. Please read the section below for instructions on how Street View imagery may or may not be used.

Terms of Service

To help you figure out whether your use of the Content is acceptable, first read the following documents:

- Google Terms of Service
- Google Maps/Google Earth Additional Terms of Service

Your use of the Content is first and foremost governed by the licenses above.

Fair Use

Apart from any license granted to you by Google, your use of the Content may be acceptable under principles of "fair use." Fair use is a concept under copyright law in the U.S. that, generally speaking, permits you to use a copyrighted work in certain ways without obtaining a license from the copyright holder.

There are similar, although generally more limited, concepts in other countries' copyright laws, including a concept known as "fair dealing" in a number of countries. Google can't tell you if your use of the Content from our products would be fair use or would be considered fair dealing; these are legal analyses that depend on all of the specific facts of your proposed use. We suggest you speak with an attorney if you have questions regarding fair use of copyrighted works.

Written permission

Due to limited resources and high demand, we're unable to sign any letter or contract specifying that your project or use has our explicit permission. As long as you follow the guidance on this page, and attribute the Content correctly, feel free to move forward with your project.

Attribution

All uses of the Content must provide attribution to both Google and our data providers. We require clear, visible attribution when the Content is shown. You may not move the attribution to the end credits or fade it out after a few seconds.

Note that if you embed a classic map, Street View panorama or My Map; use one of our APIs on the web or in an application; or export a video or JPEG from Google Earth Pro, the necessary attribution is already baked into the map and no further credit is needed. Learn more about how to properly credit, as well as how to identify providers, on our attribution guidelines page

If you are unwilling to meet our attribution requirements, contact our data provider(s) directly to inquire about purchasing the rights to use the Content directly. You'll find provider contact information listed on their websites.

Personalizing your map

You may annotate our maps with additional information—like points, lines or labels. In fact, many of our tools have built-in features that make it easy to do just that. For example, Google My Maps lets you draw lines and shapes on a Google map. We also offer a Styled Maps API that allows you to edit the colors of individual map components (for example, changing water to purple), as well as toggle visibility for each component (for example, making roads invisible). If neither of those fit your needs, you may save an image from Google Earth and use Photoshop to add custom text labels.

While we encourage annotations, you must not significantly alter how Google Maps, Google Earth or Street View would look online. For example, you're not allowed to make any changes to the colors of the product interface or alter how imagery appears (such as adding clouds or other natural elements, blurring, etc.).

USES IN PRINT

Google Maps and Google Earth have built-in print functionality. You may print Content for non-commercial use and enlarge it (for example, a map with directions). In all uses where you will distribute printed materials that include the Content, first be sure to read the general guidelines above, especially with regard to fair use and attribution.

Proposed use	OK to use?	Additional information
Books	Yes	It’s fine to use a handful of images, as long as you’re not distributing more than 5,000 copies or using the Content in guidebooks.
Periodicals	Yes	This includes newspapers, magazines and journals.
Reports and presentations	Yes	This includes research papers, internal reports, presentations, proposals and other related professional documents.
Guidebooks	No	You may not use the Content as a core part of printed navigational material (for example, tour books).
Consumer	No	This includes retail products or retail product packaging (for example, t-shirts, beach towels,

goods		shower curtains, mugs, posters, stationery, etc.).
Print advertisements	No	See the advertisements section for more guidance on digital and TV uses.